

OMEN-SED 1.0: A new, numerically efficient sediment module for the coupling to Earth System Models

Dominik Hülse¹, Sandra Arndt^{1,2}, Stuart Daines³, Pierre Regnier², and Andy Ridgwell^{1,4}

¹School of Geographical Sciences, University of Bristol, Clifton, Bristol BS8 1SS, UK

²Department of Earth and Environmental Sciences, Université Libre de Bruxelles, Brussels, Belgium

³Earth System Science, University of Exeter, North Park Road, Exeter EX4 4QE, UK

⁴Department of Earth Sciences, University of California, Riverside, CA 92521, USA

Correspondence to: Dominik Hülse (Dominik.Huelse@bristol.ac.uk)

Abstract. We present the first version of a new, analytical early diagenetic model resolving organic matter cycling and associated biogeochemical dynamics in marine sediments called OMEN-SED (Organic Matter ENabled SEDiment model). Most biogeochemical cycles and reactions in the surface sediments can be related either directly or indirectly to the degradation of organic matter (OM).

- Despite its fundamental importance for global biogeochemical cycling, in most Earth system models sediment-water dynamics are either neglected or treated in a very simplistic way. To provide a more realistic description of OM degradation and nutrient cycles in marine sediments we have developed OMEN-SED, a new, one-dimensional, numerically efficient reactive transport model. OMEN-SED is the first analytical model to explicitly describe organic matter cycling as well as associated dynamics of the most important terminal electron acceptors (i.e. O₂, NO₃, SO₄), related reduced substances (NH₄, H₂S), the full suite of secondary-redox reactions, macronutrients (PO₄) and associated pore water quantities (ALK, DIC). To represent a redox-dependent sedimentary P cycle we consider the formation and burial of Fe-bound P and authigenic Ca-P minerals. Thus, OMEN-SED captures most of the features of a complex, numerical diagenetic model, however, its computational efficiency allows the coupling to global Earth System models and therefore the investigation of coupled global biogeochemical dynamics over different timescales. This paper provides a detailed description of the new sediment model, as well as an extensive sensitivity analysis using a novel method which considers the entire cumulative distribution functions of the model outputs. OMEN-SED's performance is evaluated through comprehensive comparisons with observations and a more complex analytical model. Solid phase and dissolved porewater profiles for different ocean depths could be reproduced with good accuracy and modelled terminal electron acceptor fluxes fall well

within the range of globally observed fluxes. Furthermore, the coupling of OMEN-SED to the Earth System model cGENIE is described and the organic matter degradation rate constants were tuned to optimise the fit of modelled OM concentrations to a global database. In addition, simulated sediment
25 characteristics of the coupled model framework (such as OM degradation rates, oxygen penetration depths and sediment-water interface fluxes) are generally in good agreement with observations and in line with what one would expect on a global scale.

Contents

1	Introduction	4
30	2 Model Description	9
2.1	General Model Approach	9
2.2	Conservation Equations and Analytical Solution	13
2.2.1	Organic matter or Particulate Organic Carbon (POC)	13
2.2.2	Oxygen	14
35	2.2.3 Nitrate and Ammonium	15
2.2.4	Sulfate and Sulfide	18
2.2.5	Phosphate	20
2.2.6	Dissolved Inorganic Carbon (DIC)	21
2.2.7	Alkalinity	22
40	2.3 Determination of Integration Constants	24
2.3.1	Generic Boundary Condition Matching (GBCM)	25
2.3.2	Abstracting out the bioturbation boundary	26
2.4	Model Parameters	28
2.4.1	Transport Parameters	28
45	2.4.2 Stoichiometries and reaction parameters	29
3 Stand-alone sensitivity analysis and case studies	32	
3.1	Sensitivity Analysis	32
3.1.1	Methodology	32
3.1.2	Results	34
50	3.2 Case study: Simulations of sediment cores	37
3.2.1	Methodology	37
3.2.2	Results	37
3.3	Case study: Stand-alone simulations of global ocean transect	39
3.3.1	Methodology	39
55	3.3.2 Results	41

4 Coupled pre-industrial Earth system model simulations	43
4.1 Coupling to the cGENIE Earth system model	43
4.2 Parameterising the OM degradation rate constants in a global model	45
4.2.1 Methodology	46
4.2.2 Results	49
4.3 Modelled fluxes and sediment characteristics	52
5 Scope of applicability and model limitations	54
6 Conclusions	56
7 Code Availability	57
65 A Reaction Network	57
B Sensitivity Analysis	57
B1	57

1 Introduction

DH: Will delete the sub-headings!

Role of marine sediments for climate and global biogeochemical cycles:

- 70 Marine surface sediments are key components in the Earth system. They host the largest carbon reservoir within the surficial Earth system, provide the only long term sink for atmospheric CO₂, recycle nutrients and represent the most important geochemical archive used for deciphering past changes in biogeochemical cycles and climate (e.g. Berner, 1991; Archer and Maier-Reimer, 1994; Ridgwell and Zeebe, 2005; Arndt et al., 2013). Physical and chemical processes in sediments (i.e.
- 75 diagenetic processes) depend on the water column and vice versa: Diagenesis is controlled by the external supply of solid material (e.g. organic matter, calcium carbonate, opal) from the water column and is affected by overlying bottom water concentrations of solutes. At the same time, sediments impact the water column directly either by short- and long-term storage of deposited material or diagenetic processing of deposited material and diffusion of some of the resulting products (e.g.
- 80 nutrients, DIC) to the overlying bottom waters. This so-called benthic-pelagic coupling is essential for understanding global biogeochemical cycles and climate (e.g. Archer and Maier-Reimer, 1994; Archer et al., 2000; Soetaert et al., 2000; Mackenzie, 2005).

Biological primary production of organic matter (OM, CH₂O in equation R1) and the reverse process of degradation can be written in a greatly simplified reaction as:



On geological timescales production of OM is generally greater than degradation which results in some organic matter being buried in marine sediments and oxygen accumulating in the atmosphere.

Thus burial of OM leads to net oxygen input to, and CO₂ removal from the atmosphere (Berner, 2004).

90 On shorter timescales, the upper few meters of the sediments where early diagenesis occurs are specifically important as this zone controls whether a substance is recycled to the water column or buried for a longer period of time in the deeper sediments (Hensen et al., 2006). Most

biogeochemical cycles and reactions in this part of marine sediments can be related either directly or indirectly to the degradation of organic matter (Arndt et al., 2013). Oxygen and nitrate for instance,

the most powerful electron acceptors, are consumed in the course of the degradation of organic mat-

95 ter, resulting in the release of ammonium and phosphorus to the pore water. As such, degradation of OM in the sediments can profoundly affect the oxygen and nutrient inventory of the ocean and thus primary productivity (Van Cappellen and Ingall, 1994; Lenton and Watson, 2000). Furthermore,

organic matter degradation releases metabolic CO₂ to the pore water, causing it to have a lower pH and provoking the dissolution of calcium carbonate CaCO₃ (Emerson and Bender, 1981).

100 Nutrient recycling from marine sediments has been suggested to play a key role for climate and ocean biogeochemistry for different events during Earth history. For example, feedbacks between phosphorus storage and erosion from shelf sediments and marine productivity have been hypothesised to play an important role for glacial/interglacial atmospheric CO₂ changes (Broecker, 1982;

Ruttenberg, 1993). Furthermore, nutrient recycling from anoxic sediments has been invoked to explain the occurrence of more extreme events in Earth history, for instance Oceanic Anoxic Events (OAEs, e.g. Mort et al., 2007; Tsandev and Slomp, 2009). OAEs represent severe disturbances of the global carbon, oxygen and nutrient cycles of the ocean and are usually characterized by widespread bottom water anoxia and photic zone euxinia (Jenkyns, 2010). One way to explain the genesis and persistence of OAEs is increased oxygen demand due to enhanced primary productivity. Increased nutrient inputs to fuel primary productivity may have come from marine sediments as the burial efficiency of phosphorus declines when bottom waters become anoxic (Ingall and Jahnke, 1994; Van Cappellen and Ingall, 1994). The recovery from OAE like conditions is thought to involve the permanent removal of excess CO₂ from the atmosphere and ocean by burying carbon in the form of organic matter in marine sediments (e.g. Arthur et al., 1988; Jarvis et al., 2011), which is consistent with the geological record of widespread black shale formation (Stein et al., 1986). However, the overall amount, exact timing and the rate of organic matter burial remain a topic of an ongoing debate. Therefore, globally quantifying the burial and degradation of organic matter in marine sediments and related biogeochemical dynamics is important for understanding climate and the cycling of many chemical elements on various timescales.

120 Diagenetic Models in general:

Quantifications of diagenetic processes are possible through the application of idealised mathematical representations of diagenesis, or so-called diagenetic models (see e.g. Berner, 1980; Boudreau, 1997). The number of research questions that can be addressed with diagenetic models is infinite and a plethora of different approaches have been developed, mainly following two distinct directions (Arndt et al., 2013). First, state-of-the art vertically resolved numerical models simulating the entire suite of essential coupled redox and equilibrium reactions within marine sediments (e.g. BRNS, Aguilera et al., 2005; CANDI, Boudreau, 1996; MEDIA, Meysman et al., 2003; STEADYSED, Van Cappellen and Wang, 1996). These “complete”, non-steady-state models, thus resolve the resulting characteristic redox-zonation of marine sediments through explicitly including oxic OM degradation, denitrification, oxidation by manganese and iron (hydr)oxides, sulfate reduction and methanogenesis as well as the reoxidation of reduced byproducts (i.e. NH₄, Mn²⁺, Fe²⁺, H₂S, CH₄, see e.g. Regnier et al., 2011; Arndt et al., 2013). Furthermore, they incorporate various mineral dissolution and precipitation reactions, as well as fast equilibrium sorption processes for example of NH₄, PO₄ and metal ions (i.e. Mn²⁺, Fe²⁺ and Mg²⁺, compare Van Cappellen and Wang, 1996; Meysman et al., 2003). Modelled, depth-dependent, transport processes usually comprise advection, diffusion, bioturbation and bio-irrigation. This group of diagenetic models generally uses a so-called multi-G approach (Jørgensen, 1978; Berner, 1980), thus dividing the bulk organic matter pool into a number of compound classes that are characterised by different degradabilities k_i , which are generally dependent on the type and concentration of the specific terminal electron acceptor (TEA).

140 Alternative approaches, in particular reactive continuum models (Boudreau and Ruddick, 1991),

assume a continuous distribution of reactive types but are much less often used. These complex, “complete” models have a great potential for quantifying OM degradation dynamics for sites where enough observations are available to constrain its model parameters (see e.g. Boudreau et al., 1998; Wang and Van Cappellen, 1996; Thullner et al., 2009, for applications). However, due to the high degree of coupled processes and depth-varying parameters the diagenetic equation needs to be solved numerically, thus resulting in a very high computational demand and consequently rendering their application in an Earth system model (ESM) framework prohibitive. Additionally, their global applicability is limited by the restricted transferability of model parameters from one site to the global scale (Arndt et al., 2013).

The second group of models solves the diagenetic equation analytically or semi-analytically, thus providing an alternative and computational more efficient approach. However, finding an analytical solution, especially when complex reaction networks are to be considered, is not straightforward and generally requires the assumption of steady state. The complexity of the reaction network can be reduced by dividing the sediment column into distinct zones and accounting for the most pertinent biogeochemical processes within each zone, thus increasing the likelihood of finding an analytical solution. In general, analytical diagenetic models are less sophisticated and comprehensive than numerical models and are used for the coupling to global ESMs (e.g. HAMOCC and NorESM use the model of Heinze et al. (1999)) or box models (e.g. DCESS, Shaffer et al., 2008 or MBM using MEDUSA, Munhoven, 2007). These analytic or semi-analytical models account for the most important transport processes (i.e advection, bioturbation and molecular diffusion) through basic parametrizations and include fewer biogeochemical reactions which are generally restricted to the upper, bioturbated 10 cm of the sediments. They assume that the sedimentary organic matter pool is composed of just a single compound class which is either degraded with a globally invariant degradation rate constant (Munhoven, 2007) or a fixed rate constant depending on local oxygen concentrations (Shaffer et al., 2008; Palastanga et al., 2011). Pore water tracers explicitly represented in DCESS (Shaffer et al., 2008) and the HAMOCC model of Heinze et al. (1999) and Palastanga et al. (2011) are restricted to DIC, TA, PO₄ and O₂. The MEDUSA model (Munhoven, 2007) considers CO₂, HCO₃⁻, CO₃²⁻ and O₂. Other species produced or consumed during OM degradation are neglected. Thus, with oxygen being the only TEA explicitly modelled the influence of reduced species is only implicitly included in the boundary conditions for O₂. A newer versions of the HAMOCC model, being a notable exception, as Ilyina et al. (2013) include NO₃ and denitrification explicitly. Furthermore, the version of Palastanga et al. (2011) represents an redox-dependent explicit sedimentary phosphorus cycle. Yet, reoxidation of reduced byproducts, so-called secondary redox-reactions, or sorption processes are not included in any of the discussed models.

How are sediments resolved in Earth system models:

A suitable sediment model for the coupling to an ESM has to provide a robust quantification of organic (and inorganic) carbon burial fluxes, as well as benthic uptake/return fluxes of oxygen, growth-

DH: I shortened this paragraph a bit. I think, it should be somehow included as it talks specifically about diagenetic models in ESMs!?

limiting nutrients and reduced species. As a consequence, the reaction network must account for the most important primary and secondary redox reactions, equilibrium reactions, mineral precipitation/dissolution and adsorption/desorption, resulting in a complex set of coupled reaction-transport equations. Even though there are more appropriate sediment representations available, in most current ESMs sediment-water dynamics are either neglected or treated in a very simplistic way (Soetaert et al., 2000; Hülse et al., 2017). Most Earth system Models of Intermediate Complexity (EMICs) and also some of the higher resolution global carbon cycle models represent the sediment-water interface either as a reflective or a conservative/semi-reflective boundary (Hülse et al., 2017). Thus, all particulate material deposited on the seafloor is either instantaneously consumed (reflective boundary), or a fixed fraction is buried in the sediments (conservative/semi-reflective boundary). Both highly simplified approaches furthermore completely neglect the exchange of solute species through the sediment-water interface and, therefore, cannot resolve the complex benthic-pelagic coupling. However, due to their computational efficiency, both representations are often used in global biogeochemical models (e.g. Najjar et al., 2007; Ridgwell et al., 2007; Goosse et al., 2010). The most complex description of diagenetic organic matter degradation in Earth system models is the second group of vertically resolved diagenetic models as discussed above (e.g. Heinze et al., 1999; Munhoven, 2007; Shaffer et al., 2008). These models solve the one-dimensional reaction-transport equation for a number of solid and dissolved species for the upper, bioturbated 10 cm of the sediments. Examples of global ESMs employing a vertically resolved diagenetic model are NorESM (Tjiputra et al., 2013) and HAMOCC (Palastanga et al., 2011; Ilyina et al., 2013), both using a version of Heinze et al. (1999). None of the EMICs reviewed by Hülse et al. (2017) use such a sediment representation. DCESS (Shaffer et al., 2008) and MBM (Munhoven, 2007) are box models employing a vertically resolved diagenetic model. However, in general oxygen is the only TEA explicitly modelled and secondary redox reactions and reduced species are completely neglected in these approaches. Furthermore, all models represent the bulk OM pool as a single fraction with a fixed degradation rate constant.

Problem with that:

Obviously, such a simplification of the OM pool can neither account for the observed vast structural complexity in natural organic matter and its resulting different degradation rates nor for the rapid decrease in OM degradability in the uppermost centimetres of the sediments (Arndt et al., 2013). It has been suggested that at least a 3G approach is necessary to accurately represent organic matter dynamics in this part of the sediments where most OM is degraded (e.g. Soetaert et al., 1996). Even more restrictive is the use of O₂ as the only TEA and the complete absence of reduced substances and related secondary redox reactions. Even though for the majority of the modern sediments (i.e. in the deep-ocean) O₂ is the primary electron acceptor and Archer et al. (2002) suggested that aerobic degradation accounts for 66% of total organic matter respiration more recent model and data studies have reported that sulfate reduction is the dominant degradation pathway on a global average (with

215 contributions of 55–76% Canfield et al., 2005; Jørgensen and Kasten, 2006; Thullner et al., 2009). Oxygen becomes progressively less important as TEA with decreasing seafloor depth and sulfate reduction has been shown to account for 83% of OM degradation in coastal sediments (Krumins et al., 2013). In these environments most O₂ is used to reoxidise reduced substances produced during anaerobic degradation (Canfield et al., 2005; Thullner et al., 2009). Thus, the in situ production of
220 e.g. NO₃ and SO₄ through oxidation of NH₄ and H₂S forms an important sink for O₂ which is entirely neglected in current sediment representations in global models. In addition, due to the lack of an appropriate sedimentary P cycle (with the exception of the HAMOCC version of Palastanga et al. (2011), no current global ESM is able to model the redox dependent P release from marine sediments and its implications for primary productivity, global biogeochemical cycles and climate.

225 **Solution presented here:**

Analytical approaches with distinct biogeochemical zones were implemented and used in the seventies and eighties to describe observed pore water profiles (e.g. Vanderborgh and Billen, 1975; Vanderborgh et al., 1977; Billen, 1982; Goloway and Bender, 1982) and later for inclusion into 1-D ecosystem models (e.g. Ruardij and Van Raaphorst, 1995) and global Earth system models (Tromp 230 et al., 1995). However, alongside the oxic zone these models only describe one anoxic zone explicitly, either a denitrification (Vanderborgh and Billen, 1975; Vanderborgh et al., 1977; Billen, 1982; Goloway and Bender, 1982; Ruardij and Van Raaphorst, 1995) or a sulfate reduction zone (Tromp et al., 1995). Furthermore, the approaches of Vanderborgh and Billen (1975), Goloway and Bender (1982) and Tromp et al. (1995) do not explicitly model the produced reduced species (i.e. 235 NH₄ and H₂S, respectively). In addition, the model of Tromp et al. (1995) ignores reoxidation of H₂S produced during sulfate reduction. In order to provide a more realistic description of organic matter degradation and nutrient cycles in marine sediments we have developed the OrganicMatter ENabled SEDiment model (OMEN-SED), a new, one-dimensional, numerically efficient reactive transport model. OMEN-SED is the first analytical model to explicitly describe OM cycling as well 240 as associated dynamics of the most important TEAs (i.e. O₂, NO₃, SO₄), related reduced substances (NH₄, H₂S), the full suite of secondary-redox reactions, macronutrients (PO₄) and associated pore water quantities (ALK, DIC). To represent a redox-dependent sedimentary P cycle we consider the formation and burial of Fe-bound P and authigenic Ca-P minerals. Thus, OMEN-SED captures most 245 of the features of a complex, numerical diagenetic model, however, its computational efficiency allows the coupling to global Earth system models and therefore the investigation of coupled global biogeochemical dynamics over different timescales. Here, the model is presented as a 2G-approach, however, a third, non-degradable OM fraction can easily be added and OMEN-SED can be further extended to a Multi-G approach.

The first part of the paper provides a detailed description of OMEN-SED (Section 2). This includes descriptions of the general model approach (Section 2.1), of the conservation equations for all explicitly represented biogeochemical tracers (Section 2.2), as well as a summary of global re-

lationships used to constrain reaction and transport parameters in OMEN-SED (Section 2.4). In addition, a generic algorithm is described which is used to match internal boundary conditions and to determine the integration constants for the analytical solutions (Section 2.3). In order to validate
255 the stand-alone version of OMEN-SED the second part of the paper performs an extensive sensitivity analysis for the most important model parameters and resulting sediment-water interface fluxes are compared with a global database (Section 3.1). In addition, results of the stand-alone model are compared with observed pore water profiles from different ocean depths (Section 3.2) and OMEN-SED simulations of TEA-fluxes along a typical ocean transect are compared with observations and results
260 from a complete, numerical diagenetic model (Section 3.3). Thereafter, the coupling of OMEN-SED to the carbon-centric version of the “GENIE” Earth system model (cGENIE, Ridgwell et al., 2007) is describe (Section 4.1). Sensitivity studies are carried out using this coupled model and modelled organic matter concentrations in the surface sediments are compared to a global database (Seiter et al., 2004, Section 4.2). Finally, potential applicabilities of OMEN-SED are suggested and model
265 limitations are critically analyzed (Section 5).

2 Model Description

OMEN-SED is a new, one-dimensional, computationally efficient reaction-transport model is designed for the coupling to regional/global biogeochemical and Earth system models. OMEN-SED is implemented as a Fortran version that can be easily coupled to a pelagic model via the coupling
270 routine **OMEN_SED_main**. In addition, OMEN-SED exists as a stand-alone version implemented in MATLAB and the entire model can be executed on a standard personal computer in less than 0.1 seconds. The source code of both, the Fortran and the MATLAB stand-alone version, as well as instructions for executing OMEN-SED and for plotting model results are available as a supplement to this paper. The following section provides a detailed description of OMEN-SED and the
275 fundamental equations underlying the model are highlighted. Tables 1 and 15 summarise the bio-geochemical reaction network and Tables 9 and 10 provide a glossary of model parameters along with their respective units.

SA: maybe include some examples and test figures in supplement?

2.1 General Model Approach

In OMEN-SED, the calculation of benthic uptake, recycling and burial fluxes is generally based on
280 the vertically resolved conservation equation for solid and dissolved species in porous media (e.g. Berner, 1980; Boudreau, 1997):

$$\frac{\partial \xi C_i}{\partial t} = -\frac{\partial}{\partial z} \left(-\xi D_i \frac{\partial C_i}{\partial z} + \xi w C_i \right) + \xi \sum_j R_i^j \quad (1)$$

where C_i is the concentration of biogeochemical species i , ξ equals the porosity ϕ for solute species and $(1-\phi)$ for solid species. The term z is the sediment depth, t denotes the time, D_i is the apparent

285 diffusion coefficient of species i ($D_i = D_{i,0} + D_{\text{bio}} = D_{\text{mol},i} \cdot f_{ir} + D_{\text{bio}}$ for dissolved species and $D_i = D_{\text{bio}}$ for solid species), w is the burial rate and $\sum_j R_i^j$ represents the sum of all biogeochemical rates j affecting species i .

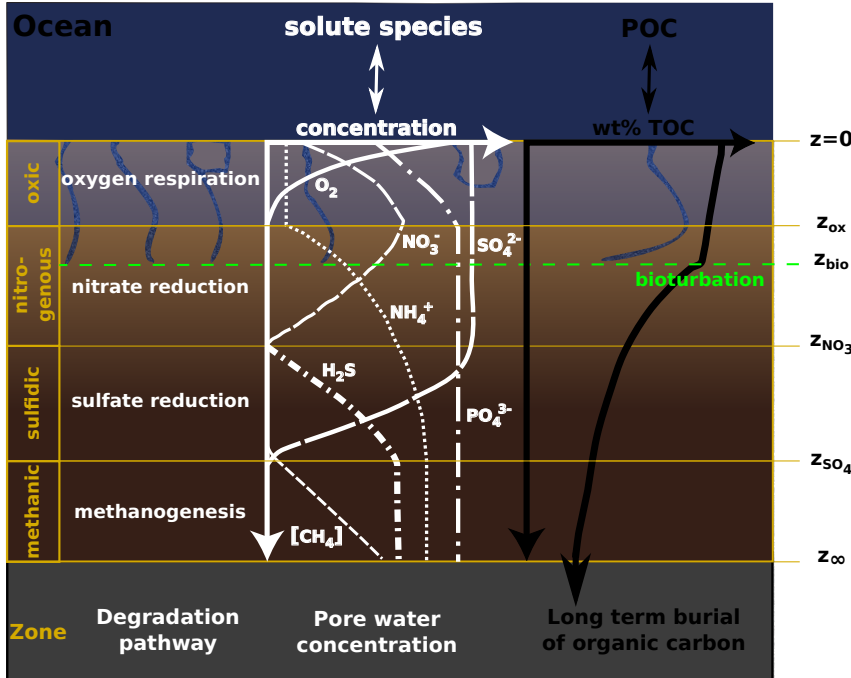


Figure 1. Schematic of the different modelled species and zones in OMEN-SED. Here showing the case $z_{ox} < z_{bio} < z_{NO_3^-} < z_{SO_4^{2-}}$.

OMEN-SED accounts for both the advective, as well as the diffusive transport of dissolved and solid species. Solid and dissolved species are buried in the sediment according to a constant burial rate w , thus neglecting the effect of sediment compaction (i.e. $\frac{\partial \phi}{\partial z} = 0$) due to mathematical constraints. The molecular diffusion of dissolved species is described by Fick's law applying a species-specific apparent diffusion coefficient, $D_{\text{mol},i}$. In addition, the activity of infaunal organisms in the bioturbated zone is simulated using a diffusive term (e.g. Boudreau, 1986), with a constant bioturbation coefficient D_{bio} in the bioturbated zone, while D_{bio} is set to zero below the maximum 290 bioturbation depth, z_{bio} . The pumping activity by burrow-dwelling animals and the resulting ventilation of tubes, the so-called bioirrigation, is encapsulated in a factor f_{ir} that enhances the molecular diffusion coefficient (hence, $D_{i,0} = D_{\text{mol},i} \cdot f_{ir}$, Soetaert et al., 1996). The reaction network of 295 OMEN-SED accounts for the most important primary and secondary redox reactions, equilibrium reactions, mineral dissolution and precipitation, as well as adsorption and desorption processes that affect the dissolved and solid species explicitly resolved in OMEN-SED. Tables 1 and 15 provide a 300

Table 1. Reactions and biogeochemical tracers implemented in the reaction network of OMEN-SED. The primary and secondary redox reactions are listed in the sequence they occur with increasing sediment depth.

Description	
Primary redox reactions	Degradation of organic matter via aerobic degradation, denitrification, sulfate reduction, methanogenesis (implicit)
Secondary redox reactions	Oxidation of ammonium and sulfide by oxygen, anaerobic oxidation of methane by sulfate
Adsorption/Desorption	Ad-/Desorption of P on/from Fe(OH) ₃ , NH ₄ adsorption, PO ₄ adsorption
Mineral precipitation	Formation of authigenic P
Biogeochemical tracers	Organic matter (2-G), oxygen, nitrate, ammonium, sulfate, sulfide (hydrogen sulfide), phosphate, Fe-bound P, DIC, ALK

summary of the reactions and biogeochemical tracers considered in OMEN-SED together with their respective reaction stoichiometries.

All parameters in Eq. (1) may vary with depth and many reaction rate expressions depend on the concentration of other species. Expressing Eq. (1) for a set of chemical species thus results in
305 a non-linear, coupled set of equations that can only be solved numerically. However, OMEN-SED is designed for the coupling to Earth system models and, therefore, cannot afford a computationally expensive numerical solution. Yet, a computationally efficient analytical solution of Eq. (1) can be derived by 1) assuming steady state conditions (i.e. $\frac{\partial C_i}{\partial t} = 0$) and 2) reducing the vertical variability in parameters and reaction rate expressions by dividing the sediment column into a number
310 of functional biogeochemical zones (Fig. 1, compare e.g. Billen, 1982; Goloway and Bender, 1982; Tromp et al., 1995; Gypens et al., 2008, for similar solutions). More specifically, OMEN-SED divides the sediment column into: I) a bioturbated and II) a non-bioturbated zone defined by an imposed, constant bioturbation depth z_{bio} (Fig. 1). Furthermore, it resolves the dynamic redox stratification of marine sediments by dividing the sediment into 1) an oxic zone delineated by the
315 oxygen penetration depth z_{ox} ; 2) a denitrification (or nitrogenous) zone situated between z_{ox} and the nitrate penetration depth z_{NO_3} ; 3) a sulfate reduction zone situated between z_{NO_3} and the sulfate penetration depth z_{SO_4} ; and 4) a methanogenic zone situated below z_{SO_4} (Fig. 1). In each of these zones Eq. (1) is applied with depth invariant parameters. Yet, parameter values may differ across zones. The biogeochemical zones are linked by stating continuity in both concentrations and fluxes
320 at the dynamic, internal boundaries ($z_b \in \{z_{\text{bio}}, z_{\text{ox}}, z_{\text{NO}_3}, z_{\text{SO}_4}\}$, compare e.g. Billen, 1982; Ruardij and Van Raaphorst, 1995). These boundaries are dynamic because their depth varies in response to changing ocean boundary conditions and forcings (see Section 2.3.1 for details). Furthermore, the maximum bioturbation depth is not restricted to a specific biogeochemical zone, hence OMEN-SED allows bioturbation to occur in the anoxic zones of the sediment (here all zones $z > z_{\text{ox}}$ combined).
325 In addition, the formulation of the reaction term in Eq. (1) varies between zones and encapsulates

the most pertinent reaction processes within the respective zone (see Section 2.2), thus simplifying the mathematical description of the reaction network while retaining most of its biogeochemical complexity.

All consumption or production processes of dissolved species related to the degradation of organic matter are a function of the organic matter concentration and, because first-order decay is assumed in the kinetic expression, can be expressed as a series of exponential terms ($\sum_j \alpha_j \exp(-\beta_j z)$, see Eq. (2)). In addition, slow adsorption/desorption and mineral precipitation processes can be expressed as zero or first order (reversible) reaction (Q or $k \cdot (C_i - \tilde{C})$, in Eq. (2)). Fast adsorption is described as an instantaneous equilibrium reaction using a constant adsorption coefficient K_i . The reoxidation of reduced substances is accounted for implicitly by adding a (consumption/production) flux to the internal boundary conditions (see Sections 2.2.2, 2.2.3 and 2.2.4 **SA: make reference to the section where this is explained in detail**). This simplification has been used previously by Gypens et al. (2008) for nitrate and ammonium and can be justified as it has been shown that the reoxidation mainly occurs within a thin layer at the oxic/anoxic interface (Soetaert et al., 1996). The general reaction-transport equation of OMEN-SED is thus given by:

$$\frac{\partial C_i}{\partial t} = 0 = \frac{D_i}{1+K_i} \frac{\partial^2 C_i}{\partial z^2} - w \frac{\partial C_i}{\partial z} - \frac{1}{1+K_i} \left(\sum_j \alpha_j \exp(-\beta_j z) + \sum_l k_l \cdot C_i - \sum_m Q_m \right) \quad (2)$$

where $1/\beta_j$ can be interpreted as the length scale and α_j as the relative importance (or the magnitude at $z = 0$) of reaction j (Boudreau, 1997), k_l are generic first order reaction rate constants and Q_m are zeroth-order (or constant) reaction rates.

DH: Do you mean these sections? Not discussed in further details anywhere else

The analytical solution of Eq. (2) is of the general form:

$$C_i(z) = A \exp(az) + B \exp(bz) + \sum_j \frac{\alpha_j}{D\beta_j^2 - w\beta_j - \sum_l k_l} \cdot \exp(-\beta_j z) + \frac{\sum_m Q_m}{\sum_l k_l} \quad (3)$$

with

$$a = \frac{w - \sqrt{w^2 + 4 \cdot D \cdot \sum_l k_l}}{2 \cdot D}, \quad b = \frac{w + \sqrt{w^2 + 4 \cdot D \cdot \sum_l k_l}}{2 \cdot D} \quad (4)$$

where A and B are integration constants that can be determined by applying a set of internal boundary conditions (see Section 2.3).

Based on Eq. (2) and its analytical solution Eq. (3), OMEN-SED returns the fraction of particulate organic carbon (POC) buried in the sediment, f_{POC} , as well as the benthic uptake/return fluxes F_{C_i} of dissolved species C_i (in $\text{mol cm}^{-2} \text{ year}^{-1}$) in response to changing boundary conditions and

355 forcings:

$$f_{\text{POC}} = \frac{\text{POC}(z_\infty)}{\text{POC}(0)} \quad (5)$$

$$F_{C_i} = \phi(0) \left(D_i \frac{\partial C_i(z)}{\partial z} \Big|_{z=0} - w \cdot C_i(0) \right) \quad (6)$$

where w is the deposition rate, D_i is the diffusion coefficient and $\text{POC}(0)$, $\text{POC}(z_\infty)$, $C_i(0)$ denotes
360 the concentration of POC and dissolved species i at the SWI and at the lower sediment boundary,
respectively.

2.2 Conservation Equations and Analytical Solution

2.2.1 Organic matter or Particulate Organic Carbon (POC)

In marine sediments, particulate organic carbon (POC) is degraded by heterotrophic activity coupled to the sequential utilisation of terminal electron acceptors according to the free energy gain
365 of the half-reaction ($\text{O}_2 > \text{NO}_3^- > \text{MnO}_2 > \text{Fe(OH)}_3 > \text{SO}_4^{2-}$, e.g. Stumm and Morgan, 2012). Here, organic matter degradation is described via a multi G-model approach (Arndt et al., 2013, and references therein), dividing the bulk OM into a number i of discrete compound classes POC_i characterised by class-specific first-order degradation rate constants k_i . The conservation equation
370 for organic matter dynamics is thus given by:

$$\frac{\partial \text{POC}_i}{\partial t} = 0 = D_{\text{POC}_i} \frac{\partial^2 \text{POC}_i}{\partial z^2} - w \frac{\partial \text{POC}_i}{\partial z} - k_i \cdot \text{POC}_i \quad (7)$$

with $D_{\text{POC}_i} = D_{\text{bio}}$ for $z \leq z_{\text{bio}}$ and $D_{\text{POC}_i} = 0$ for $z > z_{\text{bio}}$. Integration of equations (7) yields the following general solutions:

375 I. Bioturbated zone ($z \leq z_{\text{bio}}$)

$$\text{POC}_i^I(z) = A_{1i} \cdot \exp(a_{1i}z) + B_{1i} \cdot \exp(b_{1i}z)$$

which using the boundary condition at $z = 0$ can be rewritten as:

$$380 \text{POC}_i^I(z) \stackrel{\text{BC1}}{=} A_{1i} \cdot [\exp(a_{1i}z) - \exp(b_{1i}z)] + \text{POC}_{0i} \cdot \exp(b_{1i}z) \quad (8)$$

II. Non-bioturbated zone ($z_{\text{bio}} < z$)

$$\text{POC}_i^{II}(z) = A_{2i} \cdot \exp(a_{2i}z) \quad (9)$$

where

$$385 a_{1i} = \frac{w - \sqrt{w^2 + 4 \cdot D_{\text{POC}_i} \cdot k_i}}{2 \cdot D_{\text{POC}_i}}, \quad b_{1i} = \frac{w + \sqrt{w^2 + 4 \cdot D_{\text{POC}_i} \cdot k_i}}{2 \cdot D_{\text{POC}_i}}, \quad a_{2i} = -\frac{k_i}{w} \quad (10)$$

Determining the integration constants ($A_{1,i}$, $B_{1,i}$, $A_{2,i}$) requires the definition of a set of boundary conditions (Table 2). For organic matter, OMEN-SED applies a known concentration/flux at the sediment-water interface and assumes continuity across the bottom of the bioturbated zone, z_{bio} .

See Section 2.3.1 for further details on how to find the analytical solution.

Table 2. OM Boundary conditions applied in OMEN-SED. For the boundaries we define: $z_{\text{bio}}^- := \lim_{h \rightarrow 0} (z_{\text{bio}} - h)$ and $z_{\text{bio}}^+ := \lim_{h \rightarrow 0} (z_{\text{bio}} + h)$.

Boundary	Condition	
$z = 0$	known concentration	1) $\text{POC}_i(0) = \text{POC}_{0i}$
$z = z_{\text{bio}}$	continuity	2) $\text{POC}_i(z_{\text{bio}}^-) = \text{POC}_i(z_{\text{bio}}^+)$ 3) $-D_{\text{bio}} \cdot \frac{\partial \text{POC}_i}{\partial z} \Big _{z_{\text{bio}}^-} = 0$

390 2.2.2 Oxygen

OMEN-SED explicitly accounts for oxygen consumption by the aerobic degradation of organic matter within the oxic zone, as well as the oxidation of reduced species (i.e. NH_4 , H_2S) produced in the anoxic zones of the sediment. In the oxic zone ($z < z_{\text{ox}}$), the aerobic degradation consumes oxygen with a fixed $\text{O}_2 : \text{C}$ ratio (O_2C , Tab. 10). A predefined fraction, γ_{NH_4} , of the ammonium produced 395 during the aerobic degradation of OM is nitrified to nitrate, consuming two moles of oxygen per mole of ammonium produced. In addition, OMEN-SED implicitly accounts for the oxygen consumption due to oxidation of reduced species (NH_4 , H_2S) produced below the oxic zone through the flux boundary condition at the dynamically calculated (see section 2.4.2 for details) oxygen penetration depth z_{ox} . All oxygen consumption processes can thus be formulated as a function of organic matter 400 degradation. The conservation equation for oxygen is given by: **SA: I'd show the POC substitution in the equations below:**

$$\frac{\partial \text{O}_2}{\partial t} = 0 = D_{\text{O}_2} \frac{\partial^2 \text{O}_2}{\partial z^2} - w \frac{\partial \text{O}_2}{\partial z} - \frac{1-\phi}{\phi} \sum_i k_i \cdot [\text{O}_2\text{C} + 2\gamma_{\text{NH}_4} \text{NC}_i] \cdot \text{POC}_i(z) \quad (11)$$

405 which, using Eq. (8) and (9) for the depth-distribution of $\text{POC}_i(z)$, can be written as:

DH: you mean the way I did it or in the solution?
I think it's easier to understand (also how to get the solution) if it's done in the ODE

I Bioturbated zone ($z \leq z_{\text{bio}}$)

$$\begin{aligned} \frac{\partial \text{O}_2^I}{\partial t} = 0 &\stackrel{8}{=} D_{\text{O}_2}^I \frac{\partial^2 \text{O}_2}{\partial z^2} - w \frac{\partial \text{O}_2}{\partial z} \\ &- \frac{1-\phi}{\phi} \sum_i k_i \cdot [\text{O}_2\text{C} + 2\gamma_{\text{NH}_4} \text{NC}_i] \cdot \left(A_{1i} \cdot [\exp(a_{1i}z) - \exp(b_{1i}z)] + \text{POC}_{0i} \cdot \exp(b_{1i}z) \right) \end{aligned}$$

II Non-bioturbated zone ($z_{\text{bio}} < z < z_{\text{ox}}$)

$$\frac{\partial \text{O}_2^{II}}{\partial t} = 0 \stackrel{9}{=} D_{\text{O}_2}^{II} \frac{\partial^2 \text{O}_2}{\partial z^2} - w \frac{\partial \text{O}_2}{\partial z} - \frac{1-\phi}{\phi} \sum_i k_i \cdot [\text{O}_2\text{C} + 2\gamma_{\text{NH}_4} \text{NC}_i] \cdot \left(A_{2i} \cdot \exp(a_{2i}z) \right)$$

410 where $D_{\text{O}_2}^I$ and $D_{\text{O}_2}^{II}$ denote the O_2 diffusion coefficient for the bioturbated and non-bioturbated zone, respectively. The term $\frac{1-\phi}{\phi}$ accounts for the volume conversion from solid to dissolved phase and NC_i is the nitrogen to carbon ratio in OM. Integration yields the following analytical solution for each zone:

I Bioturbated zone ($z \leq z_{\text{bio}}$):

$$O_2^I(z) = A_{O_2}^1 + B_{O_2}^1 \cdot \exp(b_{O_2}^1 z) + \sum_i \Phi_{1,i}^I \cdot \exp(a_{1i} z) + \sum_i \Phi_{1,i}^{II} \cdot \exp(b_{1i} z) + \sum_i \Phi_{1,i}^{III} \cdot \exp(b_{1i} z) \quad (12)$$

420

II Non-bioturbated zone ($z_{\text{bio}} < z < z_{\text{ox}}$)

$$O_2^{II}(z) = A_{O_2}^2 + B_{O_2}^2 \cdot \exp(b_{O_2}^2 z) + \sum_i \Phi_{i,2}^I \cdot \exp(a_{2i} z) \quad (13)$$

425 with

$$\begin{aligned} b_{O_2}^1 &= \frac{w}{D_{O_2}^I}, \quad b_{O_2}^2 = \frac{w}{D_{O_2}^{II}} \\ \Phi_{1,i}^I &= \frac{1-\phi}{\phi} \cdot \frac{k_i \cdot (O_2 C + 2\gamma_{NH_4} NC_i) \cdot A_{1i}}{D_{O_2}^I(-a_{1i})^2 - w \cdot (-a_{1i})}, \quad \Phi_{1,i}^{II} = -\frac{1-\phi}{\phi} \cdot \frac{k_i \cdot (O_2 C + 2\gamma_{NH_4} NC_i) \cdot A_{1i}}{D_{O_2}^I(-b_{1i})^2 - w \cdot (-b_{1i})} \\ \Phi_{1,i}^{III} &= \frac{1-\phi}{\phi} \cdot \frac{k_i \cdot (O_2 C + 2\gamma_{NH_4} NC_i) \cdot POC_{0i}}{D_{O_2}^I(-b_{1i})^2 - w \cdot (-b_{1i})} \\ \Phi_{i,2}^I &:= \frac{1-\phi}{\phi} \cdot \frac{k_i \cdot (O_2 C + 2\gamma_{NH_4} NC_i) \cdot A_{2i}}{D_{O_2}^{II}(-a_{2i})^2 - w \cdot (-a_{2i})} \end{aligned}$$

430

Determining the four integration constants ($A_{O_2}^1, B_{O_2}^1, A_{O_2}^2, B_{O_2}^2$, see Section 2.3 for details), as well as the *a priori* unknown oxygen penetration depth requires the definition of five boundary conditions (see Table 3). At the sediment-water interface, OMEN-SED applies a Dirichlet condition (i.e. known concentration) and assumes concentration and flux continuity across the bottom of the bioturbated zone, z_{bio} . The oxygen penetration depth z_{ox} marks the lower boundary and is dynamically calculated as the depth at which $O_2(z) = 0$. Therefore, OMEN-SED applies a Dirichlet boundary condition $O_2(z_{\text{ox}}) = 0$. In addition, a flux boundary is applied that implicitly accounts for the oxygen consumption by the partial oxidation of NH_4 and H_2S diffusing into the oxic zone from below (BC 4.2, Table 3). It is assumed that respective fractions (γ_{NH_4} and γ_{H_2S}) are directly reoxidised at the oxic/anoxic interface and the remaining fraction escapes reoxidation. OMEN-SED iteratively solves for z_{ox} by first testing if there is oxygen left at z_∞ (i.e. $O_2(z_\infty) > 0$) and, otherwise, by finding the root for the flux boundary condition 4.2 (Table 3). If $z_{\text{ox}} = z_\infty$, a zero diffusive flux boundary condition is applied as lower boundary condition.

2.2.3 Nitrate and Ammonium

445 Nitrogen dynamics in OMEN-SED are controlled by the metabolic production of ammonium, nitrification, denitrification as well as ammonium adsorption. Ammonium is produced by organic matter degradation in both the oxic and anoxic zones, while denitrification consumes nitrate in the denitrification zone with a fixed $NO_3^- : C$ ratio (NO_3^-C , Tab. 10) **SA: need explanation**. The adsorption of ammonium to sediment particles is formulated as an equilibrium process with constant equilibrium adsorption coefficient K_{NH_4} , thus assuming that the adsorption is fast compared with the characteristic time scales of transport processes (Wang and Van Cappellen, 1996). In addition, a defined

DH: Edited explanation of finding z_{ox}

DH: explanation sufficient?

Table 3. Boundary conditions for oxygen. For the boundaries we define: $z_{\text{bio}}^- := \lim_{h \rightarrow 0} (z_{\text{bio}} - h)$ and $z_{\text{bio}}^+ := \lim_{h \rightarrow 0} (z_{\text{bio}} + h)$.

Boundary	Condition	
$z = 0$	known concentration	1) $O_2(0) = O_{20}$
$z = z_{\text{bio}}$	continuity	2) $O_2(z_{\text{bio}}^-) = O_2(z_{\text{bio}}^+)$
$z = z_{\text{ox}}$	O_2 consumption ($z_{\text{ox}} = z_\infty$)	3) $-(D_{O_2,0} + D_{\text{bio}}) \cdot \frac{\partial O_2}{\partial z} \Big _{z_{\text{bio}}^-} = -D_{O_2,0} \cdot \frac{\partial O_2}{\partial z} \Big _{z_{\text{bio}}^+}$ 4) IF ($O_2(z_\infty) > 0$) 4.1) $\frac{\partial O_2}{\partial z} \Big _{z_{\text{ox}}} = 0$ ELSE
	$(z_{\text{ox}} < z_\infty)$ with	4.2) $O_2(z_{\text{ox}}) = 0 \quad \text{and} \quad -D_{O_2} \cdot \frac{\partial O_2}{\partial z} \Big _{z_{\text{ox}}} = F_{\text{red}}(z_{\text{ox}})$ $F_{\text{red}}(z_{\text{ox}}) = \frac{1-\phi}{\phi} \cdot \int_{\tilde{z}_{\text{NO}_3}}^{\infty} \sum_i (2\gamma_{\text{NH}_4} \text{NC}_i + 2\gamma_{\text{H}_2\text{S}} \text{SO}_4 \text{C}) k_i \text{POC}_i dz$

Note: $\tilde{z}_{\text{NO}_3} = z_{\text{ox}}$ as upper boundary here, as z_{NO_3} is not known at this point.

fraction, γ_{NH_4} , of metabolically produced ammonium is directly nitrified to nitrate in the oxic zone, while the nitrification of upward diffusing ammonium produced in the sulfidic and methanic zones is implicitly accounted for in the boundary conditions. The conservation equations for ammonium

455 and nitrate are thus given by:

1. Oxic zone ($z \leq z_{\text{ox}}$)

$$\frac{\partial \text{NO}_3^I}{\partial t} = 0 = D_{\text{NO}_3} \frac{\partial^2 \text{NO}_3^I}{\partial z^2} - w \frac{\partial \text{NO}_3^I}{\partial z} + \gamma_{\text{NH}_4} \frac{1-\phi}{\phi} \cdot \sum_i \text{NC}_i \cdot k_i \cdot \text{POC}_i(z) \quad (14)$$

$$\frac{\partial \text{NH}_4^I}{\partial t} = 0 = \frac{D_{\text{NH}_4}}{1 + K_{\text{NH}_4}} \frac{\partial^2 \text{NH}_4^I}{\partial z^2} - w \frac{\partial \text{NH}_4^I}{\partial z} + \frac{1 - \gamma_{\text{NH}_4}}{1 + K_{\text{NH}_4}} \cdot \frac{1-\phi}{\phi} \cdot \sum_i \text{NC}_i \cdot k_i \cdot \text{POC}_i(z) \quad (15)$$

460

2. Denitrification (or nitrogenous) zone ($z_{\text{ox}} < z \leq z_{\text{NO}_3}$)

$$\frac{\partial \text{NO}_3^{II}}{\partial t} = 0 = D_{\text{NO}_3} \frac{\partial^2 \text{NO}_3^{II}}{\partial z^2} - w \frac{\partial \text{NO}_3^{II}}{\partial z} - \frac{1-\phi}{\phi} \text{NO}_3 \text{C} \cdot \sum_i k_i \cdot \text{POC}_i(z) \quad (16)$$

$$465 \quad \frac{\partial \text{NH}_4^{II}}{\partial t} = 0 = \frac{D_{\text{NH}_4}}{1 + K_{\text{NH}_4}} \frac{\partial^2 \text{NH}_4^{II}}{\partial z^2} - w \frac{\partial \text{NH}_4^{II}}{\partial z} \quad (17)$$

3. Sulfidic and methanic zone ($z_{\text{NO}_3} < z \leq z_\infty$)

$$\frac{\partial \text{NH}_4^{III}}{\partial t} = 0 = \frac{D_{\text{NH}_4}}{1 + K_{\text{NH}_4}} \frac{\partial^2 \text{NH}_4^{III}}{\partial z^2} - w \frac{\partial \text{NH}_4^{III}}{\partial z} + \frac{1}{1 + K_{\text{NH}_4}} \cdot \frac{1-\phi}{\phi} \cdot \sum_i \text{NC}_i \cdot k_i \cdot \text{POC}_i(z) \quad (18)$$

where D_{NO_3} and D_{NH_4} denote the diffusion coefficients for NO_3 and NH_4 which depend on 470 the bioturbation status of the respective geochemical zone (compare Section 2.3.1). Integration of

Table 4. Boundary conditions for nitrate and ammonium. For the boundaries we define: $z_-^- := \lim_{h \rightarrow 0} (z_- - h)$ and $z_-^+ := \lim_{h \rightarrow 0} (z_- + h)$.

Boundary	Condition	
$z = 0$	known concentration	1) $\text{NO}_3(0) = \text{NO}_{30}$
$z = z_{\text{bio}}$	continuity	2) $\text{NO}_3(z_{\text{bio}}^-) = \text{NO}_3(z_{\text{bio}}^+)$
$z = z_{\text{ox}}$	continuity	3) $-(D_{\text{NO}_3,0} + D_{\text{bio}}) \cdot \frac{\partial \text{NO}_3}{\partial z} _{z_{\text{bio}}^-} = -D_{\text{NO}_3,0} \cdot \frac{\partial \text{NO}_3}{\partial z} _{z_{\text{bio}}^+}$
	where:	4) $\text{NO}_3(z_{\text{ox}}^-) = \text{NO}_3(z_{\text{ox}}^+)$
$z = z_{\text{NO}_3}$	NO_3 consumption ($z_{\text{NO}_3} = z_\infty$)	5) $-D_{\text{NO}_3} \cdot \frac{\partial \text{NO}_3}{\partial z} _{z_{\text{ox}}^-} + \gamma_{\text{NH}_4} \cdot F_{\text{NH}_4}(z_{\text{ox}}) = -D_{\text{NO}_3} \cdot \frac{\partial \text{NO}_3}{\partial z} _{z_{\text{ox}}^+}$ $F_{\text{NH}_4}(z_{\text{ox}}) = \frac{1}{1+K_{\text{NH}_4}} \cdot \frac{1-\phi}{\phi} \cdot \int_{z_{\text{NO}_3}}^\infty \sum_i \text{NC}_i \cdot k_i \cdot \text{POC}_i dz$
		6) IF ($\text{NO}_3(z_\infty) > 0$)
		6.1) $\frac{\partial \text{NO}_3}{\partial z} _{z_{\text{NO}_3}} = 0$
		ELSE
		6.2) $\text{NO}_3(z_{\text{NO}_3}) = 0 \quad \text{and} \quad \frac{\partial \text{NO}_3}{\partial z} _{z_{\text{NO}_3}} = 0$
$z = 0$	known concentration	1) $\text{NH}_4(0) = \text{NH}_{40}$
$z = z_{\text{bio}}$	continuity	2) $\text{NH}_4(z_{\text{bio}}^-) = \text{NH}_4(z_{\text{bio}}^+)$
$z = z_{\text{ox}}$	continuity	3) $-\frac{D_{\text{NH}_4,0} + D_{\text{bio}}}{1+K_{\text{NH}_4}} \cdot \frac{\partial \text{NH}_4}{\partial z} _{z_{\text{bio}}^-} = -\frac{D_{\text{NH}_4,0}}{1+K_{\text{NH}_4}} \cdot \frac{\partial \text{NH}_4}{\partial z} _{z_{\text{bio}}^+}$
	where:	4) $\text{NH}_4(z_{\text{ox}}^-) = \text{NH}_4(z_{\text{ox}}^+)$
$z = z_{\text{NO}_3}$	continuity flux	5) $-\frac{D_{\text{NH}_4}}{1+K_{\text{NH}_4}} \cdot \frac{\partial \text{NH}_4}{\partial z} _{z_{\text{ox}}^-} - \gamma_{\text{NH}_4} \cdot F_{\text{NH}_4}(z_{\text{ox}}) = -\frac{D_{\text{NH}_4}}{1+K_{\text{NH}_4}} \cdot \frac{\partial \text{NH}_4}{\partial z} _{z_{\text{ox}}^+}$ $F_{\text{NH}_4}(z_{\text{ox}}) = \frac{1}{1+K_{\text{NH}_4}} \cdot \frac{1-\phi}{\phi} \cdot \int_{z_{\text{NO}_3}}^\infty \sum_i \text{NC}_i \cdot k_i \cdot \text{POC}_i dz$
$z = z_\infty$	zero NH_4 flux	6) $\text{NH}_4(z_{\text{NO}_3}^-) = \text{NH}_4(z_{\text{NO}_3}^+)$
		7) $-\frac{D_{\text{NH}_4}}{1+K_{\text{NH}_4}} \cdot \frac{\partial \text{NH}_4}{\partial z} _{z_{\text{NO}_3}^-} = -\frac{D_{\text{NH}_4}}{1+K_{\text{NH}_4}} \cdot \frac{\partial \text{NH}_4}{\partial z} _{z_{\text{NO}_3}^+}$
		8) $\frac{\partial \text{NH}_4}{\partial z} _{z_\infty} = 0$

Eq. (14) - (18) yields the analytical solutions, which are not further developed here but follow the procedure outlined in Section 2.2.2 for oxygen (also see Section 2.3.1 for more details on how to find the analytical solution). Table 4 summarises the boundary conditions applied in OMEN-SED to solve Eq. (14) - (18) and to find the *a priori* unknown nitrate penetration depth, z_{NO_3} . The model assumes known bottom water concentrations for both NO_3 and NH_4 , the complete consumption of nitrate at the nitrate penetration depth (in case $z_{\text{NO}_3} < z_\infty$) and no change in ammonium flux at z_∞ . In addition, concentration and diffusive flux continuity across z_{bio} and z_{ox} is considered for NO_3 and NH_4 . Furthermore, the reoxidation of upward-diffusing reduced ammonium is accounted for in the oxic-anoxic boundary condition for nitrate and ammonium. OMEN-SED iteratively solves for z_{NO_3} by first testing if there is nitrate left at z_∞ (i.e. $\text{NO}_3(z_\infty) > 0$) and, otherwise, by finding the root for the flux boundary condition 6.2 (Table 4).

2.2.4 Sulfate and Sulfide

Below the denitrification zone ($z > z_{\text{NO}_3}$), organic matter degradation is coupled to sulfate reduction, consuming sulfate and producing hydrogen sulfide with a fixed $\text{SO}_4 : \text{C}$ ratio (SO_4C , Tab. 10).

485 In addition, the anaerobic oxidation of upward diffusing methane (AOM) produced below the sulfate penetration and the associated consumption of sulfate and production of sulfide; as well as the production of sulfate and consumption of sulfide through sulfide oxidation are implicitly accounted for through the boundary conditions (Table 5). The conservation equations for sulfate and sulfide are thus given by:

490

1. Oxic and nitrogenous zone ($z \leq z_{\text{NO}_3}$)

$$\frac{\partial \text{SO}_4^I}{\partial t} = 0 = D_{\text{SO}_4} \frac{\partial^2 \text{SO}_4^I}{\partial z^2} - w \frac{\partial \text{SO}_4^I}{\partial z} \quad (19)$$

495

$$\frac{\partial \text{H}_2\text{S}^I}{\partial t} = 0 = D_{\text{H}_2\text{S}} \frac{\partial^2 \text{H}_2\text{S}^I}{\partial z^2} - w \frac{\partial \text{H}_2\text{S}^I}{\partial z} \quad (20)$$

2. Sulfidic zone ($z_{\text{NO}_3} < z \leq z_{\text{SO}_4}$)

$$\frac{\partial \text{SO}_4^{II}}{\partial t} = 0 = D_{\text{SO}_4} \frac{\partial^2 \text{SO}_4^{II}}{\partial z^2} - w \frac{\partial \text{SO}_4^{II}}{\partial z} - \frac{1-\phi}{\phi} \cdot \sum_i \text{SO}_4\text{C} \cdot k_i \cdot \text{POC}_i(z) \quad (21)$$

$$\frac{\partial \text{H}_2\text{S}^{II}}{\partial t} = 0 = D_{\text{H}_2\text{S}} \frac{\partial^2 \text{H}_2\text{S}^{II}}{\partial z^2} - w \frac{\partial \text{H}_2\text{S}^{II}}{\partial z} + \frac{1-\phi}{\phi} \cdot \sum_i \text{SO}_4\text{C} \cdot k_i \cdot \text{POC}_i(z) \quad (22)$$

500 3. Methanic zone ($z_{\text{SO}_4} < z \leq z_\infty$)

$$\frac{\partial \text{H}_2\text{S}^{III}}{\partial t} = 0 = D_{\text{H}_2\text{S}} \frac{\partial^2 \text{H}_2\text{S}^{III}}{\partial z^2} - w \frac{\partial \text{H}_2\text{S}^{III}}{\partial z} \quad (23)$$

where D_{SO_4} and $D_{\text{H}_2\text{S}}$ denote the diffusion coefficients for SO_4 and H_2S which depend on the bioturbation status of the respective geochemical zone (compare Section 2.3.1). Integration of Eq. 505 (19) - (23) yields the analytical solution and Table 5 summarises the boundary conditions applied. OMEN-SED assumes known concentrations at the sediment-water interface and continuity across the bioturbation depth and the nitrate penetration depth. The reoxidation of reduced H_2S to SO_4 is accounted for implicitly via the oxic-anoxic boundary condition for both species, while reduction of SO_4 and the associated production of H_2S via AOM is accounted for through the respective 510 boundary conditions at z_{SO_4} . In case $z_{\text{SO}_4} < z_\infty$, OMEN-SED assumes zero sulfate concentration at z_{SO_4} and its diffusive flux must equal the amount of methane produced below (with a methane to carbon ratio of MC); or, in case $z_{\text{SO}_4} = z_\infty$, a zero diffusive flux condition for sulfate is considered. OMEN-SED iteratively solves for z_{SO_4} by first testing if there is sulfate left at z_∞ (i.e. $\text{SO}_4(z_\infty) > 515$ 0) and, otherwise, by finding the root for the flux boundary condition 8.2 (Table 5). At the lower boundary z_∞ zero diffusive flux of H_2S is considered.

Table 5. Boundary conditions for sulfate and sulfide. For the boundaries we define: $z_-^- := \lim_{h \rightarrow 0} (z_- - h)$ and $z_-^+ := \lim_{h \rightarrow 0} (z_- + h)$.

Boundary	Condition	
$z = 0$	known concentration	1) $\text{SO}_4(0) = \text{SO}_4$
$z = z_{\text{bio}}$	continuity	2) $\text{SO}_4(z_{\text{bio}}^-) = \text{SO}_4(z_{\text{bio}}^+)$
	flux	3) $-(D_{\text{SO}_4,0} + D_{\text{bio}}) \cdot \frac{\partial \text{SO}_4}{\partial z} _{z_{\text{bio}}^-} = -D_{\text{SO}_4,0} \cdot \frac{\partial \text{SO}_4}{\partial z} _{z_{\text{bio}}^+}$
$z = z_{\text{ox}}$	continuity	4) $\text{SO}_4(z_{\text{ox}}^-) = \text{SO}_4(z_{\text{ox}}^+)$
	flux	5) $-D_{\text{SO}_4} \cdot \frac{\partial \text{SO}_4}{\partial z} _{z_{\text{ox}}^-} + \gamma_{\text{H}_2\text{S}} \cdot F_{\text{H}_2\text{S}}(z_{\text{ox}}) = -D_{\text{SO}_4} \cdot \frac{\partial \text{SO}_4}{\partial z} _{z_{\text{ox}}^+}$
	where:	$F_{\text{H}_2\text{S}}(z_{\text{ox}}) = \frac{1-\phi}{\phi} \cdot \left(\int_{z_{\text{NO}_3}}^{\text{SO}_4} \sum_i \text{SO}_4 \cdot k_i \cdot \text{POC}_i dz + \gamma_{\text{CH}_4} \cdot \int_{z_{\text{SO}_4}}^{\infty} \sum_i \text{MC} \cdot k_i \cdot \text{POC}_i dz \right)$
$z = z_{\text{NO}_3}$	continuity	6) $\text{SO}_4(z_{\text{NO}_3}^-) = \text{SO}_4(z_{\text{NO}_3}^+)$
	flux	7) $-D_{\text{SO}_4} \cdot \frac{\partial \text{SO}_4}{\partial z} _{z_{\text{NO}_3}^-} = -D_{\text{SO}_4} \cdot \frac{\partial \text{SO}_4}{\partial z} _{z_{\text{NO}_3}^+}$
$z = z_{\text{SO}_4}$	SO ₄ consumption ($z_{\text{SO}_4} = z_\infty$)	8) IF ($\text{SO}_4(z_\infty) > 0$) 8.1) $\frac{\partial \text{SO}_4}{\partial z} _{z_{\text{SO}_4}} = 0$ ELSE
	($z_{\text{SO}_4} < z_\infty$) with	8.2) $\text{SO}_4(z_{\text{SO}_4}) = 0 \quad \text{and} \quad -D_{\text{SO}_4} \cdot \frac{\partial \text{SO}_4}{\partial z} _{z_{\text{SO}_4}} = \gamma_{\text{CH}_4} \cdot F_{\text{CH}_4}(z_{\text{SO}_4})$ $F_{\text{CH}_4}(z_{\text{SO}_4}) = \frac{1-\phi}{\phi} \cdot \int_{z_{\text{SO}_4}}^{\infty} \sum_i \text{MC} \cdot k_i \cdot \text{POC}_i dz$
$z = 0$	known concentration	1) $\text{H}_2\text{S}(0) = \text{H}_2\text{S}_0$
$z = z_{\text{bio}}$	continuity	2) $\text{H}_2\text{S}(z_{\text{bio}}^-) = \text{H}_2\text{S}(z_{\text{bio}}^+)$
	flux	3) $-(D_{\text{H}_2\text{S},0} + D_{\text{bio}}) \cdot \frac{\partial \text{H}_2\text{S}}{\partial z} _{z_{\text{bio}}^-} = -D_{\text{H}_2\text{S},0} \cdot \frac{\partial \text{H}_2\text{S}}{\partial z} _{z_{\text{bio}}^+}$
$z = z_{\text{ox}}$	continuity	4) $\text{H}_2\text{S}(z_{\text{ox}}^-) = \text{H}_2\text{S}(z_{\text{ox}}^+)$
	flux	5) $-D_{\text{H}_2\text{S}} \cdot \frac{\partial \text{H}_2\text{S}}{\partial z} _{z_{\text{ox}}^-} - \gamma_{\text{H}_2\text{S}} F_{\text{H}_2\text{S}}(z_{\text{ox}}) = -D_{\text{H}_2\text{S}} \cdot \frac{\partial \text{H}_2\text{S}}{\partial z} _{z_{\text{ox}}^+}$
	where:	$F_{\text{H}_2\text{S}}(z_{\text{ox}}) = \frac{1-\phi}{\phi} \cdot \left(\int_{z_{\text{NO}_3}}^{\text{SO}_4} \sum_i \text{SO}_4 \cdot k_i \cdot \text{POC}_i dz + \gamma_{\text{CH}_4} \cdot \int_{z_{\text{SO}_4}}^{\infty} \sum_i \text{MC} \cdot k_i \cdot \text{POC}_i dz \right)$
$z = z_{\text{NO}_3}$	continuity	6) $\text{H}_2\text{S}(z_{\text{NO}_3}^-) = \text{H}_2\text{S}(z_{\text{NO}_3}^+)$
	flux	7) $-D_{\text{H}_2\text{S}} \cdot \frac{\partial \text{H}_2\text{S}}{\partial z} _{z_{\text{NO}_3}^-} = -D_{\text{H}_2\text{S}} \cdot \frac{\partial \text{H}_2\text{S}}{\partial z} _{z_{\text{NO}_3}^+}$
$z = z_{\text{SO}_4}$	continuity flux (with AOM) where:	8) $\text{H}_2\text{S}(z_{\text{SO}_4}^-) = \text{H}_2\text{S}(z_{\text{SO}_4}^+)$ 9) $-D_{\text{H}_2\text{S}} \cdot \frac{\partial \text{H}_2\text{S}}{\partial z} _{z_{\text{SO}_4}^-} + \gamma_{\text{CH}_4} \cdot F_{\text{CH}_4}(z_{\text{SO}_4}) = -D_{\text{H}_2\text{S}} \cdot \frac{\partial \text{H}_2\text{S}}{\partial z} _{z_{\text{SO}_4}^+}$ $F_{\text{CH}_4}(z_{\text{SO}_4}) = \frac{1-\phi}{\phi} \cdot \int_{z_{\text{SO}_4}}^{\infty} \sum_i \text{MC} \cdot k_i \cdot \text{POC}_i dz$
$z = z_\infty$	zero H ₂ S flux	10) $\frac{\partial \text{H}_2\text{S}}{\partial z} _{z_\infty} = 0$

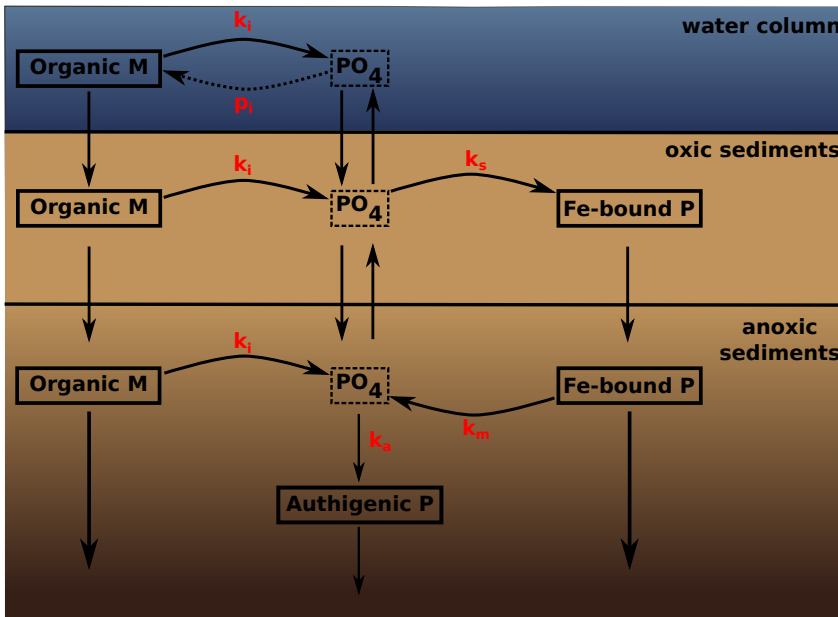


Figure 2. A schematic of the sedimentary P cycle in OMEN-SED. Red numbers represent kinetic rate constants for phosphorus dynamics (compare Table 10; p_i represents uptake rate of PO_4 via primary production in shallow environments). Adapted from Slomp et al. (1996).

2.2.5 Phosphate

The biogeochemical description of phosphorus (P) dynamics builds on the work of Slomp et al. (1996) and accounts for phosphorus recycling through organic matter degradation, adsorption onto sediments and iron(III) hydroxides (Fe-bound P), as well as carbonate fluorapatite (CFA or authigenic P) formation (see Figure 2 for a schematic overview of the sedimentary P cycle). In the oxic zone of the sediment, PO_4 liberated through organic matter degradation can adsorb to iron(III) hydroxides forming Fe-bound P (or FeP, Slomp et al., 1998). Below the oxic zone, PO_4 is not only produced via organic matter degradation but can also be released from the Fe-bound P pool due to the reduction of iron(III) hydroxides under anoxic conditions. Furthermore, in these zones phosphate concentrations build up and pore waters can thus become supersaturated with respect to carbonate fluorapatite, thus triggering the authigenic formation of CFA (Van Cappellen and Berner, 1988). Phosphorus bound in these authigenic minerals represents a permanent sink for reactive phosphorus (Slomp et al., 1996). As for ammonium, the adsorption of P to the sediment matrix is treated as an equilibrium processes, parameterised with dimensionless adsorption coefficients for the oxic and anoxic zone, respectively ($K_{\text{PO}_4}^{\text{ox}}$, $K_{\text{PO}_4}^{\text{anox}}$ Slomp et al., 1998). The sorption and desorption of P to iron(III) hydroxides as well as the authigenic fluorapatite formation are described as first-order reactions with rate constants k_s , k_m and k_a , respectively (Table 10). The rate of the respective process is

calculated as the product of the rate constant and the difference between the current concentration (of PO₄ and FeP) and an equilibrium or asymptotic concentration Slomp et al. (1996). The asymptotic
535 Fe-bound P concentration is FeP[∞] and the equilibrium concentration for P sorption and authigenic fluorapatite formation are PO₄^s and PO₄^a, respectively (Table 10). The last term in Eq. (24) and (25) represents sorption of PO₄ to FeP in the oxic zone, the last term in Eq. (26) and (27) is the release of PO₄ from the FeP pool and the 4th term in Eq. (27) represents the permanent loss of PO₄ to authigenic fluorapatite formation. The conservation equations for phosphate and Fe-bound P are
540 thus given by:

1. Oxic zone ($z \leq z_{\text{ox}}$)

$$\frac{\partial \text{PO}_4^I}{\partial t} = \frac{D_{\text{PO}_4}}{1 + K_{\text{PO}_4}^{\text{ox}}} \frac{\partial^2 \text{PO}_4^I}{\partial z^2} - w \frac{\partial \text{PO}_4^I}{\partial z} + \frac{1-\phi}{\phi} \frac{1}{1 + K_{\text{PO}_4}^{\text{ox}}} \sum_i (\text{PC}_i \cdot k_i \cdot \text{POC}_i(z)) - \frac{k_s}{1 + K_{\text{PO}_4}^{\text{ox}}} (\text{PO}_4^I - \text{PO}_4^s) \quad (24)$$

$$545 \frac{\partial \text{FeP}^I}{\partial t} = D_{\text{FeP}} \frac{\partial^2 \text{FeP}^I}{\partial z^2} - w \frac{\partial \text{FeP}^I}{\partial z} + \frac{\phi}{1-\phi} k_s (\text{PO}_4^I - \text{PO}_4^s) \quad (25)$$

2. Anoxic zones ($z_{\text{ox}} < z \leq z_{\infty}$)

$$\frac{\partial \text{FeP}^{II}}{\partial t} = D_{\text{FeP}} \frac{\partial^2 \text{FeP}^{II}}{\partial z^2} - w \frac{\partial \text{FeP}^{II}}{\partial z} - k_m (\text{FeP}^{II} - \text{FeP}^{\infty}) \quad (26)$$

$$550 \frac{\partial \text{PO}_4^{II}}{\partial t} = \frac{D_{\text{PO}_4}}{1 + K_{\text{PO}_4}^{\text{anox}}} \frac{\partial^2 \text{PO}_4^{II}}{\partial z^2} - w \frac{\partial \text{PO}_4^{II}}{\partial z} + \frac{1-\phi}{\phi} \frac{1}{1 + K_{\text{PO}_4}^{\text{anox}}} \sum_i (\text{PC}_i \cdot k_i \cdot \text{POC}_i(z)) - \frac{k_a}{1 + K_{\text{PO}_4}^{\text{anox}}} (\text{PO}_4^{II} - \text{PO}_4^a) + \frac{(1-\phi)}{\phi} \frac{k_m}{1 + K_{\text{PO}_4}^{\text{anox}}} (\text{FeP}^{II} - \text{FeP}^{\infty}) \quad (27)$$

where D_{PO_4} denotes the diffusion coefficient for PO₄ which depends on the bioturbation status of the respective geochemical zone and $D_{\text{FeP}} = D_{\text{bio}}$ for $z \leq z_{\text{bio}}$ and $D_{\text{FeP}} = 0$ for $z > z_{\text{bio}}$ (compare Section 2.3.1). Integration of Eq. (24) - (27) yields the analytical solution and Table 6 summarises
555 the boundary conditions applied in OMEN-SED. The model assumes known bottom water concentrations and equal concentrations and diffusive fluxes at z_{bio} and z_{ox} for both species. Additionally OMEN-SED considers no change in phosphate flux and an asymptotic Fe-bound P concentration at z_{∞} .

2.2.6 Dissolved Inorganic Carbon (DIC)

560 OMEN-SED accounts for the production of dissolved inorganic carbon (DIC) through organic matter degradation, as well as methane oxidation. Organic matter degradation produces dissolved inorganic carbon with a stoichiometric DIC : C ratio of 1:2 in the methanic zone and 1:1 in the rest of the sediment column (DIC^{CII} and DIC^{CI} respectively). DIC production through methane oxidation is implicitly taken into account through the boundary condition at z_{SO_4} . A mechanistic description of
565 DIC production from CaCO₃ dissolution would lead to significant mathematical problems and is

DH: I think what I wrote before also applies: a asymptotic Fe-bound P concentration at z_{∞} is assumed! (but is the same as “no flux condition” as it is now?’)

Table 6. Boundary conditions for phosphate and Fe-bound P (FeP). For the boundaries we define: $z_-^- := \lim_{h \rightarrow 0} (z_- - h)$ and $z_-^+ := \lim_{h \rightarrow 0} (z_- + h)$.

Boundary	Condition	
$z = 0$	known concentration	1) $\text{PO}_4(0) = \text{PO}_{40}$
$z = z_{\text{bio}}$	continuity	2) $\text{PO}_4(z_{\text{bio}}^-) = \text{PO}_4(z_{\text{bio}}^+)$
	flux	3) $(D_{\text{PO}_4,0} + D_{\text{bio}}) \cdot \frac{\partial \text{PO}_4}{\partial z} _{z_{\text{bio}}^-} = D_{\text{PO}_4,0} \cdot \frac{\partial \text{PO}_4}{\partial z} _{z_{\text{bio}}^+}$
$z = z_{\text{ox}}$	continuity	4) $\text{PO}_4(z_{\text{ox}}^-) = \text{PO}_4(z_{\text{ox}}^+)$
	flux	5) $-\frac{D_{\text{PO}_4}}{1 + K_{\text{PO}_4}^{\text{ox}}} \cdot \frac{\partial \text{PO}_4}{\partial z} _{z_{\text{ox}}^-} = -\frac{D_{\text{PO}_4}}{1 + K_{\text{PO}_4}^{\text{anox}}} \cdot \frac{\partial \text{PO}_4}{\partial z} _{z_{\text{ox}}^+}$
$z = z_\infty$	flux	10) $\frac{\partial \text{PO}_4}{\partial z} _{z_\infty} = 0$
$z = 0$	known concentration	1) $\text{FeP}(0) = \text{FeP}_0$
$z = z_{\text{bio}}$	continuity	2) $\text{FeP}(z_{\text{bio}}^-) = \text{FeP}(z_{\text{bio}}^+)$
	flux	3) $\frac{\partial \text{FeP}}{\partial z} _{z_{\text{bio}}^-} = \frac{\partial \text{FeP}}{\partial z} _{z_{\text{bio}}^+}$
$z = z_{\text{ox}}$	continuity	4) $\text{FeP}(z_{\text{ox}}^-) = \text{FeP}(z_{\text{ox}}^+)$
	flux	5) $\frac{\partial \text{FeP}}{\partial z} _{z_{\text{ox}}^-} = \frac{\partial \text{FeP}}{\partial z} _{z_{\text{ox}}^+}$
$z = z_\infty$	asymptotic concentration	10) $\text{FeP}(z_\infty) = \text{FeP}_\infty$

therefore not included in the current version of OMEN-SED. The conservation equations for DIC are thus given by:

1. Oxic, nitrogenous and sulfidic zone ($z \leq z_{\text{SO}_4}$)

$$570 \quad \frac{\partial \text{DIC}^I}{\partial t} = 0 = D_{\text{DIC}} \frac{\partial^2 \text{DIC}^I}{\partial z^2} - w \frac{\partial \text{DIC}^I}{\partial z} + \frac{1 - \phi}{\phi} \cdot \sum_i \text{DICC}^I \cdot k_i \cdot \text{POC}_i(z) \quad (28)$$

2. Methanic zone ($z_{\text{SO}_4} < z \leq z_\infty$)

$$\frac{\partial \text{DIC}^{II}}{\partial t} = 0 = D_{\text{DIC}} \frac{\partial^2 \text{DIC}^{II}}{\partial z^2} - w \frac{\partial \text{DIC}^{II}}{\partial z} + \frac{1 - \phi}{\phi} \cdot \sum_i \text{DICC}^{II} \cdot k_i \cdot \text{POC}_i(z) \quad (29)$$

575 where D_{DIC} denotes the diffusion coefficient for DIC which depends on the bioturbation status of the respective geochemical zone. Integration of Eq. (28) and (29) yields the analytical solution and Table 7 summarises the boundary conditions applied in OMEN-SED. A Dirichlet condition is applied at the sediment-water interface. In addition, the model assumes a zero diffusive flux through the lower boundary z_∞ and continuity across the bottom of the bioturbated zone, as well as the 580 sulfate penetration depth. An additional flux boundary condition at z_{SO_4} , implicitly accounts for DIC production through anaerobic oxidation of methane (Table 7 Eq. 5).

2.2.7 Alkalinity

Organic matter degradation and secondary redox reactions exert a complex influence on alkalinity (e.g. Jourabchi et al., 2005; Wolf-Gladrow et al., 2007; Krumins et al., 2013). To model alkalinity, 885 OMEN-SED divides the sediment column into four geochemical zones, where different equations

SA: TODO: again need to mention carboantes

Table 7. Boundary conditions for DIC. For the boundaries we define: $z_-^- := \lim_{h \rightarrow 0} (z_- - h)$ and $z_-^+ := \lim_{h \rightarrow 0} (z_- + h)$.

Boundary	Condition	
$z = 0$	known concentration	1) $\text{DIC}(0) = \text{DIC}_0$
$z = z_{\text{bio}}$	continuity	2) $\text{DIC}(z_{\text{bio}}^-) = \text{DIC}(z_{\text{bio}}^+)$
	flux	3) $-(D_{\text{DIC},0} + D_{\text{bio}}) \cdot \frac{\partial \text{DIC}}{\partial z} _{z_{\text{bio}}^-} = -D_{\text{DIC},0} \cdot \frac{\partial \text{DIC}}{\partial z} _{z_{\text{bio}}^+}$
$z = z_{\text{SO}_4}$	continuity	4) $\text{DIC}(z_{\text{SO}_4}^-) = \text{DIC}(z_{\text{SO}_4}^+)$
	flux (with AOM)	5) $-D_{\text{DIC}} \cdot \frac{\partial \text{DIC}}{\partial z} _{z_{\text{SO}_4}^-} + \gamma_{\text{CH}_4} \cdot F_{\text{CH}_4}(z_{\text{SO}_4}) = -D_{\text{DIC}} \cdot \frac{\partial \text{DIC}}{\partial z} _{z_{\text{SO}_4}^+}$
	where:	$F_{\text{CH}_4}(z_{\text{SO}_4}) = \frac{1-\phi}{\phi} \cdot \int_{z_{\text{SO}_4}}^{\infty} \sum_i \text{MC} \cdot k_i \cdot \text{POC}_i dz$
$z = z_\infty$	zero DIC flux	6) $\frac{\partial \text{DIC}}{\partial z} _{z_\infty} = 0$

describe the biogeochemical processes using variable stoichiometric coefficients (compare values in Table 10). Above z_{ox} , the combined effects of NH_4 and P release due to aerobic OM degradation increases alkalinity according to ALK^{OX} whereas nitrification decreases alkalinity with stoichiometry ALK^{NIT} . In the remaining three zones anaerobic OM degradation generally results in an increase in alkalinity, with the exact magnitude depending on the nature of the terminal electron acceptor used (i.e. ALK^{DEN} , ALK^{SUL} , ALK^{MET}). In addition, the effect of secondary redox reactions, such as nitrification, sulfide and methane oxidation are implicitly accounted for in the boundary conditions. Again, a mechanistic description of ALK production from CaCO_3 dissolution would lead to significant mathematical problems and is therefore not included in the current version of OMEN-SED. In OMEN-SED, the conservation equations for alkalinity are thus given by:

1. Oxic zone ($z \leq z_{\text{ox}}$)

$$\frac{\partial \text{ALK}^I}{\partial t} = 0 = D_{\text{ALK}} \frac{\partial^2 \text{ALK}^I}{\partial z^2} - w \frac{\partial \text{ALK}^I}{\partial z} + \frac{1-\phi}{\phi} \cdot \sum_i \left(\text{ALK}^{\text{NIT}} \cdot \frac{\gamma_{\text{NH}_4}}{1 + K_{\text{NH}_4}} \text{NC}_i + \text{ALK}^{\text{OX}} \right) \cdot k_i \cdot \text{POC}_i(z) \quad (30)$$

2. Denitrification or nitrogenous zone ($z_{\text{ox}} < z \leq z_{\text{NO}_3}$)

$$\frac{\partial \text{ALK}^{II}}{\partial t} = 0 = D_{\text{ALK}} \frac{\partial^2 \text{ALK}^{II}}{\partial z^2} - w \frac{\partial \text{ALK}^{II}}{\partial z} + \frac{1-\phi}{\phi} \cdot \sum_i \text{ALK}^{\text{DEN}} \cdot k_i \cdot \text{POC}_i(z) \quad (31)$$

3. Sulfidic zone ($z_{\text{NO}_3} < z \leq z_{\text{SO}_4}$)

$$\frac{\partial \text{ALK}^{III}}{\partial t} = 0 = D_{\text{ALK}} \frac{\partial^2 \text{ALK}^{III}}{\partial z^2} - w \frac{\partial \text{ALK}^{III}}{\partial z} + \frac{1-\phi}{\phi} \cdot \sum_i \text{ALK}^{\text{SUL}} \cdot k_i \cdot \text{POC}_i(z) \quad (32)$$

4. Methanic zone ($z_{\text{SO}_4} < z \leq z_\infty$)

$$\frac{\partial \text{ALK}^{IV}}{\partial t} = 0 = D_{\text{ALK}} \frac{\partial^2 \text{ALK}^{IV}}{\partial z^2} - w \frac{\partial \text{ALK}^{IV}}{\partial z} + \frac{1-\phi}{\phi} \cdot \sum_i \text{ALK}^{\text{MET}} \cdot k_i \cdot \text{POC}_i(z) \quad (33)$$

Table 8. Boundary conditions for alkalinity. For the boundaries we define: $z_-^- := \lim_{h \rightarrow 0} (z_- - h)$ and $z_-^+ := \lim_{h \rightarrow 0} (z_- + h)$.

Boundary	Condition	
$z = 0$	known concentration	1) $\text{ALK}(0) = \text{ALK}_0$
$z = z_{\text{bio}}$	continuity	2) $\text{ALK}(z_{\text{bio}}^-) = \text{ALK}(z_{\text{bio}}^+)$
	flux	3) $-(D_{\text{ALK},0} + D_{\text{bio}}) \cdot \frac{\partial \text{ALK}}{\partial z} _{z_{\text{bio}}^-} = -D_{\text{ALK},0} \cdot \frac{\partial \text{ALK}}{\partial z} _{z_{\text{bio}}^+}$
$z = z_{\text{ox}}$	continuity	4) $\text{ALK}(z_{\text{ox}}^-) = \text{ALK}(z_{\text{ox}}^+)$
	flux	5) $-D_{\text{ALK}} \cdot \frac{\partial \text{ALK}}{\partial z} _{z_{\text{ox}}^-} + F_{\text{ALK}}(z_{\text{ox}}) = -D_{\text{ALK}} \cdot \frac{\partial \text{ALK}}{\partial z} _{z_{\text{ox}}^+}$ $F_{\text{ALK}}(z_{\text{ox}}) = \frac{1-\phi}{\phi} \cdot \left(\text{ALK}^{\text{H}_2\text{S}} \cdot \gamma_{\text{H}_2\text{S}} \int_{z_{\text{NO}_3}}^{\text{SO}_4} \sum_i \text{SO}_4 \cdot k_i \cdot \text{POC}_i dz \right) + \frac{1-\phi}{\phi} \cdot \left(\text{ALK}^{\text{NIT}} \frac{\gamma_{\text{NH}_4}}{1+k_{\text{NH}_4}} \int_{z_{\text{NO}_3}}^{\infty} \sum_i \text{NC}_i \cdot k_i \cdot \text{POC}_i dz \right)$
	where:	
$z = z_{\text{NO}_3}$	continuity	6) $\text{ALK}(z_{\text{NO}_3}^-) = \text{ALK}(z_{\text{NO}_3}^+)$
	flux	7) $-D_{\text{ALK}} \cdot \frac{\partial \text{ALK}}{\partial z} _{z_{\text{NO}_3}^-} = -D_{\text{ALK}} \cdot \frac{\partial \text{ALK}}{\partial z} _{z_{\text{NO}_3}^+}$
$z = z_{\text{SO}_4}$	continuity	8) $\text{ALK}(z_{\text{SO}_4}^-) = \text{ALK}(z_{\text{SO}_4}^+)$
	flux (with AOM)	9) $-D_{\text{ALK}} \cdot \frac{\partial \text{ALK}}{\partial z} _{z_{\text{SO}_4}^-} + F_{\text{ALK}}(z_{\text{SO}_4}) = -D_{\text{ALK}} \cdot \frac{\partial \text{ALK}}{\partial z} _{z_{\text{SO}_4}^+}$ $F_{\text{ALK}}(z_{\text{SO}_4}) = \frac{1-\phi}{\phi} \cdot \left(\text{ALK}^{\text{AOM}} \gamma_{\text{CH}_4} \cdot \int_{z_{\text{SO}_4}}^{\infty} \sum_i k_i \cdot \text{POC}_i dz \right)$
	where:	
$z = z_{\infty}$	zero ALK flux	10) $\frac{\partial \text{ALK}}{\partial z} _{z_{\infty}} = 0$

610 where D_{ALK} denotes the diffusion coefficient for alkalinity which depends on the bioturbation status of the respective geochemical zone. Integration of Eq. (30) - (33) yields the analytical solution and Table 8 summarises the boundary conditions applied in OMEN-SED. A Dirichlet boundary condition is applied at the sediment-water interface. The decrease of alkalinity due to oxidation of reduced species produced in the anoxic zones (with stoichiometry ALK^{NIT} and $\text{ALK}^{\text{H}_2\text{S}}$) is implicitly taken into account through the flux boundary condition at z_{ox} (Table 8 Eq. 5). Furthermore, the oxidation of methane by sulfate reduction increases alkalinity with stoichiometry ALK^{AOM} which is accounted for through the flux boundary condition at z_{SO_4} (Table 8 Eq. 9). At the lower boundary z_{∞} a zero diffusive flux condition is applied.

2.3 Determination of Integration Constants

620 The integration constants of all general analytical solutions derived above change in response to changing boundary conditions. Thus, OMEN-SED has to re-determine integration constants for each dynamic zone (i.e. $z_{\text{ox}}, z_{\text{bio}}, z_{\text{NO}_3}$ and z_{SO_4}) at every time step for all biogeochemical tracers. The bioturbation boundary poses a particular challenge as it can theoretically occur in any of the dynamic geochemical zones (Fig. 3). Therefore, in order to generalise and simplify this recurring boundary 625 matching problem, an independent, generic algorithm is implemented (rather than using multiple fully-worked-out algebraic solutions for each possible case and every biogeochemical tracer). The algorithm only has to solve a two-simultaneous-equation problem.

2.3.1 Generic Boundary Condition Matching (GBCM)

As discussed in Section 2.1, the solution of the general steady-state transport-reaction equation (Eq. 630 (2)) for a generic tracer C is of the general form:

$$C(z) = A \exp(az) + B \exp(bz) + \sum_j \frac{\alpha_j}{D\beta_j^2 - w\beta_j - k} \cdot \exp(-\beta_j z) + \frac{Q}{k} \quad (34)$$

and can therefore be expressed as:

635 $C(z) = A \cdot E(z) + B \cdot F(z) + G(z) \quad (35)$

where $E(z)$, $F(z)$ are the homogeneous solutions of the ODE, $G(z)$ the particular integral (collectively called the basis functions), and A , B are the integration constants that must be determined with the boundary conditions (shown in Fig. 3 for the whole sediment column).

Each internal boundary matching problem (i.e. excluding $z = 0$ and $z = z_\infty$) involves matching 640 continuity and flux for the two solutions of the respective reaction-transport equation above, $C_U(z)$ (= 'upper'), and below, $C_L(z)$ (= 'lower'), the dynamic boundary at $z = z_b$:

$$C_U(z) = A_U \cdot E_U(z) + B_U \cdot F_U(z) + G_U(z) \quad (36)$$

$$C_L(z) = A_L \cdot E_L(z) + B_L \cdot F_L(z) + G_L(z). \quad (37)$$

645 OMEN-SED generally applies concentration continuity and flux boundary conditions at its internal, dynamic boundaries:

Continuity (where for generality we allow a discontinuity V_b)

$$C_U(z_b) = C_L(z_b) + V_b \quad (38)$$

650 Flux

$$D_U C'_U(z_b) + w C_U(z_b) = D_L C'_L(z_b) + w C_L(z_b) + F_b \quad (39)$$

where w is advection, D are the diffusion coefficients and F_b is any flux discontinuity (e.g. resulting from secondary redox reactions).

655 Considering that the advective flux above and below the boundary is equal (i.e. $w C_U(z_b) = w C_L(z_b)$) and substituting the general ODE solutions (36), (37), the boundary conditions can be represented as two equations connecting the four integration constants:

$$\begin{pmatrix} E_U & F_U \\ D_U E'_U & D_U F'_U \end{pmatrix} \begin{pmatrix} A_U \\ B_U \end{pmatrix} = \begin{pmatrix} E_L & F_L \\ D_L E'_L & D_L F'_L \end{pmatrix} \begin{pmatrix} A_L \\ B_L \end{pmatrix} + \begin{pmatrix} G_L - G_U + V_b \\ D_L G'_L - D_U G'_U + F_b - wV_b \end{pmatrix} \quad (40)$$

where the ODE solutions E , F , G are all evaluated at z_b .

660 Equation (40) can now be solved to give A_U and B_U as a function of the integration constants from the layer below (A_L and B_L), thereby constructing a piecewise solution for both layers, with just two integration constants (this is implemented in the function **benthic_utils.matchsoln** of OMEN-SED):

$$\begin{pmatrix} A_U \\ B_U \end{pmatrix} = \begin{pmatrix} c_1 & c_2 \\ c_3 & c_4 \end{pmatrix} \begin{pmatrix} A_L \\ B_L \end{pmatrix} + \begin{pmatrix} d_1 \\ d_2 \end{pmatrix}. \quad (41)$$

665 Using Eq. (41), $C_U(z)$ in (36) can now be rewritten as a function of A_L and B_L (implemented in **benthic_utils.xformsoln**):

$$C_U(z) = (c_1 A_L + c_2 B_L + d_1) \cdot E_U(z) + (c_3 A_L + c_4 B_L + d_2) \cdot F_U(z) + G_U(z) \quad (42)$$

and hence define the “transformed” basis functions $E_U^*(z)$, $F_U^*(z)$, $G_U^*(z)$ such that:

$$C_U(z) = A_L \cdot E_U^*(z) + B_L \cdot F_U^*(z) + G_U^*(z) \quad (43)$$

670 where

$$\begin{aligned} E_U^*(z) &= c_1 E_U(z) + c_3 F_U(z) \\ F_U^*(z) &= c_2 E_U(z) + c_4 F_U(z) \\ G_U^*(z) &= G_U(z) + d_1 E_U(z) + d_2 F_U(z) \end{aligned} \quad (44)$$

675 Equations (41), (43) and (44) can now be consecutively applied for each of the dynamic biogeochemical zone boundaries, starting at the bottom of the sediment column. The net result is a piecewise solution of the whole sediment column with just two integration constants (coming from the lowest layer), which can then be solved for by applying the boundary conditions at the sediment-water interface and the bottom of the sediments.

680 2.3.2 Abstracting out the bioturbation boundary

The bioturbation boundary affects the diffusion coefficient of the modelled solutes, as well as the conservation equation of organic matter (and thereby the exact form of each reaction-transport equation). This boundary is particularly inconvenient as it can, in principle, occur in the middle of any of the dynamically shifting biogeochemical zones and therefore generate multiple cases (Fig. 3). The 685 GBCM algorithm described above is thus not only used to construct a piecewise solution of the whole sediment column, but also to abstract out the bioturbation boundary. For each biogeochemical zone the “bioturbation-status” is initially tested (i.e. fully bioturbated, fully non-bioturbated, or crossing the bioturbation boundary). Therefore, the upper and lower boundaries for the different zones (e.g. for the nitrogenous zone: $z_U = z_{\text{ox}}$, $z_L = z_{\text{NO}_3}$), as well as the respective reactive terms and diffusion coefficients (bioturbated and non-bioturbated) are passed over to the routine **zTOC.prepfg_l12**

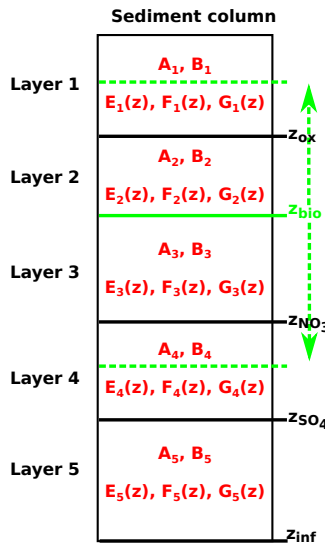


Figure 3. Schematic of the generic boundary condition matching (GBCM) problem. Showing the resulting integration constants (A_i, B_i) and ODE solutions (E_i, F_i, G_i) for the different sediment layers and the variable bioturbation boundary.

where the bioturbation-status is determined. In case the bioturbation depth is located within this zone (i.e. $z_U < z_{bio} < z_L$) a piecewise solution for this layer is constructed. Therefore, the reactive terms and diffusion coefficients are handed over to the routines **zTOC.calcfg_I1** and **zTOC.calcfg_I2** which calculate the basis functions (E_U, F_U, G_U and E_L, F_L, G_L) and their derivatives for the bioturbated and the non-bioturbated part of this specific geochemical zone. The concentration and flux for both solutions at z_{bio} are matched and the coefficients $c_1, c_2, c_3, c_4, d_1, d_2$ (as in Eq. (41)) are calculated by the routine **benthic_utils.matchsoln**. These coefficients and the "bioturbation-status" of the layer are passed back to the main GBCM algorithm where they can be used by the routine **benthic_utils.xformsoln** to calculate the "transformed" basis functions ($E_U^*(z), F_U^*(z), G_U^*(z)$) such that both layers are expressed in the same basis (compare Eq. (42 - 44)).

For instance, in the case of sulfate, **zTOC.prepfg_I12** is called three times before the actual profile is calculated (once per zone: oxic, nitrogenous, sulfidic) and hands back the information about the "bioturbation-status" of the three layers and the coefficients $c_1, c_2, c_3, c_4, d_1, d_2$ for the biogeochemical zone including the bioturbation depth. When calculating the complete piecewise solution for the sediment column, this information is passed to the function **zTOC.calcfg_I12** which sorts out the correct solution type to use. The main GBCM algorithm therefore never needs to know whether it is dealing with a piecewise solution (i.e. matched across the bioturbation boundary) or a "simple" solution (i.e. the layer is fully bioturbated or fully non-bioturbated).

2.4 Model Parameters

710 The following section provides a summary of global relationships used to constrain reaction and transport parameters in OMEN-SED. Table 9 synthesises sediment and transport parameters, while table 10 provides an overview of all biogeochemical parameters used in OMEN-SED.

2.4.1 Transport Parameters

715 The burial of sediments and pore water is directly related to the accumulation of new material on the seafloor (i.e. sedimentation, Burdige, 2006). This results in a downward advective flux of older sediment material and pore water in relation to the sediment-water interface. When coupled to an ocean model, its sedimentation flux can be readily used in OMEN-SED. The stand-alone version of OMEN-SED uses the empirical global relationship between sediment accumulation rate (cm yr^{-1}) and seafloor depth (m) of Middelburg et al. (1997):

720 $w = 3.3 \cdot 10^{-0.87478367 - 0.00043512 \cdot \text{depth}},$ (45)

As mentioned before (Section 2.1), the diffusion coefficient of species i is calculated as $D_i = D_{i,0} + D_{\text{bio}} = D_{\text{mol},i} \cdot f_{ir} + D_{\text{bio}}$ for dissolved species and $D_i = D_{\text{bio}}$ for solid species. The bioturbation coefficient D_{bio} ($\text{cm}^2 \text{ yr}^{-1}$) is constant in the bioturbated zone and also follows the empirical relationship by Middelburg et al. (1997):

725 $D_{\text{bio}} = 5.2 \cdot 10^{0.76241122 - 0.00039724 \cdot \text{depth}}$ (46)

Observations indicate that bioturbation is largely restricted to the upper 10 cm of the sediments and is only marginally related to seafloor depth (e.g. Boudreau, 1998; Teal et al., 2010). Therefore, OMEN-SED imposes a globally invariant bioturbation depth z_{bio} of 10 cm. In case the bottom water oxygen concentration is below 5 nmol cm^{-3} infaunal activity is assumed to cease and $z_{\text{bio}} = 0.01$ cm. We choose a low value unequal to zero in order to simplify the implementation of the model. This approach ensures that the sediment column always consists of a bioturbated (even though very small for the low oxygen condition) and a non-bioturbated zone, thus the same GBCM algorithm can be used to solve the conservation equations. Furthermore, when OMEN-SED is coupled to an Earth system model the same method can be used to convert the POC depositional flux into a SWI concentration (i.e. the flux needs to be converted assuming bioturbation, see Section 4.1).

Bioirrigation (i.e. the pumping activity by burrow-dwelling animals) exchanges burrow water with overlying water and may enhance the SWI-flux of solutes (Aller, 1984, 1988). Several approaches exist to incorporate this into a 1-D diagenetic model, for instance as a non-local transport/exchange process (Boudreau, 1984; Emerson et al., 1984) or as an enhancement factor of the molecular diffusion coefficient (Devol and Christensen, 1993; Soetaert et al., 1996). In OMEN-SED the latter approach is applied and the apparent “bio-diffusion” coefficient is calculated as $D_{i,0} = D_{\text{mol},i} \cdot f_{ir}$. Soetaert et al. (1996) derived an empirical relationship between f_{ir} and seafloor

SA: need to explain why not 0; **DH:** Decent explanation?

depth ($f_{ir} = \text{Min}\{1; 15.9 \cdot \text{depth}^{-0.43}\}$) based on observations from Archer and Devol (1992) and Devol and Christensen (1993). As this relationship just varies for depth below ~ 623 m (with a maximum value of 3 at ~ 50 m) a constant value of $f_{ir} = 1$ is used in the default OMEN-SED configuration. The specific molecular diffusion coefficients $D_{\text{mol},i}$ are corrected for sediment porosity ϕ , tortuosity F and are linearly interpolated for an ambient temperature T using zero-degree coefficients D_i^0 and temperature-dependent diffusion coefficients D_i^T (Soetaert et al., 1996):

$$D_{\text{mol},i} = (D_i^0 + D_i^T \cdot T) \cdot \frac{1}{\phi \cdot F}.$$

Tortuosity can be expressed in terms of porosity as $F = \frac{1}{\phi^m}$ (Ullman and Aller, 1982) with the exponent m varying according to the type of sediment (here $m=3$ is used). Values for D_i^T and D_i^0 are summarised in Table 9 and are adapted from Li and Gregory (1974), Schulz (2006) and Gypens et al. (2008).

2.4.2 Stoichiometries and reaction parameters

The first-order organic matter degradation constants of compound class i , k_i (yr^{-1}), are assumed invariant along the sediment column and therefore independent of the nature of the terminal electron acceptor. The rate constants can be altered manually to fit observed sediment profiles (compare Section 3.2) or related to a master variable provided by a coupled Earth system model (e.g. sedimentation rate, compare Section 4.2). The partitioning of the bulk OM pool into reactivity classes (f_i) is also done manually in the stand-alone version or is provided by the ESM. Organic matter degradation releases N, P and DIC to the pore water using Redfield molar ratios (Redfield, 1963) and consumes TEA with specific stoichiometries (O_2C , NO_3C , SO_4C) as summarised in Table 10. Table 15 in the appendix provides a list of reactions and their stoichiometries as implemented in OMEN-SED. The effect of OM degradation and secondary redox reactions on total alkalinity is also accounted for via reaction specific stoichiometries representing the release of NH_4 , H_2S and P and is based on Jourabchi et al. (2005). The secondary redox parameters (i.e. γ_{NH_4} , $\gamma_{\text{H}_2\text{S}}$, γ_{CH_4}), accounting for the fraction of reduced substances that are reoxidised, would be ideally parameterised for instance in relation to bottom water oxygen concentration or oxygen penetration depth (z_{ox}). Gypens et al. (2008) for example expressed γ_{NH_4} as a function of oxygen penetration depth ($\gamma_{\text{NH}_4} = 0.243 \cdot \ln(z_{\text{ox}}) + 1.8479$) based on a fitting exercises to a numerical model and showed that the fraction varies between 0.2 for $z_{\text{ox}} = 0.1\text{cm}$ and 1.0 for $z_{\text{ox}} > 3\text{cm}$. Due to mathematical constraints for finding an analytical solution to the model equations these fractions take constant values generally representing oxygenated deep sea conditions. The instantaneous equilibrium adsorption coefficients of NH_4 and PO_4 (K_{NH_4} , $K_{\text{PO}_4}^{\text{ox}}$, $K_{\text{PO}_4}^{\text{anox}}$) are based on Wang and Van Cappellen (1996) and Slomp et al. (1998), respectively. The first order rate constants for sorption of PO_4 to Fe oxides (k_s), release of PO_4 from Fe-bound P due to Fe-oxide reduction (k_m) and authigenic CFA precipitation (k_a), as well as the pore water equilibrium concentrations for P sorption and CFA precipitation

Table 9. Sediment characteristics and transport parameters.

Parameter	Unit	Value	Description/Source
ρ_{sed}	g cm^{-3}	2.6	Sediment density
w	cm yr^{-1}	Fct. of seafloor depth or from ESM	Advection/Sediment accumulation rate (Middelburg et al., 1997)
z_{bio}	cm	10 or 0.01	Bioturbation depth (Boudreau, 1998; Teal et al., 2010)
D_{bio}	$\text{cm}^2 \text{yr}^{-1}$	Fct. of seafloor depth	Bioturbation coefficient (Middelburg et al., 1997)
ϕ	-	0.85	Porosity
F	-	$\frac{1}{\phi^m}$	Tortuosity, here m=3
f_{ir}	-	1	Irrigation factor
Diffusion coefficients (Li and Gregory, 1974; Schulz, 2006; Gypens et al., 2008)			
$D_{\text{O}_2}^0$	$\text{cm}^2 \text{yr}^{-1}$	348.62	Molecular diffusion coefficient of oxygen at 0°C
$D_{\text{O}_2}^T$	$\text{cm}^2 \text{yr}^{-1} \text{°C}^{-1}$	14.09	Diffusion coefficient for linear temp. dependence of oxygen
$D_{\text{NO}_3}^0$	$\text{cm}^2 \text{yr}^{-1}$	308.42	Molecular diffusion coefficient of nitrate at 0°C
$D_{\text{NO}_3}^T$	$\text{cm}^2 \text{yr}^{-1} \text{°C}^{-1}$	12.26	Diffusion coefficient for linear temp. dependence of nitrate
$D_{\text{NH}_4}^0$	$\text{cm}^2 \text{yr}^{-1}$	309.05	Molecular diffusion coefficient of ammonium at 0°C
$D_{\text{NH}_4}^T$	$\text{cm}^2 \text{yr}^{-1} \text{°C}^{-1}$	12.26	Diffusion coefficient for linear temp. dependence of ammonium
$D_{\text{SO}_4}^0$	$\text{cm}^2 \text{yr}^{-1}$	157.68	Molecular diffusion coefficient of sulfate at 0°C
$D_{\text{SO}_4}^T$	$\text{cm}^2 \text{yr}^{-1} \text{°C}^{-1}$	7.88	Diffusion coefficient for linear temp. dependence of sulfate
$D_{\text{H}_2\text{S}}^0$	$\text{cm}^2 \text{yr}^{-1}$	307.48	Molecular diffusion coefficient of sulfide at 0°C
$D_{\text{H}_2\text{S}}^T$	$\text{cm}^2 \text{yr}^{-1} \text{°C}^{-1}$	9.64	Diffusion coefficient for linear temp. dependence of sulfide
$D_{\text{PO}_4}^0$	$\text{cm}^2 \text{yr}^{-1}$	112.91	Molecular diffusion coefficient of phosphate at 0°C
$D_{\text{PO}_4}^T$	$\text{cm}^2 \text{yr}^{-1} \text{°C}^{-1}$	5.59	Diffusion coefficient for linear temp. dependence of phosphate
D_{DIC}^0	$\text{cm}^2 \text{yr}^{-1}$	151.69	Molecular diffusion coefficient of DIC at 0°C
D_{DIC}^T	$\text{cm}^2 \text{yr}^{-1} \text{°C}^{-1}$	7.93	Diffusion coefficient for linear temp. dependence of DIC
D_{ALK}^0	$\text{cm}^2 \text{yr}^{-1}$	151.69	Molecular diffusion coefficient of ALK at 0°C
D_{ALK}^T	$\text{cm}^2 \text{yr}^{-1} \text{°C}^{-1}$	7.93	Diffusion coefficient for linear temp. dependence of ALK
Note: DIC and ALK coefficients are the values of HCO_3^- from Schulz (2006).			

Table 10. Values for biogeochemical parameters used in OMEN-SED. The variables x , y and z denote the atomic ratio of carbon, nitrogen and phosphorus of the degrading organic matter (here set to $C : N : P = 106 : 16 : 1$).

Parameter/Variable	Unit	Value	Description
Stoichiometric factors and molecular ratios			
NC _i	mol/mol	$\frac{y}{x} = \frac{16}{106}$	Nitrogen to carbon ratio
PC _i	mol/mol	$\frac{z}{x} = \frac{1}{106}$	Phosphorus to carbon ratio
MC	mol/mol	0.5	Methane to carbon ratio produced during methanogenesis
DICC ^I	mol/mol	1.0	DIC to carbon ratio until z _{SO₄}
DICC ^{II}	mol/mol	0.5	DIC to carbon ratio below z _{SO₄}
O ₂ C	mol/mol	$\frac{x+2y}{x} = \frac{138}{106}$	Oxygen to carbon ratio
NO ₃ C	mol/mol	$\frac{4x+3y}{5x} = \frac{94.4}{106}$	Nitrate to carbon ratio
SO ₄ C	mol/mol	$\frac{1}{2}O_2C = \frac{138}{212}$	Sulfate to carbon ratio
ALK ^{OX}	mol/mol	$\frac{y-2z}{x} = \frac{14}{106}$	ALK from aerobic degradation
ALK ^{NIT}	mol/mol	-2	ALK from nitrification
ALK ^{DEN}	mol/mol	$\frac{4x+3y-10z}{5x} = \frac{92.4}{106}$	ALK from denitrification
ALK ^{SUL}	mol/mol	$\frac{x+y-2z}{x} = \frac{120}{106}$	ALK from sulfate reduction
ALK ^{MET}	mol/mol	$\frac{y-2z}{x} = \frac{14}{106}$	ALK from methanogenesis
ALK ^{H₂S}	mol/mol	-2	ALK from H ₂ S oxidation
ALK ^{AOM}	mol/mol	2	ALK from AOM
Secondary reaction parameters			
γ _{NH₄}	-	0.9	Fraction of NH ₄ that is nitrified
γ _{H₂S}	-	0.95	Fraction of H ₂ S that is oxidised
γ _{CH₄}	-	0.99	Fraction of CH ₄ that is oxidised
Adsorption coefficients (Wang and Van Cappellen, 1996; Slomp et al., 1998)			
K _{NH₄}	-	1.4	NH ₄ adsorption coefficient
K _{PO₄} ^{ox} , K _{PO₄} ^{anox}	-	200.0, 2.0	PO ₄ adsorption coefficient (oxic, anoxic)
P related parameters (Slomp et al., 1996)			
k _s	yr ⁻¹	94.9	Rate constant for PO ₄ sorption
k _m	yr ⁻¹	0.193	Rate constant for Fe-bound P release
k _a	yr ⁻¹	0.365	Rate constant for authigenic CFA precipitation
PO ₄ ^s	mol cm ⁻³	$1 \cdot 10^{-9}$	Equilibrium conc. for P sorption
FeP [∞]	mol cm ⁻³	$1.99 \cdot 10^{-10}$	Asymptotic concentration for Fe-bound P
PO ₄ ^a	mol cm ⁻³	$3.7 \cdot 10^{-9}$	Equilibrium conc. for authigenic P precipitation

DH: ALK^{OX} correct?
y=NH₄ prod.; -2z=P release

(PO₄^s, PO₄^a) and the asymptotic concentration for Fe-bound P (FeP[∞]) are taken from Slomp et al. (1996). See Table 10 for a complete summary of the parameters and their values.

780 **3 Stand-alone sensitivity analysis and case studies****3.1 Sensitivity Analysis****3.1.1 Methodology**

Model parameters implicitly account for processes that are not explicitly resolved. Therefore, model parameters are notoriously difficult to constrain and a source of uncertainty for numerical and analytical models. A comprehensive sensitivity analysis (SA) can help quantify this uncertainty and identify the most sensitive parameters. More specifically, sensitivity analysis is used to investigate how the variations in the outputs (y_1, \dots, y_N) of a model can be attributed to variations in the different input parameters (x_1, \dots, x_M , Pianosi et al., 2016). Different types of sensitivity indices, which quantify the relative influence of parameter x_i on output y_j with a scalar $S_{i,j}$ (for $i \in \{1, \dots, M\}$ and $j \in \{1, \dots, N\}$), can be calculated, ranging from simple one-at-a-time methods to statistical evaluations of the output distribution (e.g. variance-based or density-based approaches Pianosi et al., 2016). The latter indices take values between zero and one ($S_{i,j} \in [0, 1]$), where zero indicates a non-influential parameter and a higher value a more influential parameter. Here, SA is used mainly to identify which parameters have the largest impact on the different model outputs and therefore require careful calibration. As the probability density functions of our model outputs (i.e. the resulting SWI-fluxes) are generally highly-skewed towards extreme organic matter degradation rates (not shown) variance-based sensitivity indices may not be a suitable proxy for output uncertainty (Pianosi et al., 2016). Hence the novel density-based PAWN method by Pianosi and Wagener (2015) is employed which considers the entire conditional and unconditional Cumulative Distribution Function (CDF) of the model output rather than its variance only. The unconditional CDF, $F_y(y)$, of output y is obtained when all uncertain parameters (x_1, \dots, x_M) are varied simultaneously, and the conditional CDFs, $F_{y|x_i}(y)$, are obtained when all inputs but the i -th parameter are varied (i.e. x_i is fixed to a so-called conditioning value). The sensitivity index of parameter i is measured by the distance between the two CDFs using the Kolmogorov-Smirnov statistic (Kolmogorov, 1933; Smirnov, 1939), i.e.:

$$S_i = \max_{x_i} \max_y |F_y(y) - F_{y|x_i}(y)|. \quad (47)$$

Since $F_{y|x_i}(y)$ accounts for what happens when the variability due to x_i is removed, the distance between the two CDFs provides a measure of the effects of x_i on the output y . Due to the model complexity it is impossible to compute the sensitivity indices analytically. Therefore, they are approximated from a Latin-Hypercube sampling of parameter inputs and calculated outputs. For a brief description of the methodology see Fig. 4. For more details we refer the interested reader to Pianosi and Wagener (2015).

The PAWN method, as implemented within the Sensitivity Analysis for Everyone (SAFE) matlab toolbox (Pianosi et al., 2015), is used to investigate $M = 11$ model parameters for ranges as specified

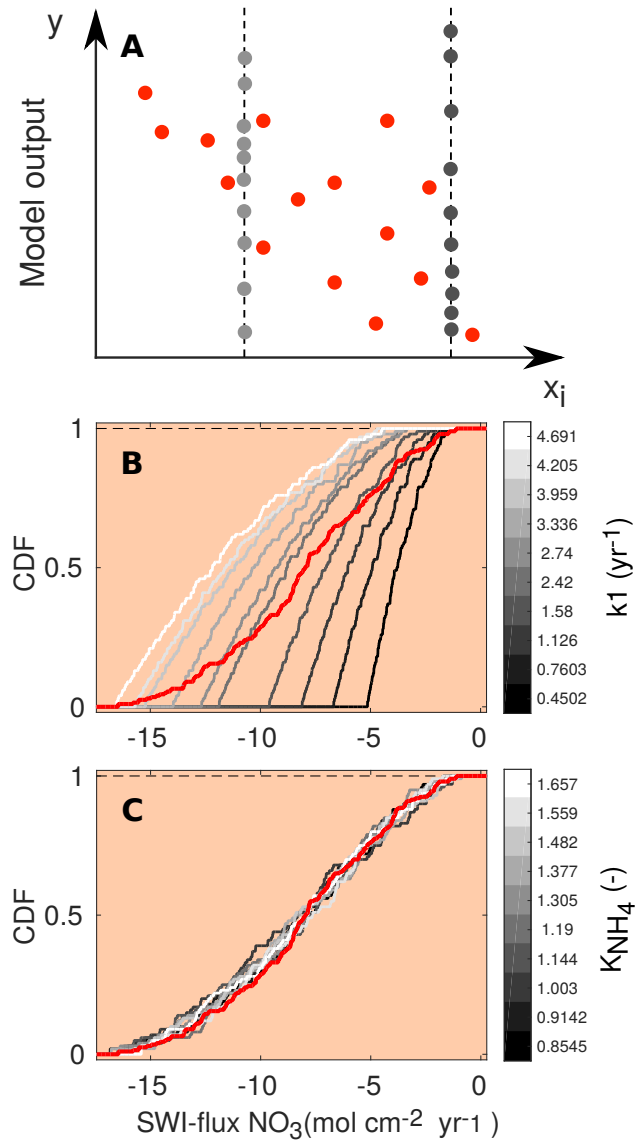


Figure 4. A: Schematic of the PAWN method, plotting an uncertain parameter (x_i) against a generic model output (y). Red dots represent points for calculating the unconditional CDF (NU, here 15), grey dots are points for calculating each conditional CDF (NC, here 10) with $n = 2$ conditioning points as an example. The user can change the values of NU, NC and n . The number of model evaluations equals $N_{\text{eval}} = \text{NU} + n \cdot \text{NC} \cdot M$, where M is the number of uncertain input parameters. B + C: Two examples of CDFs of the model calculated SWI-flux of NO_3 using NU = 200, NC = 100 and $n = 10$. The red lines are the unconditional distribution functions $F_y(\text{NO}_3)$ and the grey lines are the conditional distribution functions $F_{y|x_i}(\text{NO}_3)$ at different fixed values of the input parameters k_1 (B) and K_{NH_4} (C). As the maximal distance between conditional CDFs and unconditional CDF is greater for k_1 , this parameter is more influential for the model output (here SWI-flux of NO_3 , compare Fig. 5).

Table 11. Range of model parameters used for sensitivity analysis of model predicted output.

Parameter	Description	Units	Minimum	Maximum	Source
k_1	labile OM degradation constant	yr^{-1}	$1e^{-4}$	5.0	(1)
\tilde{k}_2	order of refractory OM degradation constant ($k_2 = \tilde{k}_2 \cdot k_1$)	-	$1e^{-4}$	$1e^{-1}$	(1)
f_1	fraction of labile OM	-	0.02	0.98	-
K_{NH_4}	Adsorption coefficient	-	0.8	1.7	(2)
γ_{NH_4}	NH_4 fraction oxidised		0.5	1.0	-
$\gamma_{\text{H}_2\text{S}}$	H_2S fraction oxidised		0.5	1.0	-
$K_{\text{PO}_4}^{\text{ox}}$	Adsorption coeff. oxic	-	100.0	400.0	(3)
$K_{\text{PO}_4}^{\text{anox}}$	Adsorption coeff. anoxic	-	1.3	2.0	(3)
k_s	kinetic P sorption	yr^{-1}	0.1	100.0	(4, 5)
k_m	Fe-bound P release	yr^{-1}	0.015	0.02	(4, 5)
k_a	authigenic P formation	yr^{-1}	0.001	10.0	(4, 6)

Sources: (1) Arndt et al. (2013); (2): Van Cappellen and Wang (1996); (3): Krom and Berner (1980)
(4): Gypens et al. (2008); (5): Slomp et al. (1996); (6): Van Cappellen and Berner (1988)

Table 12. Model boundary conditions for the two idealised sediment conditions used for the sensitivity analysis (Fig. 5 and 6). All solute concentrations are in nmol cm^{-3} .

Depth (m)	Temp. ($^{\circ}\text{C}$)	OC (wt%)	O_2	NO_3	SO_4	PO_4	z_{bio} (cm)
400	8.0	2.0	0.0	40.0	28,000	40.0	0.001
4000	1.5	1.0	300.0	20.0	28,000	40.0	10.0

- 815 in Table 11. Sensitivity indices for all resulting SWI-fluxes for two idealised sediment conditions (i.e. anoxic at 400 m and oxic at 4000 m, see Table 12) are calculated. We use $\text{NU} = 200$ samples to estimate the unconditional CDF, $\text{NC} = 100$ samples to estimate the conditional CDFs and $n = 10$ conditioning points. Thus as $N_{\text{eval}} = 200 + 100 \cdot 10 \cdot 11$, 11200 model evaluations are performed for each sediment condition. The resulting indices are then translated into a color code and summarised
820 in a pattern plot to simplify comparison (Fig. 5).

3.1.2 Results

Fig. 5 summarises results of the sensitivity analysis as a colour map. Results indicate that generally the most significant parameters for all model outputs are the degradation rate constant for the labile OM pool (k_1) and the fraction of this pool to the total OM stock (f_1). Other parameters play a minor
825 role for the SWI-fluxes, with the exception of the secondary redox parameters (i.e. γ_{NH_4} , $\gamma_{\text{H}_2\text{S}}$) in the oxic scenario. Here, NH_4 , SO_4 and H_2S are very sensitive to changes in γ_{NH_4} and $\gamma_{\text{H}_2\text{S}}$, as these parameters determine how much of the respective TEA is produced in situ via reoxidation,

thus affecting the resulting SWI-fluxes. For the oxic scenario, the reoxidation of H₂S produced in the sulfidic layer (γ_{H_2S} , Table 8 Eq. 5) also has a strong influence on alkalinity as it decreases alkalinity by 2 moles per mole of S oxidized (ALK^{H₂S}, Table 10). For the anoxic scenario the secondary redox parameters are essentially non-influential as no O₂ is available for the reoxidation of reduced substances. Especially for the oxic condition the PO₄ SWI-flux appears to be insensitive to P-related parameters (i.e. $K_{PO_4}^{ox}$, $K_{PO_4}^{anox}$, k_s , k_m , k_a) as the majority is absorbed to Fe-oxides. The sensitivities change if other PO₄ related equilibrium concentrations PO₄^s, PO₄^a and FeP[∞] are used (not shown). Overall the results of the sensitivity analysis are in line with what one would expect from a diagenetic model and thus provide ground to confirm that OMEN-SED provides sensible results.

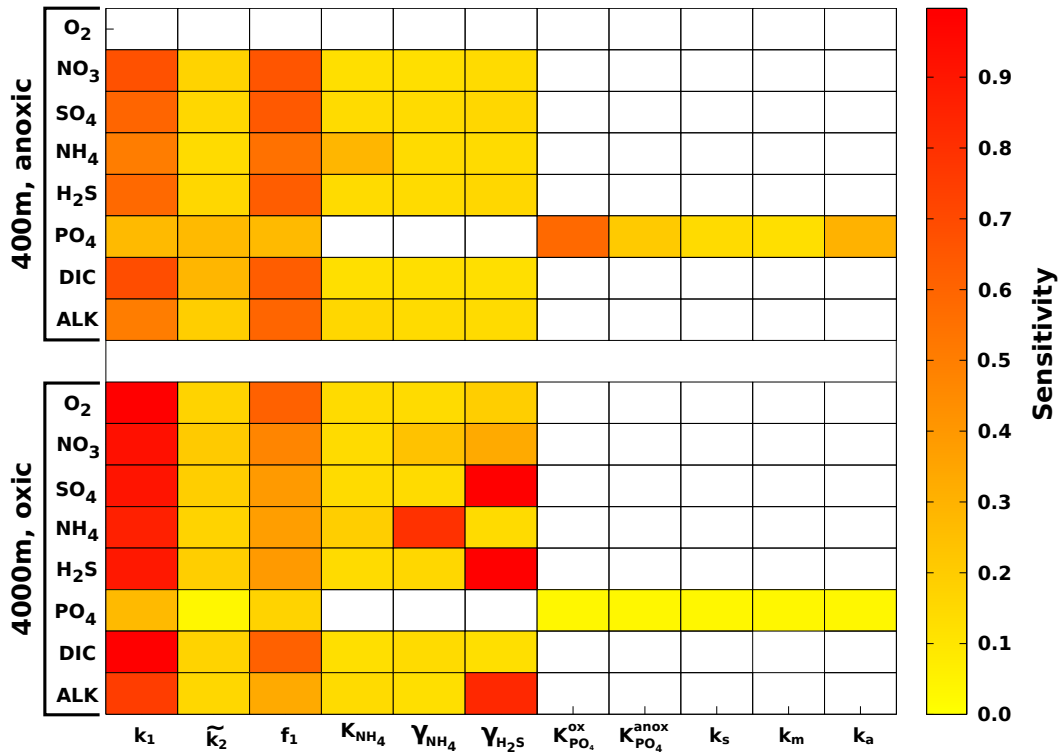


Figure 5. Pattern plot, showing the output sensitivity for each SWI flux (i.e. the chemical compounds on the vertical axis) and each input factor (i.e. the model parameters on the horizontal axis) for two idealised sediment cores. White patterns are assigned where the SWI flux is independent of the specific parameter.

We further explore the sensitivity of simulated sediment-water exchange fluxes to variations in organic matter degradation parameters by varying k₁, f₁ and k̃₂ while all other model parameters are set to their default values (Tables 9 and 10). Minimum and maximum values for k₁, k̃₂ and f₁ in the shallow ocean are as in Table 11. For the deep sea condition we account for the presence of more

refractory OM by sampling $f_1 \in [0.02, 0.3]$, whereas the variation of k_1 and \tilde{k}_2 is as in the shallow ocean. The parameter space is sampled using another Latin-Hypercube approach with sample sizes of $N = 3500$ for each idealised sediment condition. Figure 6 summarises the results of the sensitivity 845 study and the ranges of observed O_2 and NO_3 sediment-water interface fluxes extracted from a global database (Stolpovsky et al., 2015) are indicated on the colour scale. Figure 6 shows that the ranges of SWI-fluxes simulated with OMEN-SED are comparable to the observed ranges reported by Stolpovsky et al. (2015). The colour patterns in Figure 6 A and B also reveal the complex interplay 850 between the amount of labile OM f_1 and its degradation rate k_1 for the resulting SWI-fluxes of NO_3 in anoxic sediments and O_2 in aerobic sediments. In general, a higher degradation rate in combination with more labile OM available leads to a higher SWI-flux. However, higher fluxes extend over a larger range of k_1 -values when the amount of labile OM f_1 is high. The absence of a colour pattern in Figure 6 C highlights the limited interaction of the two model parameters for NO_3 SWI-fluxes under oxic conditions.

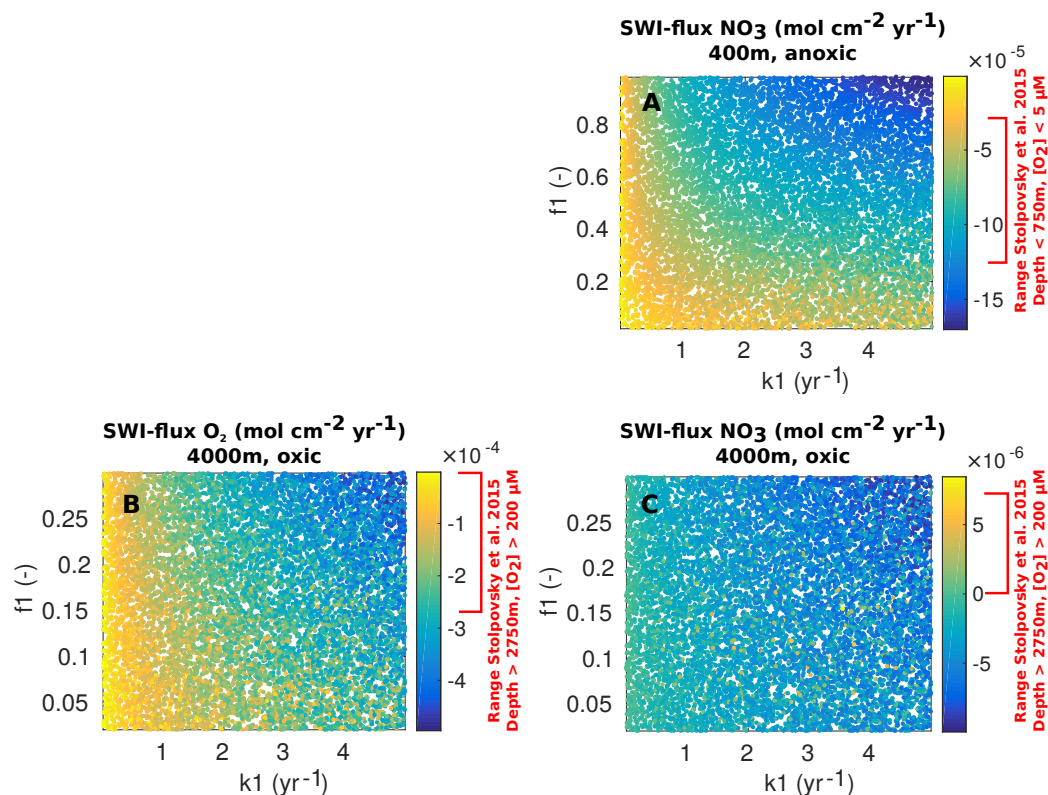


Figure 6. Scatter plots (k_1 vs f_1) of resulting OMEN-SED SWI-fluxes for the 400m anoxic (A: NO_3) and 4000m oxic (B: O_2 , C: NO_3) scenario. Negative values represent a flux from the water column into the sediments. Ranges indicated in red on the colour scale correspond to observed benthic fluxes as reported in the global database of Stolpovsky et al. (2015).

855 **3.2 Case study: Simulations of sediment cores**

3.2.1 Methodology

In order to illustrate the capabilities of OMEN-SED, comprehensive datasets from the Santa Barbara Basin (Reimers et al., 1996), as well as from the Iberian margin and the Nazaré Canyon (Epping et al., 2002) are modelled. Modelled profiles are compared with measured pore water data from 860 different depths including the continental shelf (108 m) and the lower slope (2213 m) located at the Iberian margin, the upper slope (585 m) from the Santa Barbara Basin, and a deep sea site (4298 m) in the Nazaré Canyon. The Santa Barbara Basin is characterised by anoxic bottom waters, high POC concentrations and varved sediments (Reimers et al., 1990), therefore the depth of bioturbation in 865 OMEN-SED is restricted to the upper 0.01 cm. In the uppermost sediments iron(III) hydroxides are reduced, releasing Fe^{2+} which reacts with sulfide to form iron sulfides. Thus, the Fe cycle exerts a strong control on sulfide concentrations in the sediments of this basin (Reimers et al., 1996). In addition, the sediments are generally supersaturated with respect to carbonate fluorapatite by and below 2 cm (Reimers et al., 1996). The Iberian margin, situated in the northeastern Atlantic, generally belongs to the more productive regions of the global ocean (Longhurst et al., 1995), however, sea- 870 sonal changes in upwelling creates a strong temporal variability in primary productivity and organic carbon deposition. Submarine canyons in this area (like the Nazaré Canyon) may deliver organic carbon from the shelf to the ocean interior (van Weering et al., 2002; Epping et al., 2002). For a more detailed description of the study areas and the experimental work, the interested reader is referred to the publications by Reimers et al. (1996) and Epping et al. (2002).

875 In OMEN-SED sediment characteristics and boundary conditions are set to the observed values where available (Table 13). Other sediment characteristics (e.g. sedimentation rate, porosity, density), stoichiometric factors and secondary reaction parameters are set to the default value (see Tables 9 and 10). Organic matter is modelled as two fractions, with different first-order degradation rate constants. The POC and pore water profiles were fitted by optimizing the POC partitioning into 880 the fast and slow degrading pool and their respective first-order degradation rate constants (priority is given to reproduce the POC and O_2 profiles). For phosphorus the equilibrium concentration for authigenic P formation (PO_4^{a}) was adjusted to fit the PO_4 concentration at z_∞ .

3.2.2 Results

Fig. 7 compares modelled and observed sediment profiles for the Santa Barbara Basin and the Iberian 885 margin. Results show that OMEN-SED is able to capture the main diagenetic features across a range of different environments without changing model parameters (e.g. stoichiometric ratios or secondary reaction parameters) to site specific conditions. For the two open Iberian margin stations (108 and 2213 m) OMEN-SED fits all observations well. OMEN-SED does especially well at seafloor depth (SFD) 2213 m by reproducing the deep O_2 penetration and the subsurface maximum

Table 13. Model boundary conditions for the simulated sediment profiles in the Santa Barbara basin (108 and 2213 m) and Iberian margin (585 and 4298 m) reported in Figure 7. For all sites a DIC bottom water concentration of 2,400 nmols cm⁻³ is assumed.

Sediment characteristics:							
Depth (m)	Temp. (°C)	z_{bio} (cm)	D_{bio} (cm ² yr ⁻¹)	POC ₁ (wt%)	POC ₂ (wt%)	k ₁ (yr ⁻¹)	k ₂ (yr ⁻¹)
108	12.5	1.0	0.02	2.64	1.8	0.65	$1.0e^{-5}$
585	5.85	0.01	0.02	2.0	3.5	0.2	$8.0e^{-4}$
2213	3.2	10.0	0.17	0.45	0.5	0.1	$4.0e^{-4}$
4298	2.5	4.2	0.18	0.83	1.2	0.052	$1e^{-5}$

Bottom water concentrations of solutes (all in nmol cm⁻³):								
Depth	O ₂	NO ₃	SO ₄	NH ₄	H ₂ S	PO ₄	PO ₄ ^a	Alkalinity
108	210	9.6	28,000	0.4	0.0	0.0	15.0	2,400
585	10	25.0	28,000	0.0	0.0	50.0	90.0	2,480
2213	250	25.0	28,000	0.6	0.0	0.0	5.0	2,400
4298	243	30.1	28,000	0.22	0.0	0.0	5.0	2,400

890 in NO₃ concentration due to the nitrification of NH₄ (note, that NH₄ is overestimated at this SFD). For the anoxic Santa Barbara Basin (585 m) the decrease in SO₄ and the increase in ALK concentration with sediment depth is well represented, indicating the importance of sulfate reduction as the primary pathway of OM degradation at this site (compare with Meysman et al., 2003). However, a misfit is observed for H₂S and PO₄ in the upper 20 cm of this sediment core. The discrepancy 895 for H₂S can be explained by high iron(III) hydroxide concentrations, which is reduced to degrade organic matter (especially in the 2 – 4 cm depth interval), therefore placing the beginning of the sulfate reduction zone and the production of H₂S to the deeper sediments (Reimers et al., 1996). Iron processes are currently not dynamically represented in OMEN-SED. In addition, produced dissolved Fe reacts with H₂S to form iron sulfides (e.g. pyrite, FeS₂) and thus further inhibits the rise 900 of H₂S (Reimers et al., 1990). The iron cycle also plays a critical role for phosphorus, as the reduction of iron(III) hydroxides in the surface sediments releases sorbed phosphate, leading to pore waters around and below 2 cm which are supersaturated with respect to fluorapatite, thus initiating CFA precipitation. Reimers et al. (1996) could even show that the accumulation of CFA is mainly restricted to the near-surface sediments (~ 5 cm) instead of throughout the sediment column. As 905 OMEN-SED does not include an iron-cycle, and Fe-bound P and CFA processes are highly parameterised, the model is not able to capture these complex, non-steady state phosphorus dynamics at this specific site. For the Nazaré Canyon station (4298 m) satisfactory fits could be realised apart from NH₄. However, also Epping et al. (2002) could not obtain a better fit using a more complex diagenetic model. They suggested non-local solute exchange resulting from bioirrigation being re-

910 sponsible for the higher NH_4 concentrations at this site which is neglected in their model, as well
 as in OMEN-SED. Furthermore, the fractured POC profile (indicating episodic depositional events
 through the canyon) could have been approximated using a different partitioning of the bulk POC
 into labile and refractory pool with different degradation rate constants, thus potentially leading to a
 better fit of the NH_4 profile. In general, better approximations of the data could have potentially been
 915 acquired by applying a sensitivity study using different NC-ratios (e.g. Epping et al., 2002, report
 different ratios from Redfield stoichiometry) and exploring the parameter space for the secondary re-
 action parameters (γ_{NH_4} , $\gamma_{\text{H}_2\text{S}}$). However, considering these generalisations and our assumption of
 steady-state, which might not be valid, particularly for the complex Santa Barbara basin, the shallow
 core and the Nazaré Canyon, which are affected by seasonality and biology, OMEN-SED performs
 920 well in capturing the main diagenetic processes.

3.3 Case study: Stand-alone simulations of global ocean transect

3.3.1 Methodology

In this section it is tested to which degree OMEN-SED is capable of capturing the dynamics of or-
 ganic matter degradation pathways and related TEA-fluxes as simulated with a complete, numerical
 925 diagenetic model. Therefore, we reproduce the simulations of typical conditions along a global ocean
 hypsometry of Thullner et al. (2009) and compare our modelled TEA-fluxes with the results of the
 complete model as well as with observations from Middelburg et al. (1996). To explore the global
 degradation of OM in the seafloor Thullner et al. (2009) quantified various diagenetic processes
 930 using the Biogeochemical Reaction Network Simulator (BRNS, Aguilera et al., 2005), a flexible
 simulation environment suitable for reactive transport simulations of complex biogeochemical prob-
 lems (e.g. Jourabchi et al., 2005; Thullner et al., 2005). Thullner et al. (2009) used seafloor depth
 (SFD) as the master variable and calculated model parameters, such as w , D_{bio} and ϕ , from existing
 empirical relationships (e.g. Van Cappellen and Wang, 1995; Middelburg et al., 1997). Organic mat-
 ter degradation was described with a 1-G approach, thus assuming a single pool of organic matter
 935 of uniform reactivity. The first order rate constant was related to the burial velocity, w (cm year^{-1}),
 following the empirical relationship of Boudreau (1997):

$$k = 0.38 \cdot w^{0.59}. \quad (48)$$

This rate constant can be assumed as the mean reactivity of the organic matter fractions which
 are degraded in the upper, bioturbated 10 – 20 cm of the sediments. Thus, more reactive fractions
 940 (degraded during days/weeks close to the SWI) and more refractory fractions (degraded on longer
 time scales deeper in the sediments) are not captured by this relationship (Boudreau, 1997). BRNS
 simulations were performed using boundary conditions and parameters for depths representative for
 shelf, slope and deep sea sediments (i.e. SFD of 100m, 200m, 500m, 1000m, 2000m, 3500m and
 5000m). In order to reproduce these results, OMEN-SED is configured here as a 1-G model and

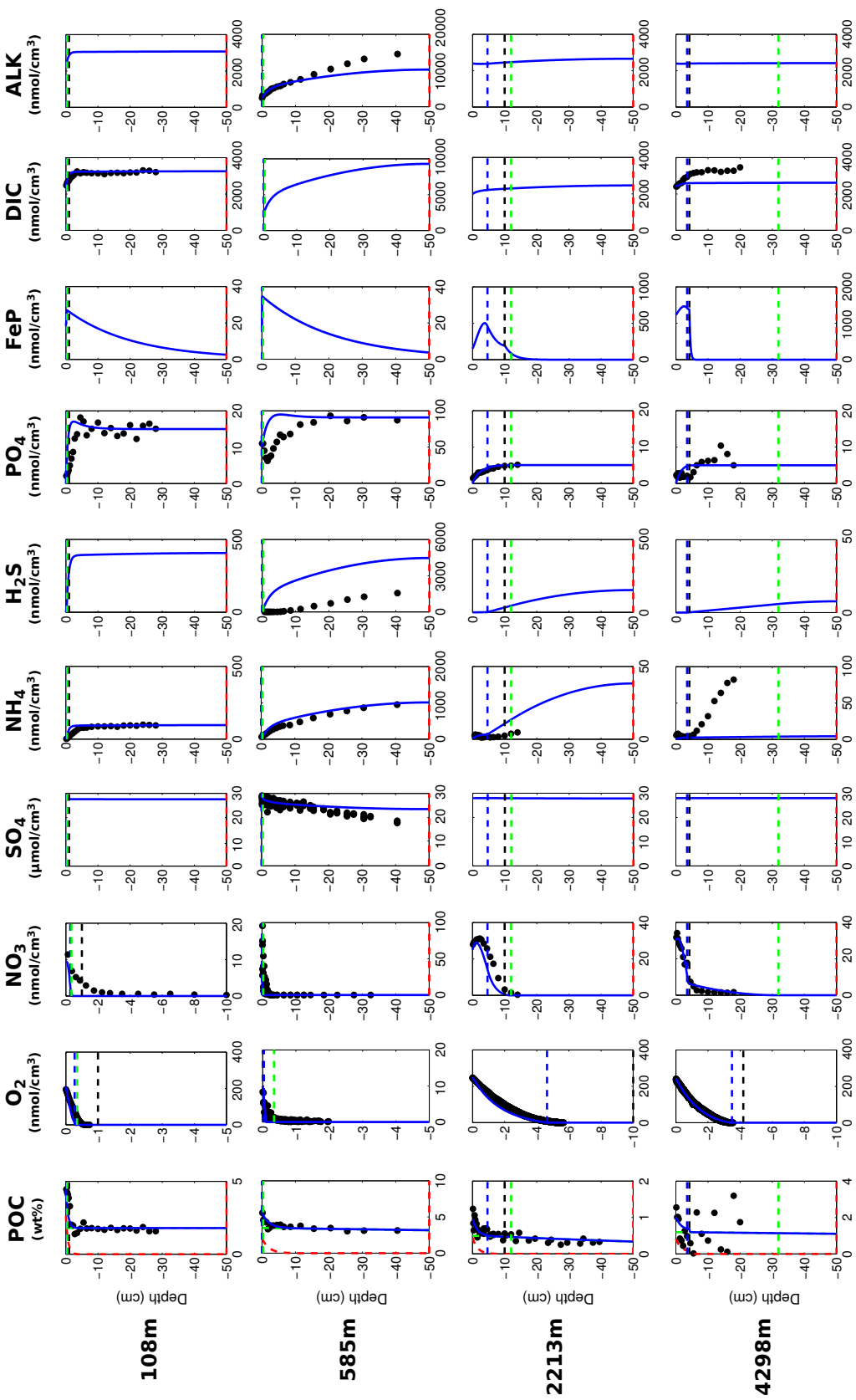


Figure 7. Modelled (curves) and measured (filled dots) solid phase and dissolved pore water profiles for four different sediment cores. Note that different scales are used for different stations. The blue POC curve represents the sum of the refractory (green) and labile (red) POC fraction. The horizontal dashed lines in each panel indicate the bioturbation depth (black) and the penetration depths of oxygen (blue), nitrate (green) and sulfate (red) as calculated by OMEN-SED.

boundary conditions and model parameters are defined as in Thullner et al. (2009, see Table 14). As OMEN-SED assumes a fixed fraction of reduced substances to be reoxidised, which exerts a large impact on the resulting SWI-fluxes (compare Section 3.1), two sets of simulations are performed in order to show the range of possible model outputs. In the first setup 95% of the reduced substances are reoxidised (i.e. $\gamma_{NH_4} = \gamma_{H_2S} = 0.95$) and in the second only 5% are reoxidised (all other model parameters and boundary conditions are equal).

Table 14. Seafloor depth dependency of key model parameters and boundary conditions (adapted from Thullner et al., 2009).

	Seafloor depth						
	100 m	200 m	500 m	1000 m	2000 m	3500 m	5000 m
Model parameters							
w^a (cm yr ⁻¹)	3.98×10^{-1}	3.60×10^{-1}	2.67×10^{-1}	1.62×10^{-1}	5.94×10^{-2}	1.32×10^{-2}	2.94×10^{-3}
D_{bio}^a (cm ² yr ⁻¹)	27.5	25.1	19.0	12.1	4.83	1.23	0.310
ϕ^b	0.85	0.85	0.80	0.80	0.80	0.80	0.80
T ^c (°C)	10.3	9.7	8.1	5.8	3.0	1.5	1.4
ρ_{sed}^c (g cm ⁻³)	2.5	2.5	2.5	2.5	2.5	2.5	2.5
k^d (yr ⁻¹)	0.221	0.208	0.174	0.130	0.0718	0.0296	0.0122
Upper boundary conditions							
POC _{flux} ^a (μmol cm ⁻² yr ⁻¹)	510	467	357	228	93.0	24.3	6.33
POC ^e (wt%)	0.79	0.78	0.55	0.50	0.42	0.32	0.25
O _{2,0} ^c (nmol cm ⁻³)	132	129	121	114	116	135	141
NO _{3,0} ^c (nmol cm ⁻³)	17.3	18.6	22.1	26.5	31.0	31.6	31.6
SO _{4,0} ^b (nmol cm ⁻³)	28,000	28,000	28,000	28,000	28,000	28,000	28,000

^a Derived from Middelburg et al. (1997).

^b Derived from Van Cappellen and Wang (1995).

^c Derived from Conkright et al. (2002).

^d Derived from Boudreau (1997).

^e Calculated with OMEN-SED from POC_{flux}.

950

3.3.2 Results

Figure 8 compares simulated SWI-fluxes of TEAs (i.e. O₂, NO₃ and SO₄) along the global hypsometry using OMEN-SED (black lines) with the results of Thullner et al. (2009) (red lines). Observations for O₂ and NO₃ fluxes are taken from Middelburg et al. (1996). Due to the applied empirical relations organic matter flux to the seafloor decreases by 2 orders of magnitude from 100 to 5000 m and its degradation rate constant by 1 order of magnitude (Table 14). Therefore, the rate of organic matter degradation is about 50 times greater at 100 m than at 5000 m (compare Thullner et al., 2009), thus resulting in a decrease of TEA-fluxes along the hypsometry (Figure 8). The 95%-reoxidation experiments (dots) show proportionally higher O₂ in-fluxes than the the 5%-reoxidation experiments

960 (triangles) because more O_2 is utilised for in situ production of NO_3^- and SO_4^{2-} in the sediments. This is also mirrored by the increased NO_3^- out-flux and decreased SO_4^{2-} in-flux for shallower SFDs. This is in line with the results of Thullner et al. (2009) which showed that in situ production is an important pathway of SO_4^{2-} supply in the sediment, which is responsible for $\sim 80\%$ of the total OM degradation at depths between 100 and 2000 m (SO_4^{2-} is not used for OM degradation in OMEN-SED 965 below 2000m). In general, Figure 8 shows that OMEN-SED captures the main trends in observed TEA fluxes well and fluxes calculated with BRNS fall within the range of possible OMEN-SED results.

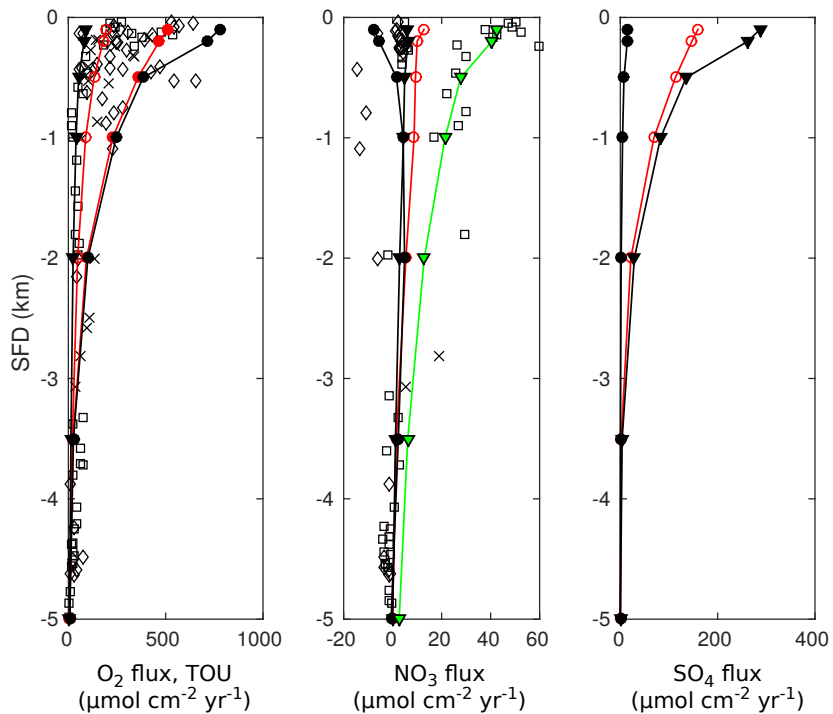


Figure 8. Fluxes of O_2 , NO_3^- and SO_4^{2-} to the sediment along the global hypsometry. Red lines (with open symbols) are modelled fluxes from Thullner et al. (2009) using BRNS; black lines are results from OMEN-SED (\bullet : $\gamma_{NH_4} = \gamma_{H_2S} = 0.95$; \blacktriangledown : $\gamma_{NH_4} = \gamma_{H_2S} = 0.05$). Observations of TEA fluxes are taken from Middelburg et al. (1996) (\diamond : Atlantic, \square : Pacific, \times : Arctic/Indian Ocean). Also plotted in Figure (A) are the total oxygen uptake (TOU) estimates of Thullner et al. (2009) (filled red symbols). The green line indicates OMEN-SED results for low oxygen/high nitrate levels and the lower NC-ratio. Negative values are directed out of the sediments.

In particular, the observed O_2 fluxes in the upper 2000m are well predicted by the two OMEN-SED simulations. Oxygen fluxes for the deep-sea sediments, however, are slightly underestimated. 970 These deviations can presumably be related to the assumed 1-G description of organic matter degradation, which neglects the more labile OM pool. This highly reactive pool is degraded close to the

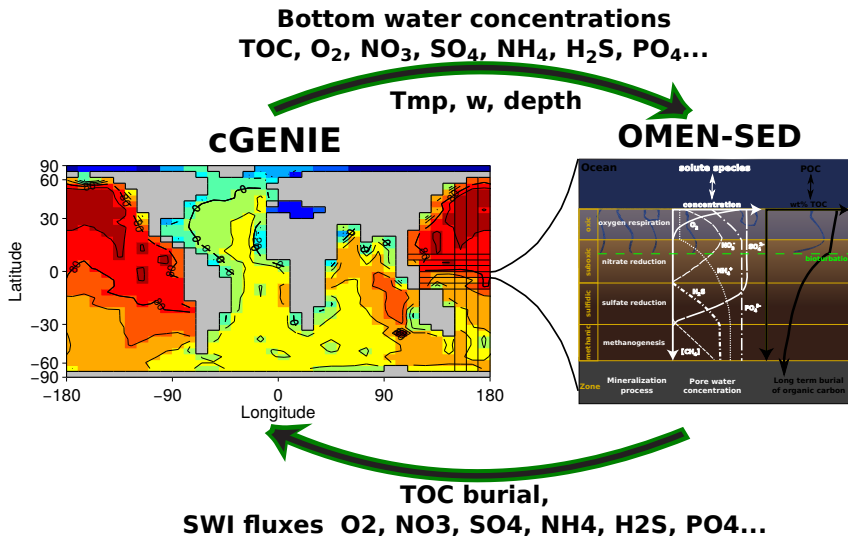


Figure 9. Schematic of the relationship between OMEN-SED and cGENIE. Arrows represent the information transferred between models.

sediment surface, thus promoting higher aerobic degradation rates and higher O₂ fluxes. Nitrate fluxes in the upper 500m of the Atlantic Ocean are well predicted. However, as in Middelburg et al. (1996) the direction of calculated nitrate fluxes in the upper 1000m of the Pacific Ocean differ from the observations. Middelburg et al. (1996) related these discrepancies to the globally averaged model parameters and the applied boundary conditions. They could reduce the disagreements significantly by using more representative bottom water concentrations for the eastern Pacific and a higher flux of labile organic matter for their 2-G model. By changing the boundary conditions and the NC-atomic ratio of organic matter for the whole hypsometry, it is possible to obtain a better model-data fit with OMEN-SED for the shallow Pacific Ocean (green line in Fig. 8B). Bohlen et al. (2012) report that the atomic NC-ratio strongly deviates from Redfield stoichiometry (0.151) with specifically lower values for the East Pacific Ocean. The use of their globally averaged value of 0.067 allows reconciling modelled and observed values provided that bottom water conditions are also changed to the low oxygen/high nitrate levels more likely to be found in the shallow Pacific Ocean (O₂ = 10 nmol cm⁻³ and NO₃ = 80 nmol cm⁻³).

4 Coupled pre-industrial Earth system model simulations

4.1 Coupling to the cGENIE Earth system model

OMEN-SED is coupled to the carbon-centric version of the “GENIE” Earth system model (cGENIE, Ridgwell et al., 2007) to illustrate the abilities of the newly developed model. The following section provides a brief description of cGENIE and the coupling procedure (Fig. 9). cGENIE is a model

of Intermediate Complexity based on the efficient climate model “C-GOLDSTEIN” of Edwards and Marsh (2005), featuring a frictional-geostrophic 3D-ocean circulation model coupled to a fast Energy-Moisture Balance 2D-atmosphere together with a dynamic-thermodynamic sea-ice component. The version of cGENIE used here includes the marine geochemical cycling of carbon, oxygen, phosphorus and sulfur (Ridgwell et al., 2007), preservation of carbonates in deep-sea sediments (SEDGEM, Ridgwell and Hargreaves, 2007) and terrestrial weathering (Colbourn et al., 2013). The ocean model is implemented on a 36×36 equal-area horizontal grid with 16 vertical levels using the pre-industrial continental configuration and bathymetry as in Archer et al. (2009). A finer grid (72×72) is used for the sediments (see Fig. 11C) and OMEN-SED is called by SEDGEM for each wet ocean grid point. Depending on the overlying biogeochemical ocean model, processes can be included or excluded in OMEN-SED and stoichiometric factors need to be adjusted to ensure preservation of mass. As nitrogen is not modelled explicitly in the employed cGENIE configuration, NC_i , ALK^{NIT} and ALK^{DEN} in OMEN-SED are set to zero. cGENIE, however, implicitly includes the effects of NH_4 release and its complete nitrification on alkalinity but neglects the impact of P release.

Therefore, alkalinity stoichiometries for aerobic degradation and sulfate reduction are changed to $ALK^{OX} = -16/106$ and $ALK^{SUL} = 122/106$, respectively (compare to default in Table 10).

Several biogeochemical tracers and parameters are transferred from SEDGEM to OMEN-SED and have to be converted into the required units. Bottom water concentrations of solutes are converted from $mol\ kg^{-1}$ to $mol\ cm^{-3}$ and the depositional flux of POC (POC_{flux}) is converted from $cm^3\ cm^{-2}\ yr^{-1}$ to $mol\ cm^{-2}\ yr^{-1}$ assuming an average density of POC of $1.0\ cm^3\ g^{-1}$. Within the water column in cGENIE, POC is partitioned into two fractions with different degradation length scales. The labile pool degrades while sinking through the water column, whereas the refractory pool is unreactive (Ridgwell et al., 2007). Thus, depending on seafloor depth, the partitioning of bulk POC reaching the sediments is different (Fig. 10A+B). This information is used by OMEN-SED to define the parameters f_1 and f_2 . Other parameters used from cGENIE are seafloor depth and local temperature. The advection/burial rate (w) is generally taken from cGENIE from the previous time-step, however, it is assured that w is not smaller than the detrital flux (Det_{flux}) to the sediments (e.g. $w < 0$ can occur if the sediments are being eroded during the spin-up of cGENIE). In case $w \leq Det_{flux} = 0.0$ all POC is remineralised at the ocean floor. Furthermore, a minimum value of $w = 0.4\ cm\ kyr^{-1}$ is imposed as OMEN-SED tends to be unstable for lower values. The bulk POC_{flux} is separated into the labile and refractory component and the routine to find the steady-state solution for POC is called. Here, the two POC depositional fluxes are first converted into SWI concentrations ($POC_i(z=0)$, in $mol\ cm^{-3}$) by solving the flux divergence equation:

$$\frac{\partial F}{\partial z} = -\frac{\partial}{\partial z} \left(-\xi D_i \frac{\partial POC_i}{\partial z} + \xi w POC_i \right) \quad (49)$$

for $z=0$. OMEN-SED then computes the fraction of POC preserved in the sediment (f_{POC} , see Eq. (5)) and subsequently calls the routines to find the steady-state solutions for the solute substances.

Note, that the calculated benthic uptake/return fluxes F_{C_i} of dissolved species C_i (compare Eq. (6)) have to be adjusted for the advective loss at the lower sediment boundary ($w \cdot C_i(z_\infty)$) to assure the preservations of mass in the coupled model:

$$1030 \quad F_{C_i} = \phi(0) \left(D_i \frac{\partial C_i(z)}{\partial z} \Big|_{z=0} - w [C_i(0) - C_i(z_\infty)] \right). \quad (50)$$

In case OMEN-SED computes unrealistic results for POC preservation (i.e. $f_{\text{POC}} < 0.0$ or $f_{\text{POC}} > 1.0$) we discard the results of OMEN-SED and all POC is remineralised at the ocean floor. Finally, f_{POC} and the SWI-fluxes of solutes (F_{C_i} , in $\text{mol cm}^{-2} \text{yr}^{-1}$) are returned to cGENIE. In case no POC is deposited on the seafloor (i.e. $\text{POC}_{\text{flux}} = 0$), OMEN-SED is not executed and f_{POC} and

1035 F_{C_i} for all i are set to zero. In order to reduce memory requirements the sediment profiles (e.g. as shown in Fig. 7) are not calculated in the FORTRAN version of OMEN-SED, however, the boundary conditions are saved at the end of the experiment and sediment profiles for specific grid-cells, ocean basins and ocean transects can be plotted using the stand-alone MATLAB version of OMEN-SED.

4.2 Parameterising the OM degradation rate constants in a global model

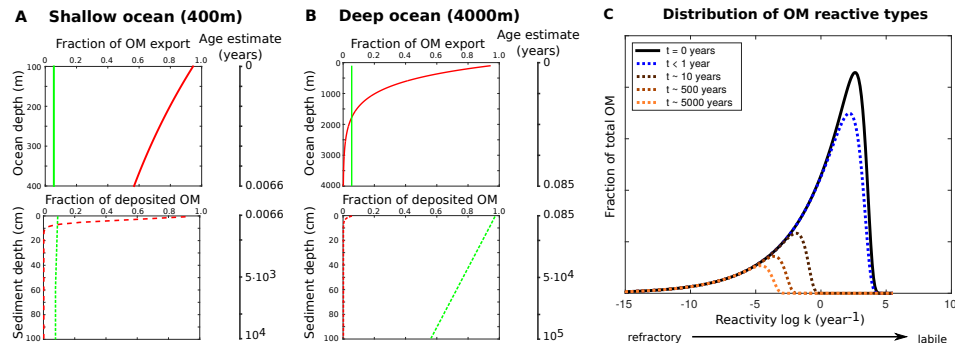


Figure 10. Idealised relationship of organic matter decomposition during remineralisation in the water column and the sediments. **A+B - Upper panels:** Water column development of the two organic matter fractions as represented in cGENIE for two ocean depths (red: labile OM with degradation length scale of 589m; green: refractory OM which is unreactive in the water column). The values are normalised to OM export at 100m. Age estimates for the OM since its export from the euphotic zone are calculated using a sinking velocity of 125m/day. **A+B - Lower panels:** Schematic representation of the development of the two OM fractions in the sediments (normalised to OM deposited on the seafloor). For the age estimates in the sediment column an advection rate of 0.01 and 0.001cm/yr is assumed, respectively. **C:** Idealised distribution functions of OM reactive types during remineralisation for different OM ages assuming a reactive continuum model for OM degradation. The initial distribution (at $t = 0$) represents fresh OM when it is exported from the euphotic zone (characterised by $a = 3e^{-4} \text{ yr}^{-1}$ and $\nu = 0.125$ Boudreau et al., 2008).

1040 As shown in our sensitivity analysis (Section 3.1) and discussed by Arndt et al. (2013) the degradation rate constants for OM (k_i) are the most influential parameters and strongly determine the

SWI-flux of redox-sensitive elements as well as the preservation of organic matter. Yet, their spatial variability is unknown at the global scale and reported rate constants in the sediments can vary by about 10 orders of magnitude or more (Middelburg et al., 1993; Arndt et al., 2013). Furthermore,
1045 when OMEN-SED is coupled to cGENIE very different timescales have to be considered for OM degradation in the sediments compared to the water column (Fig. 10A+B), thus rate constants cannot be easily adapted from cGENIE. Also, microbes tend to degrade the more reactive organic matter compounds first (Emerson and Hedges, 1988; Wakeham et al., 1997; Lee et al., 2000), thus depending on the age of OM (or depth in the sediment and water column) the reactivity distribution of its
1050 compounds changes significantly (Fig. 10). For instance, in the water column, represented by the reactivity distribution $t < 1$ year in Fig. 10C, only the most reactive OM compounds are remineralised. This explains why the POC flux in the ocean can be represented with a 1G or pseudo 2G degradation model. In the sediments much longer timescales have to be considered, thus also more reactive compounds are degraded and the reactivity distribution changes significantly already in the
1055 upper mm of the sediments ($t \sim 10$ years, Fig. 10C). Therefore, a broader range of OM reactive types must be represented by the degradation model to capture the reactivity spectrum of OM in surface sediments, explaining why at least a pseudo 3G model is required (including two degradable and one refractory fraction Soetaert et al., 1996; Boudreau, 1997; Stolpovsky et al., 2015). In addition, the advection rate in the sediments determines the age of OM at a specific sediment depth and thus
1060 its reactivity. For instance, assuming an advection rate of 0.01 cm/yr for the shallow ocean, OM at 5cm depth is about 500 years old, whereas it is one order of magnitude older for an advection rate of 0.001 cm/year in the deep ocean and thus covers a broader range of reactive types (Fig. 10C).

Thus defining appropriate OM degradation rate constants is a major challenge and source of uncertainty for diagenetic models. The rate constants in models are either determined through profile
1065 fitting for a specific site or, for global applications, they are related to a single, readily available characteristic (or master variable) of the local environmental conditions. For instance, considerable effort has been expended to relate the apparent rate constant for oxic and anoxic OM degradation to sedimentation rate (w) and various empirical relations have been proposed (Toth and Lerman, 1977; Tromp et al., 1995; Boudreau, 1997; Stolpovsky et al., 2015). Nevertheless, these relationships are
1070 generally based on limited data sets and their global applicability is questionable (Arndt et al., 2013).

4.2.1 Methodology

Our objective is not to perform and discuss a detailed calibration of the two models, as this is beyond the scope of this sediment model development paper. We rather want to showcase, that a coupling is possible and that the results show main sediment features one would expect to see on a global
1075 scale. Section 4.2.2 compares modelled mean POC weight percentages (wt%) in the upper 5cm of the sediments ($\text{POC}_{5\text{cm}}$) to the global distribution pattern of POC content in surface sediments (< 5cm sediment depth) of Seiter et al. (2004) using different parameterisations for the degradation rate

constants k_1 and k_2 . To this end, the original POC distribution pattern in $1^\circ \times 1^\circ$ grid resolution (interpolated from > 5500 measurements, compare Seiter et al., 2004) has been transformed onto the
 1080 72 \times 72 SEDGEM grid (Figure 11). The regridding of the original POC distribution obviously affects the resolution of the data, especially for the continental margin, as some sites with higher POC wt% are lost due to the restricted SEDGEM grid-resolution (compare e.g. maximum values for the East Pacific and upwelling waters of the Namibian shelf, Figure 11A + B). The colour of the points in Figures 12 - 14, which compare modelled and observed POC concentrations, represents SFD of the
 1085 respective cGENIE grid-cell. As the individual data-points are highly scattered and in order to see if a certain relation between k_1 and k_2 performs better for specific ocean depths, the data-points are binned into 6 uniform depth-classes of 1000m each (respective mean POC wt% and SFD are represented by the triangles). The regression line (and the corresponding R^2 -value) is calculated for the 6 bin-classes and included in the figures.

1090 **TODO Andy: Section describing the prescribed fields of solids (i.e. detrital, opal, CaCO_3) to the sediments!**

To parameterise the reactivity of organic matter in OMEN-SED two different approaches are compared. First, globally invariant degradation rate constants k_1 and k_2 are assumed. By providing two pools of POC from the water-column characterised by different degradation rate constants, cGENIE
 1095 accounts for the decrease in mean POC reactivity with water-depth. The rate constants for the more refractory OM pool, k_2 , is systematically varied between 0.004 and 0.006 year $^{-1}$ and the more labile OM component, described by k_1 , is assumed to degrade $x \in \{1.1, 1.2, 1.3, 1.5, 2\}$ times faster, respectively. However, although accounting for the decrease in mean POC reactivity with seafloor depth, this approach does not take into account the change in organic matter reactivity types caused
 1100 by different burial velocities and thus time scales in the sediments (Fig. 10). Therefore, the second approach uses the empirical relationship proposed by Boudreau (1997), which relates the apparent OM degradation rate constant in the upper sediments to the burial velocity, w (cm year $^{-1}$, see also Section 3.3):

$$k_{\text{app}} = 0.38 \cdot w^{0.59}. \quad (51)$$

1105 Following Boudreau (1997) and Stolpovsky et al. (2015) it can be assumed that k_{app} represents the mean OM reactivity within the upper 10-20cm of the sediments. The following assumptions are made in order to calculate the two degradation rate constants for OMEN-SED:

$$k_{\text{app}} = f_1 \cdot k_1 + f_2 \cdot k_2 \quad (52)$$

$$1110 k_1 = x \cdot k_2 \quad (53)$$

where x describes the relation between k_1 and k_2 and is subject to sensitivity experiments (with values of $x \in \{2, 5, 8, 10, 12, 15, 20, 25\}$). Note that the differences between k_1 and k_2 using this approach is significantly larger as in the invariant approach. As the fractions of labile and refractory

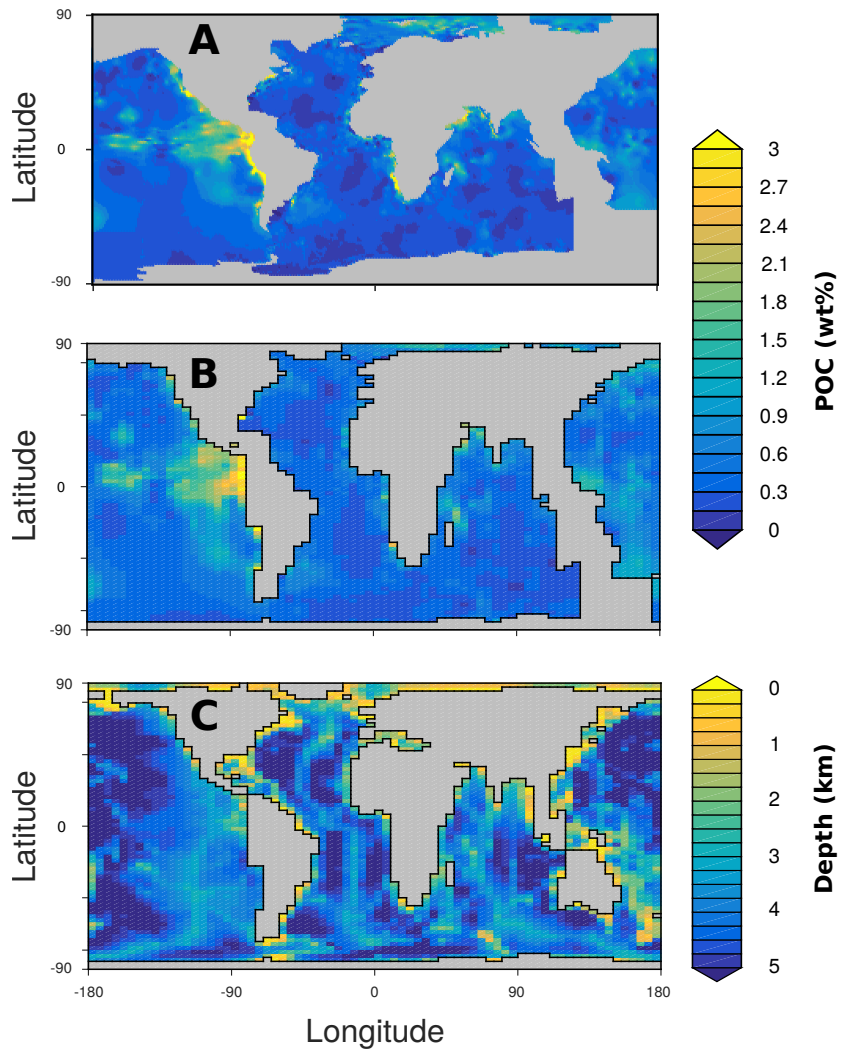


Figure 11. Observed distribution of sediment surface (< 5cm) POC wt% (A, B) and cGENIE bathymetry (C). (A) Original global distribution of POC wt% interpolated on a $1^\circ \times 1^\circ$ grid from more than 5500 individual data points (compare Seiter et al., 2004, for the interpolation procedure). (B) Observed POC wt% data transformed onto the 72×72 SEDGEM grid. Grid points without any observations are left blank (grey). (C) Gridded continental configuration and ocean bathymetry of the 16-level, 72×72 equal-area cGENIE grid.

OM reaching the sediments (f_1, f_2) is known from cGENIE, k_1 and k_2 can be calculated independently for each grid-cell. All simulations presented here are run for 10,000 years to steady-state from 1115 a 20,000 year cGENIE spin-up without OMEN-SED. The new model OMEN-SED is called for each grid-cell in every time step, feeding back the resulting SWI-fluxes and the fraction of POC preserved in the sediments to cGENIE.

4.2.2 Results

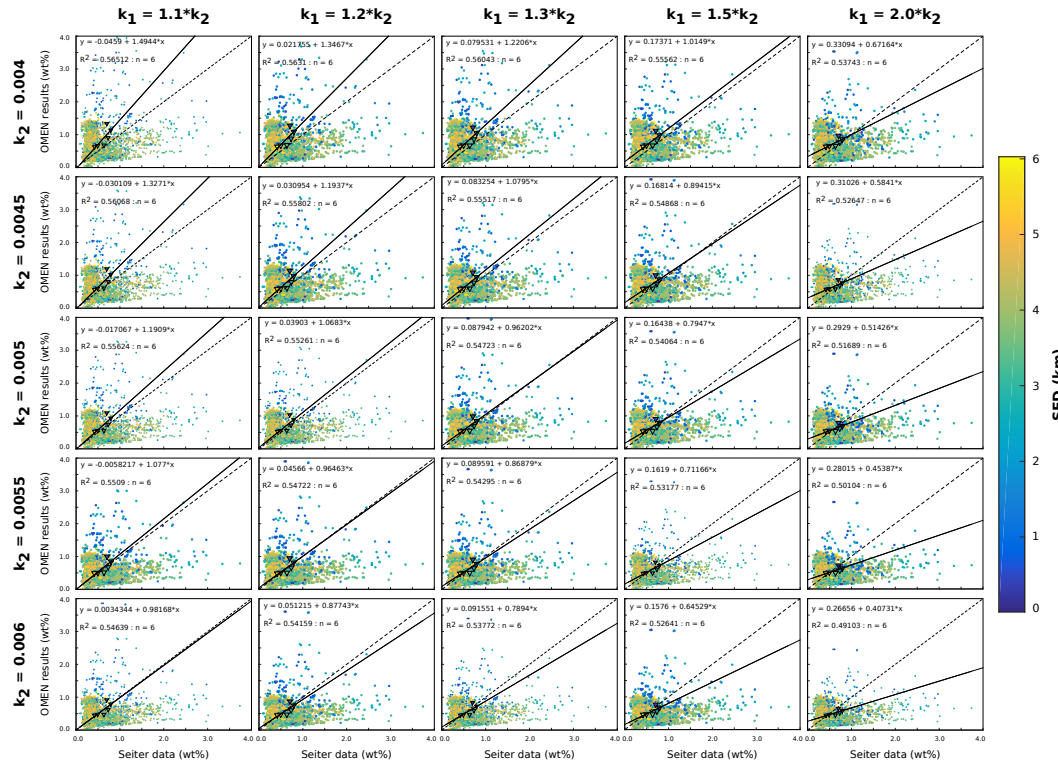


Figure 12. Crossplots comparing modelled and observed mean POC wt% in the upper 5 cm of the sediments using globally invariant degradation rate constants k_1 and k_2 . Data-points are binned into 6 uniform depth-classes of 1000m as in Fig. 13, each class is represented by a triangle. Grid-points with more than 4.0 POC wt% are not shown.

1120 Figure 12 presents results for the globally invariant degradation rate experiments. In general, using
globally invariant degradation rate constants 5 of the 6 bin-classes are located closer to the 1:1 line
as in the experiments using the Boudreau (1997) relation (Fig. 13). Also the slope of some regression
lines is close to 1.0 (e.g. $(k_2, x) \in \{(0.004, 1.5), (0.0045, 1.3), (0.005, 1.2), (0.005, 1.3), (0.0055, 1.1), (0.0055, 1.2), (0.006, 1.1)\}$),
indicating that the simpler parameterisation adequately captures the relationship between between
1125 depth and observed POC wt% by bin-class. The shallowest bin-class (between 0 and 1000m) repre-
sents an exception, as OMEN-SED tends to overestimate POC preservation for this depth class.

However, this could also be related to the regridding of the original POC distribution pattern of (Seiter et al., 2004) on to the SEDGEM grid, as some data grid-cells with higher POC wt% on the continental margin are lost due to the restricted SEDGEM resolution (compare Section 4.2). Overall, 1130 using this parameterisation a relationship where the labile POC fraction degrades not more than 1.5 times faster than the refractory fraction fits the Seiter et al. (2004) data better than a larger spread between both POC pools (i.e. $x > 2.0$).

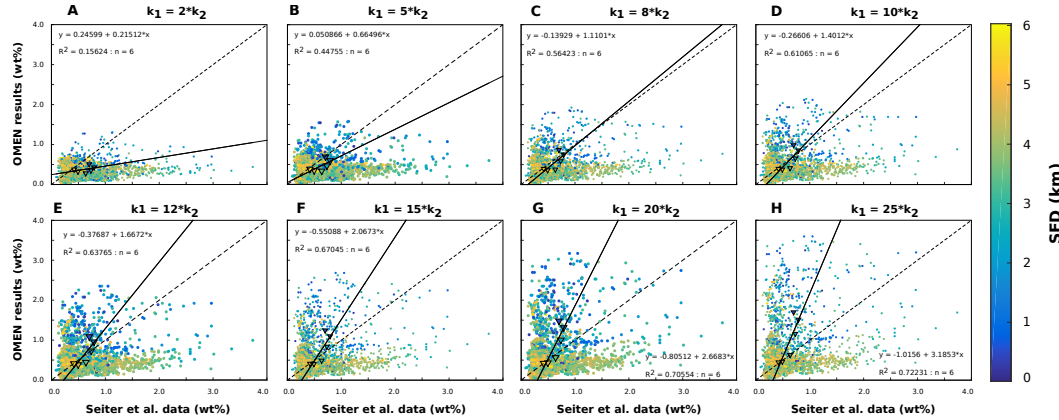


Figure 13. Crossplots comparing modelled and observed mean POC wt% in the upper 5 cm of the sediments using the relationship of Boudreau (1997) and the assumptions of Eq. (52) and (53) to calculate k_1 and k_2 . Data-points are binned into 6 uniform depth-classes of 1000m, each class is represented by a triangle. Grid-points with more than 4.0 POC wt% are not shown.

Next the relationship of Boudreau (1997) and the assumptions of Eq. (52) and (53) are used to calculate k_1 and k_2 . In Figure 13 (A-H) the relation between the two degradation rate constants 1135 (Eq. (53)) is changed globally, thus independent of the seafloor depth. The crossplots show that it is not possible to achieve a solution where all bin-classes fall onto, or close to, the 1:1 line. Also, the slope of the regression lines are generally much larger or smaller than 1.0 (with the exception of Figure 13C), indicating that the relationship between depth and observed POC wt% by bin-class is not adequately represented by the model. The R^2 values are strictly monotonically increasing for 1140 increasing x because a depth-dependency is artificially imposed for the modelled POC wt% through the relation between k_1 and k_2 . When looking at the individual bin-classes it can be seen that shallow ocean depths are better represented by smaller differences between k_1 and k_2 (e.g. $k_1 = 5 \cdot k_2$ for SFD < 1000m, Figure 13B), and the deep ocean by a larger spread (e.g. $k_1 = 25 \cdot k_2$ for SFD > 3000m, Figure 13H). These results reflect the preferential degradation of more reactive organic matter types 1145 (Wakeham et al., 1997; Lee et al., 2000) and thus the change in the distribution functions of OM reactive types for different OM ages (Fig. 10C). In the shallow ocean bulk POC consists of fresher organic matter types and is therefore generally more reactive (i.e. higher k_{app} due to higher w in the model) as in the deep ocean. In addition, OM at 5cm sediment depth in the deep ocean is generally

older as in the shallow ocean due to lower burial rates, therefore more reactive types are affected by
 1150 degradation and a larger spread between k-values is needed to capture these dynamics (compare Fig.
 10C).

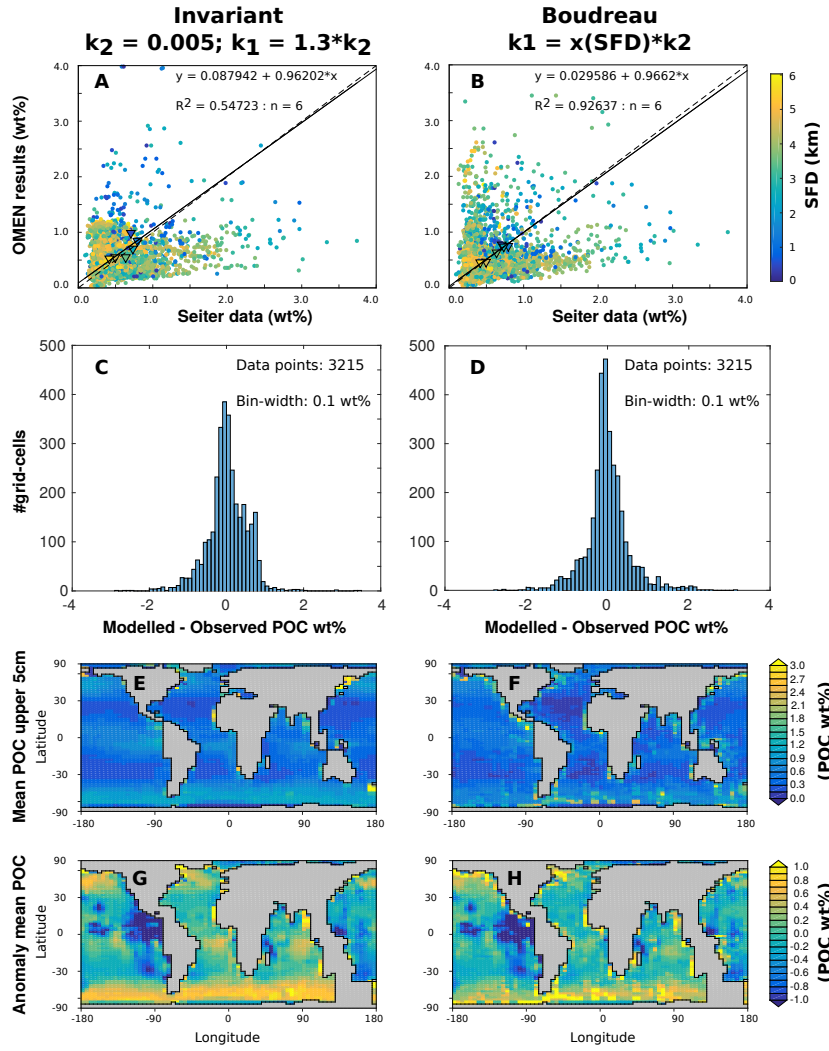


Figure 14. Mean POC concentrations in the upper 5cm of the sediments ($\text{POC}_{5\text{cm}}$) using the invariant model ($k_2 = 0.005$, $k_1 = 1.3 \cdot k_2$) and the depth dependent parameterisation $k_1 = x(\text{SFD}) \cdot k_2$ adapted from Boudreau (1997). A+B: Crossplots as shown before in Fig. 12 and 13. C+D: Histograms of the residuals of modelled minus observed $\text{POC}_{5\text{cm}}$. E+F: $\text{POC}_{5\text{cm}}$ as calculated with OMEN-SED. G+H: Difference map of $\text{POC}_{5\text{cm}}$ as calculated with OMEN-SED and interpolated data from Seiter et al. (2004).

We use these observations to create a depth dependent relationship between the two degradation rate constants, where x in Eq. (53) is a function of SFD and takes values of $x = 5$ for $\text{SFD} < 1000\text{m}$, $x = 8$ for $1000\text{m} \leq \text{SFD} < 2000\text{m}$, $x = 12$ for $2000\text{m} \leq \text{SFD} < 3000\text{m}$ and $x = 25$ for $\text{SFD} \geq$

1155 3000m for the 6 SFD bin-classes, respectively. In this depth dependent approach all bin-classes are
close to the 1:1 line and the resulting regression model accounts for 92.6% of the variance of the
modeled POC wt% around the observed mean of the bin-classes (Figure 14A). Furthermore, the
slope of the regression line (0.9662) indicates that the relationship between depth and observed POC
wt% for the bin-classes is well represented by the model. The histograms (Fig. 14C+D) visualize
1160 the difference between modelled and observed mean POC concentrations and demonstrate the high
density of data points close to the 1:1 line. For the depth dependent approach, 92.5% of the cGENIE
grid-cells show a difference between modelled and observed POC concentration of less than 1.0 POC
wt%; in 79.9% of the grid-cells, the difference is less than 0.5 POC wt% (for the invariant approach
the percentages are 95.37% and 70.95%, respectively). Both experiments reproduce minimal POC
1165 concentrations in the subtropical gyres and generally higher concentrations along the continental
margins (Fig. 14E+F). Both experiments, however, underestimate mean POC wt% in the surface
sediments of the equatorial east Pacific and overestimate POC concentrations in the North Pacific
and Southern Oceans (Fig. 14G+H). The depth dependent approach of Boudreau (1997) shows more
spatial variability in POC preservation than the other parameterisation. In general, implementing
1170 lower, anaerobic degradation rate constants when bottom water oxygen concentrations fall below a
threshold value could potentially improve the simulation of higher POC concentrations in areas with
high POC input to the sediments (Palastanga et al., 2011).

4.3 Modelled fluxes and sediment characteristics

For the globally invariant experiment A ($(k_2, x) = (0.005, 1.3)$) modelled SWI-fluxes and sediment
1175 characteristics are shown in Figure 15. Modelled total POC degradation (POC_{degr}) rates in the
upper sediments decrease from the shelves to the deep sea by up to 2 orders of magnitude (Fig.
15B). This is in agreement with data from the literature (e.g. Middelburg et al., 1993, 1997) and
other model results (e.g. Thullner et al., 2009) which indicate that the highest degradation rates in
marine sediments are found in the coastal ocean ($\text{SFD} < 200\text{m}$). Oxygen fluxes into the sediments
1180 (Fig. 15C) range from 0.0 for the deep ocean and sites without OM deposition to values of about
 $300 \mu\text{mol cm}^{-2}\text{yr}^{-1}$ for the shallow ocean with the highest POC degradation rates. Influx of SO_4
into the sediments is rather low (between 0.0 and $23.9 \mu\text{mol cm}^{-2}\text{yr}^{-1}$) because in OMEN-SED
95% of produced H_2S is reoxidised to SO_4 , therefore sulfate reduction is mainly driven by in situ
sulfide oxidation. However, in general the coupled model fluxes fall well within the ranges predicted
1185 by the stand-alone global hypsometry experiments (O_2 between 0.0 and $800 \mu\text{mol cm}^{-2}\text{yr}^{-1}$ and
 SO_4 between 0.0 and about $300 \mu\text{mol cm}^{-2}\text{yr}^{-1}$, compare Section 3.3). In accordance with the total
POC degradation rates the release of PO_4 shows a maximum value of $8.12 \text{ nmol cm}^{-2}\text{yr}^{-1}$ on the
shelves (Fig. 15D). The relative contribution of aerobic POC degradation in the upper sediments
increases from the shelves to the deep sea (Fig. 15G) which is also consistent with estimates from
1190 Thullner et al. (2009) who found that oxygen is responsible for less than 10% of POC_{degr} at 100m

$$\text{Boudreau } k_1 = x(\text{SFD}) \cdot k_2$$

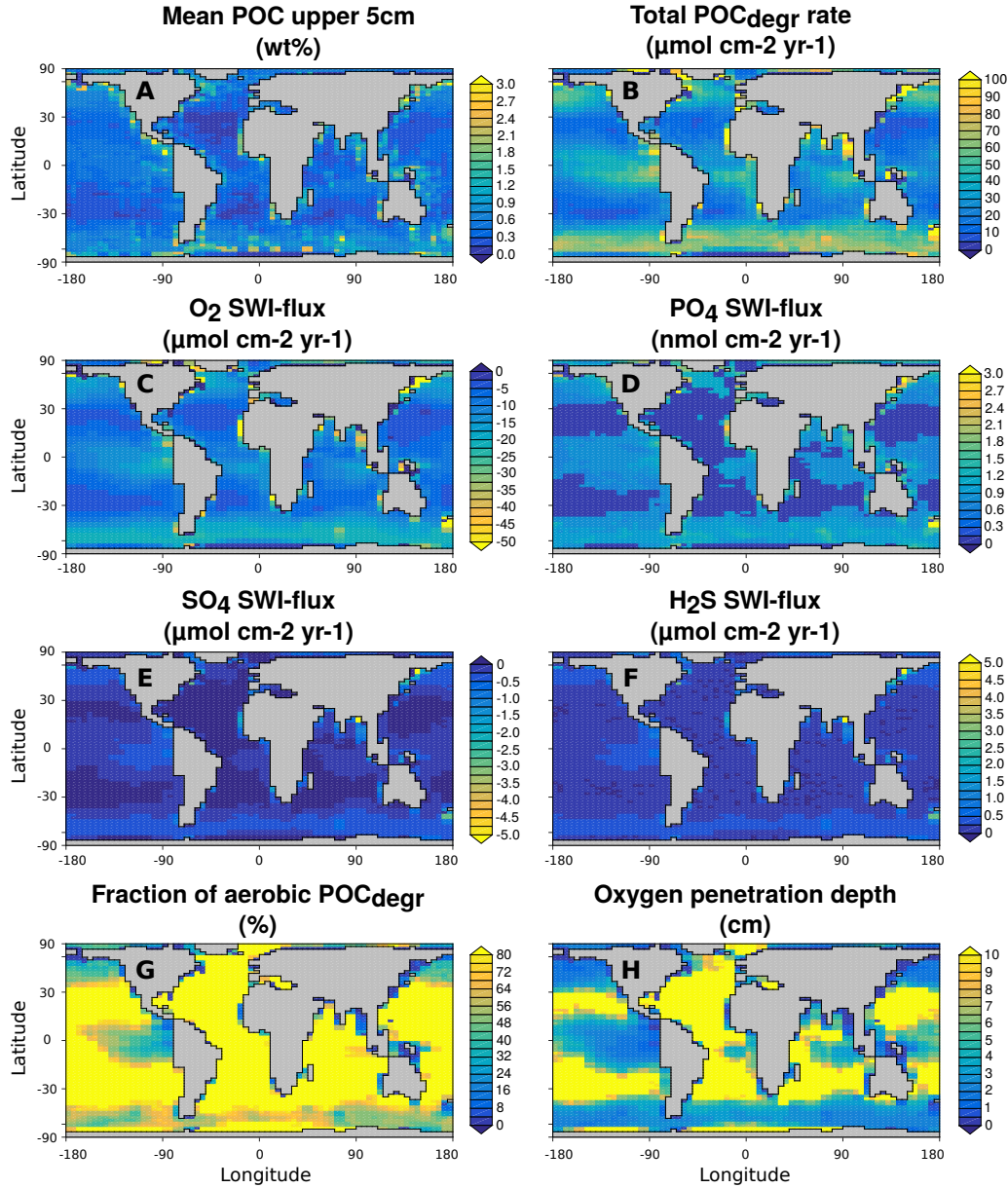


Figure 15. Sediment characteristics related to POC degradation and oxygen consumption for the depth dependent parameterisation after Boudreau (1997) with $k_1 = x(\text{SFD}) \cdot k_2$. Total POC_{degr} rate and fraction of aerobic POC_{degr} are the respective values for the first 5cm in the sediments.

SFD and for more than 80% in the deep sea. The oxygen penetration depth in OMEN-SED increases from values below 1cm at the shelves to more than 10cm in the deep ocean (Fig. 15H and 16). Small oxygen penetration depths of a few millimetres are typical for bioturbated sediments in the coastal ocean (e.g. Wenzhöfer and Glud, 2002) and the oxygen penetration depth has been shown
 1195 to increase exponentially with SFD to more than 10cm in the deep sea (Meile and Van Cappellen, 2003; Glud, 2008). Fischer et al. (2009) even found cores along a transect in the South Pacific gyre being oxygenated over their entire length (up to 8m) which is consistent with our model results (not shown). Simulated mean oxygen penetration depths for the 6 depth bin-classes also agree well with observations compiled by Meile and Van Cappellen (2003, Fig. 16).

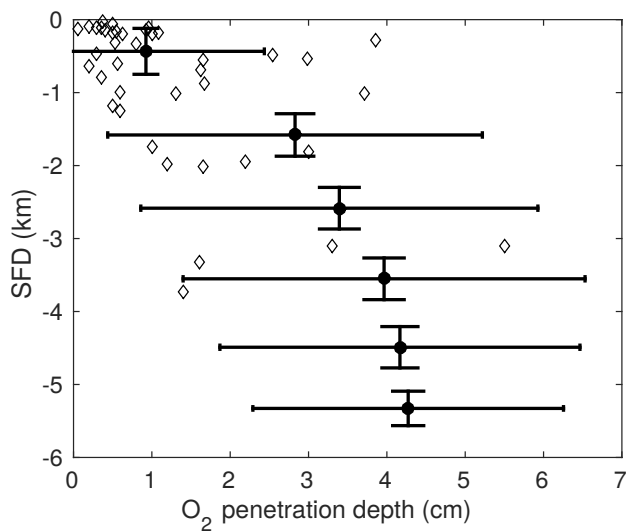


Figure 16. Seafloor depth versus O₂ penetration depth for the depth dependent parameterisation after Boudreau (1997) with $k_1 = x(\text{SFD}) \cdot k_2$. Diamonds represent the observations compiled by Meile and Van Cappellen (2003). Circles are the mean model results for the 6 SFD bin-classes (with standard deviations). Grid-cells where the entire sediment column is oxic (i.e. $z_{\text{ox}} = 100\text{cm}$) are not considered in these statistics (17, 32, 102, 300, 477 and 307 cells for the 6 bin-classes, respectively).

1200 5 Scope of applicability and model limitations

State-of-the art numerical models representing the full complexity of the diagenetic processes typically perform adequately at reproducing site-specific biogeochemical dynamics, however, tuning model parameters is laborious, the computational demand is high and, thus, their transferability to the global scale is limited. On the other hand, analytical models are very efficient, but existing approaches coupled to global models generally use highly simplified reaction networks, often restricted to oxic degradation with a limited number of explicit pore water tracers. However, our ability to
 1205

assess the role of organic matter dynamics for global biogeochemical cycles and climate requires tools that resolve the most important biogeochemical processes and tracers explicitly, while at the same time are computationally efficient and have a degree of predictive capability to extrapolate knowledge to data poor areas. The new model OMEN-SED presented here is a legitimate compromise between complexity of biogeochemical processes and computational efficiency. Its scope of applicability covers the entire range from regional to global scales. OMEN-SED's computational efficiency facilitates its use in two very different ways. Firstly, it can be coupled to global Earth system models and therefore allows the investigation of coupled global biogeochemical dynamics over different timescales. Secondly, it can be used to calculate quantitative sensitivity indices requiring large sample sizes such as variance- or density-based approaches. Therefore, OMEN-SED can help to quantitatively investigate how systematic variations in model parameters impact the model output, for instance when the model has been tuned to a site-specific problem. Due to the represented anaerobic processes and secondary-redox reactions, OMEN-SED is also useful to investigate the role of benthic-pelagic coupling on the development of ocean anoxia and euxinia for instance during extreme climate events such as OAEs. On more regional scales it can be applied to systems like continental margins or estuaries which are characterised by complex interactions between different pathways of organic matter degradation and redox reactions. Here, the model can help to disentangle the complex process interplay that drives the biogeochemical dynamics and give quantifications for upper and lower constraints of carbon and nutrient budgets for these dynamic systems. In addition, OMEN-SED can be used to model eutrophication processes in shallow coastal waters as sediment-water oxygen and nutrient exchange fluxes are explicitly modelled and depend on reoxidation of reduced substances which causes a substantial part of oxygen consumption in these environments.

However, the model presented here, despite being more complete than previous analytical models, is still associated with a certain degree of simplifications. In order to solve the diagenetic equation analytically important assumptions have been made, which limit the general applicability of the model. One of the most important simplifications is assuming steady-state. When coupled to an Earth system model this assumption is only valid if the relevant variability in boundary conditions and fluxes is generally longer than the characteristic timescales of the reaction-transport processes. In that case the sediment column can be described by a series of pseudo steady-states as it is done in OMEN-SED. Consequently, the model can be used for investigating the long term effects of changes in boundary conditions such as input of OM or bottom water oxidation state on degradation and burial dynamics, for instance during OAEs. Yet, OMEN-SED is not able to predict the system response to short-term or seasonal variations of boundary conditions. Furthermore, the separation of the sediment column into distinct biogeochemical zones and the resulting lack of overlap in degradation pathways may cause distorted organic matter degradation rates for the different TEAs. For instance, in OMEN-SED denitrification does not occur in the oxic zone, while in reality, although inhibited by the presence of oxygen, denitrification can still occur in the oxic zone, even at shallow sediments

depths with high OM contents. Manganese and iron are not represented and as such OMEN-SED
1245 is not able to model all processes important in coastal marine environments and highly accumulating upwelling regions. Furthermore, it limits the scope of applicability of the model, especially in systems characterized by high Fe oxide inputs and anoxic conditions, where redox driven iron dissolution-precipitation reactions induce a high internal recycling of the sedimentary Fe pool. This can cause problems when modelling H₂S and PO₄ profiles in anoxic environments as their concentrations are affected by these metal ions (compare Section 3.2). The model also simulates DIC and alkalinity production and, thus, has the potential to predict pH profiles within the sediment. A major limitation at this stage is the lack of representation of CaCO₃ precipitation/dissolution coupled to OM decomposition, which also controls the inorganic carbon system (Krumins et al., 2013). In addition the depth invariant porosity limits the correct calculation of the sediment-water interface flux
1250 of dissolved species as in reality porosity decreases with sediment depth.
1255

6 Conclusions

In this paper we have described and tested a new, analytical early diagenetic model resolving organic matter cycling and associated biogeochemical dynamics called OMEN-SED. Our new model is the first analytical model to explicitly represent oxic degradation, denitrification, sulfate reduction and
1260 implicitly methanogenesis, as well as the reoxidation of reduced substances produced during organic matter degradation. Pore water tracers include O₂, NO₃, NH₄, SO₄, H₂S, DIC and ALK and the solid phase includes two degradable fractions of organic matter, Fe-bound P and authigenic Ca-P minerals. We have shown that the new analytical model is able to reproduce observed pore water profiles from different ocean depths when organic matter partitioning and degradation rate constants
1265 are tuned to site specific conditions. An extensive sensitive analysis, based on the novel density-based PAWN method (Pianosi and Wagener, 2015), has been performed to asses the importance of 11 internal model parameters for all resulting SWI-fluxes. The results reveal that the degradation rate constant for labile organic matter is the most influential parameter for all model outputs. Under anoxic conditions secondary redox parameters exert an important control on related SWI-fluxes of
1270 SO₄, H₂S, NH₄ and alkalinity. In addition, the sensitivity analysis showed that produced model results fall well into the range of globally observed benthic O₂ and NO₃ fluxes. OMEN-SED is also used to quantify terminal electron acceptor fluxes across the sediment-water interface associated with organic matter degradation along a global ocean hysometry. The results demonstrate that OMEN-SED is capable of capturing most of the dynamics simulated with a complex, numerical diagenetic
1275 model and our model results fall well within the range of observed fluxes. Furthermore, the coupling of OMEN-SED to the Earth system model cGENIE is described and globally invariant degradation rate constants as well as the empirical relationship of Boudreau (1997) for the apparent first order degradation rate constant are tested to fit modelled to observed global organic matter concentrations.

Generally, large scale patterns of modelled surface sediment organic matter concentrations are in
1280 agreement with observations of Seiter et al. (2004) and calculated SWI-fluxes and sediment characteristics are consistent with estimates from the literature. However, results also show that **smaller scale OM degradation dynamics** in the sediments are too complex in time and space to be adequately represented using globally invariant or depth-independent OM rate constant parameterisations. More work is needed to develop and test mechanistic parameterisations relating degradation rate constants
1285 to available environmental parameters (e.g. bottom water oxygenation, burial rate, seafloor depth) in order to model the heterogeneous reactivity distribution of OM types due to preferential degradation and different time scales in the sediments. Due to its computational efficiency the coupled model presented here can be used to explore these questions using large simulation ensembles and objective statistical methods for sensitivity analysis. Furthermore, as the major parts of the global carbon
1290 cycle are included in the new model it is well suited to examine the role of sediments for global biogeochemical cycles and climate and for exploring feedbacks within the Earth system in response to a wide range of perturbations and over various timescales.

DH: Not sure, how to express this in a better way!?

7 Code Availability

The OMEN-SED source code (Fortran and Matlab) related to this article is provided as a supplementary package together with a ReadMe file, where hardware and software requirements, source code files and model output file management are fully described.
1295

Appendix A: Reaction Network

Appendix B: Sensitivity Analysis

B1

1300 *Acknowledgements.* We thank Claire Reimers and Filip Meysman for supplying the dataset from the Santa Barbara Basin, as well as Martin Thullner and Jack Middelburg for making the BRNS results and observations included in Section 3.3 available. We are also grateful to Andy Dale for providing the global flux database used in Section 3.1 and acknowledge BODC for the OMEXDIA dataset (check CD!). We are also grateful to Francesca Pianosi for helpful insights into sensitivity analysis. DH is supported by a graduate teaching studentship by
1305 the University of Bristol. SA is supported by funding from the European Unions Horizon 2020 research and innovation programme under the Marie Skłodowska-Curie grant agreement no. 643052 (C-CASCADES). AR acknowledge funding from the EU grant ERC-2013-CoG-617313. **TODO: add for Stuart and Pierre!**

Table 15. Primary pathways of organic matter degradation, secondary redox reactions and stoichiometries implemented in the reaction network.

Pathway	Stoichiometry
Primary Redox reactions	
Aerobic degradation	$(\text{CH}_2\text{O})_x(\text{NH}_3)_y(\text{H}_3\text{PO}_4)_z + (\text{x}+2\text{y})\text{O}_2 + (\text{y}+2\text{z})\text{HCO}_3^- \rightarrow (\text{x}+\text{y}+2\text{z})\text{CO}_2 + \text{yNO}_3^- + \text{zHPO}_4^{2-} + (\text{x}+2\text{y}+2\text{z})\text{H}_2\text{O}$
Denitrification	$(\text{CH}_2\text{O})_x(\text{NH}_3)_y(\text{H}_3\text{PO}_4)_z + \frac{(\text{4x}+3\text{y})}{5}\text{NO}_3^- \rightarrow \frac{(2\text{x}+\text{4y})}{5}\text{N}_2 + \frac{(\text{x}-3\text{y}-10\text{z})}{5}\text{CO}_2 + \frac{(\text{4x}-3\text{y}-10\text{z})}{5}\text{HCO}_3^- + \text{zHPO}_4^{2-} + \frac{(\text{3x}+3\text{y}+10\text{z})}{5}\text{H}_2\text{O}$
Sulfate reduction	$(\text{CH}_2\text{O})_x(\text{NH}_3)_y(\text{H}_3\text{PO}_4)_z + \frac{\text{x}}{2}\text{SO}_4^{2-} + (\text{y}-2\text{z})\text{CO}_2 + (\text{y}-2\text{z})\text{H}_2\text{O} \rightarrow \frac{\text{x}}{2}\text{H}_2\text{S} + (\text{x}+\text{y}-2\text{z})\text{HCO}_3^- + \text{yNH}_4^+ + \text{zHPO}_4^{2-}$
Methanogenesis	$(\text{CH}_2\text{O})_x(\text{NH}_3)_y(\text{H}_3\text{PO}_4)_z + (\text{y}-2\text{z})\text{H}_2\text{O} \rightarrow \frac{\text{x}}{2}\text{CH}_4 + \frac{\text{x}-2\text{y}+4\text{z}}{2}\text{CO}_2 + (\text{x}-2\text{z})\text{HCO}_3^- + \text{yNH}_4^+ + \text{zHPO}_4^{2-}$
Secondary Redox reactions	
Nitrification	$\text{NH}_4^+ + 2\text{O}_2 + 2\text{HCO}_3^- \rightarrow \text{NO}_3^- + 2\text{CO}_2 + 3\text{H}_2\text{O}$
Sulfide oxidation	$\text{H}_2\text{S} + 2\text{O}_2 + 2\text{HCO}_3^- \rightarrow \text{SO}_4^{2-} + 2\text{CO}_2 + 2\text{H}_2\text{O}$
AOM	$\text{CH}_4 + \text{CO}_2 + \text{SO}_4^{2-} \rightarrow 2\text{HCO}_3^- + \text{H}_2\text{S}$
Adsorption reactions and mineral precipitation	
NH ₄ adsorption	$\text{NH}_4^+ \xrightarrow{K_{\text{NH}_4}} \text{NH}_4^+(\text{ads})$
P ad-/desorption	$\text{PO}_4^{2-} \xrightarrow{K_{\text{P}\text{O}_4}^{\text{I},\text{II}}} \text{PO}_4^{2-}(\text{ads}); \quad \text{PO}_4^{2-} \xrightarrow{k_s} \text{Fe-bound P} \xrightarrow{k_m} \text{PO}_4^{2-}$
CFA precipitation	$\text{PO}_4^{2-} \xrightarrow{k_a} \text{CFA}$

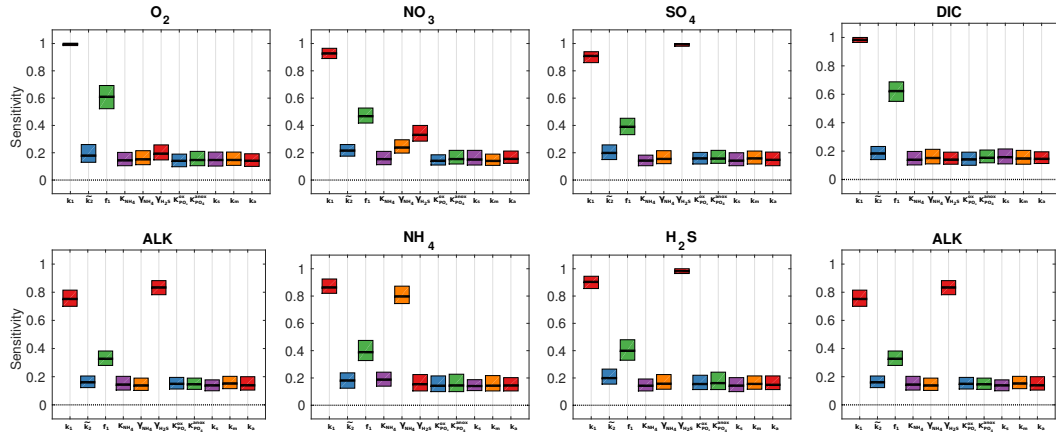


Figure 17. Move to Appendix Box plot of parameter sensitivities for the calculated SWI-fluxes for the 4000m oxic condition. Average sensitivities (black lines) and 90% confidence intervals using $N = 11200$ model evaluations and $Nboot = 100$ bootstrap resamples.

References

- Aguilera, D. R., Jourabchi, P., Spiteri, C., and Regnier, P. (2005). A knowledge-based reactive transport approach for the simulation of biogeochemical dynamics in Earth systems. *Geochemistry, Geophysics, Geosystems*, 6(7).
- Aller, R. C. (1984). The importance of relict burrow structures and burrow irrigation in controlling sedimentary solute distributions. *Geochimica et Cosmochimica Acta*, 48(10):1929–1934.
- Aller, R. C. (1988). Benthic fauna and biogeochemical processes in marine sediments: the role of burrow structures. In Blackburn, T. and Sorensen, J., editors, *Nitrogen cycling in coastal marine environments*, pages 301–338. Scope, Chichester.
- Archer, D. and Devol, A. (1992). Benthic oxygen fluxes on the Washington shelf and slope: A comparison of in situ microelectrode and chamber flux measurements. *Limnology and Oceanography*, 37(3):614–629.
- Archer, D., Eby, M., Brovkin, V., Ridgwell, A., Cao, L., Mikolajewicz, U., Caldeira, K., Matsumoto, K., Munhoven, G., Montenegro, A., and Tokos, K. (2009). Atmospheric Lifetime of Fossil Fuel Carbon Dioxide. *Annual Review of Earth and Planetary Sciences*, 37(1):117–134.
- Archer, D. and Maier-Reimer, E. (1994). Effect of Deep-Sea Sedimentary Calcite Preservation on Atmospheric Co₂ Concentration. *Nature*, 367(6460):260–263. 00506 WOS:A1994MR49400052.
- Archer, D., Winguth, A., Lea, D., and Mahowald, N. (2000). What caused the glacial/interglacial atmospheric pCO₂ cycles? *Reviews of Geophysics*, 38(2):159–189. 00414.
- Archer, D. E., Morford, J. L., and Emerson, S. R. (2002). A model of suboxic sedimentary diagenesis suitable for automatic tuning and gridded global domains. *Global Biogeochemical Cycles*, 16(1):17–1.
- Arndt, S., Jørgensen, B., LaRowe, D., Middelburg, J., Pancost, R., and Regnier, P. (2013). Quantifying the degradation of organic matter in marine sediments: A review and synthesis. *Earth-Science Reviews*, 123:53–86.

- Arthur, M. A., Dean, W. E., and Pratt, L. M. (1988). Geochemical and climatic effects of increased marine organic carbon burial at the Cenomanian/Turonian boundary. *Nature*, 335(6192):714–717.
- Berner, R. A. (1980). *Early Diagenesis: A Theoretical Approach*. Princeton University Press.
- Berner, R. A. (1991). A model for atmospheric CO₂ over Phanerozoic time. *291(4):339–376*.
- 1335 Berner, R. A. (2004). *The Phanerozoic Carbon Cycle: CO₂ and O₂*. Oxford University Press. 00000.
- Billett, G. (1982). An idealized model of nitrogen recycling in marine sediments. *American Journal of Science*, 282(4):512–541.
- Bohlen, L., Dale, A. W., and Wallmann, K. (2012). Simple transfer functions for calculating benthic fixed nitrogen losses and C:N:P regeneration ratios in global biogeochemical models. *Global Biogeochemical Cycles*, 26(3):GB3029.
- 1340 Boudreau, B. P. (1984). On the equivalence of nonlocal and radial-diffusion models for porewater irrigation. *Journal of Marine Research*, 42(3):731–735.
- Boudreau, B. P. (1986). Mathematics of tracer mixing in sediments; I, Spatially-dependent, diffusive mixing. *American Journal of Science*, 286(3):161–198.
- 1345 Boudreau, B. P. (1996). A method-of-lines code for carbon and nutrient diagenesis in aquatic sediments. *Computers & Geosciences*, 22(5):479–496.
- Boudreau, B. P. (1997). *Diagenetic models and their implementation*, volume 505. Springer Berlin.
- Boudreau, B. P. (1998). Mean mixed depth of sediments: The wherefore and the why. *Limnology and Oceanography*, 43(3):524–526.
- 1350 Boudreau, B. P., Arnosti, C., Jørgensen, B. B., and Canfield, D. E. (2008). Comment on "Physical Model for the Decay and Preservation of Marine Organic Carbon". *Science*, 319(5870):1616–1616.
- Boudreau, B. P., Mucci, A., Sundby, B., Luther, G. W., and Silverberg, N. (1998). Comparative diagenesis at three sites on the Canadian continental margin. *Journal of Marine Research*, 56(6):1259–1284.
- Boudreau, B. P. and Ruddick, B. R. (1991). On a reactive continuum representation of organic matter diagenesis. *American Journal of Science*, 291(5):507–538.
- 1355 Broecker, W. S. (1982). Ocean chemistry during glacial time. *Geochimica et Cosmochimica Acta*, 46(10):1689–1705.
- Burdige, D. J. (2006). *Geochemistry of marine sediments*, volume 398. Princeton University Press Princeton.
- Canfield, D. E., Kristensen, E., and Thamdrup, B. (2005). *Aquatic Geomicrobiology*. Gulf Professional Publishing.
- 1360 Colbourn, G., Ridgwell, A., and Lenton, T. M. (2013). The Rock Geochemical Model (RokGeM) v0.9. *Geosci. Model Dev.*, 6(5):1543–1573.
- Conkright, M. E., Locarnini, R. A., Garcia, H. E., O'Brien, T. D., Boyer, T. P., Stephens, C., and Antonov, J. I. (2002). *World Ocean Atlas 2001: Objective analyses, data statistics, and figures: CD-ROM documentation*.
- 1365 US Department of Commerce, National Oceanic and Atmospheric Administration, National Oceanographic Data Center, Ocean Climate Laboratory.
- Devol, A. H. and Christensen, J. P. (1993). Benthic fluxes and nitrogen cycling in sediments of the continental margin of the eastern North Pacific. *Journal of Marine Research*, 51(2):345–372.
- Edwards, N. R. and Marsh, R. (2005). Uncertainties due to transport-parameter sensitivity in an efficient 3-D ocean-climate model. *Climate Dynamics*, 24(4):415–433.

- Emerson, S. and Bender, M. L. (1981). Carbon fluxes at the sediment-water interface of the deep-sea: calcium carbonate preservation. *Journal of Marine Research*, 39:139–162.
- Emerson, S. and Hedges, J. I. (1988). Processes controlling the organic carbon content of open ocean sediments. *Paleoceanography*, 3(5):621–634.
- 1375 Emerson, S., Jahnke, R., and Heggie, D. (1984). Sediment-water exchange in shallow water estuarine sediments. *Journal of Marine Research*, 42(3):709–730.
- Epping, E., van der Zee, C., Soetaert, K., and Helder, W. (2002). On the oxidation and burial of organic carbon in sediments of the Iberian margin and Nazaré Canyon (NE Atlantic). *Progress in Oceanography*, 52(2–4):399–431.
- 1380 Fischer, J. P., Ferdelman, T. G., D'Hondt, S., Røy, H., and Wenzhöfer, F. (2009). Oxygen penetration deep into the sediment of the South Pacific gyre. *Biogeosciences*, 6(8):1467–1478.
- Glud, R. N. (2008). Oxygen dynamics of marine sediments. *Marine Biology Research*, 4(4):243–289.
- Goloway, F. and Bender, M. (1982). Diagenetic models of interstitial nitrate profiles in deep sea suboxic sediments1. *Limnology and Oceanography*, 27(4):624–638.
- 1385 Goosse, H., Brovkin, V., Fichefet, T., Haarsma, R., Huybrechts, P., Jongma, J., Mouchet, A., Selten, F., Barriat, P.-Y., Campin, J.-M., Deleersnijder, E., Driesschaert, E., Goelzer, H., Janssens, I., Loutre, M.-F., Morales Maqueda, M. A., Opsteegh, T., Mathieu, P.-P., Munhoven, G., Pettersson, E. J., Renssen, H., Roche, D. M., Schaeffer, M., Tartinville, B., Timmermann, A., and Weber, S. L. (2010). Description of the earth system model of intermediate complexity LOVECLIM version 1.2. *Geosci. Model Dev.*, 3(2):603–633.
- 1390 Gypens, N., Lancelot, C., and Soetaert, K. (2008). Simple parameterisations for describing n and p diagenetic processes: Application in the north sea. *Progress in Oceanography*, 76(1):89–110.
- Heinze, C., Maier-Reimer, E., Winguth, A. M. E., and Archer, D. (1999). A global oceanic sediment model for long-term climate studies. *Global Biogeochemical Cycles*, 13(1):221–250.
- Hensen, C., Zabel, M., and Schulz, H. N. (2006). Benthic Cycling of Oxygen, Nitrogen and Phosphorus. In 1395 Schulz, H. D. and Zabel, M., editors, *Marine Geochemistry*, pages 207–240. Springer Berlin Heidelberg.
- Hülse, D., Arndt, S., Wilson, J. D., Munhoven, G., and Ridgwell, A. (2017). Understanding the causes and consequences of past marine carbon cycling variability through models. *Earth-Science Reviews*, 171:349–382.
- Ilyina, T., Six, K. D., Segschneider, J., Maier-Reimer, E., Li, H., and Núñez-Riboni, I. (2013). Global ocean 1400 biogeochemistry model HAMOCC: Model architecture and performance as component of the MPI-Earth system model in different CMIP5 experimental realizations. *Journal of Advances in Modeling Earth Systems*, 5(2):287–315.
- Ingall, E. and Jahnke, R. (1994). Evidence for enhanced phosphorus regeneration from marine sediments overlain by oxygen depleted waters. *Geochimica et Cosmochimica Acta*, 58(11):2571–2575. 00302.
- 1405 Jarvis, I., Lignum, J. S., Gröcke, D. R., Jenkyns, H. C., and Pearce, M. A. (2011). Black shale deposition, atmospheric CO₂ drawdown, and cooling during the Cenomanian-Turonian Oceanic Anoxic Event. *Paleoceanography*, 26(3):n/a–n/a.
- Jenkyns, H. C. (2010). Geochemistry of oceanic anoxic events. *Geochemistry, Geophysics, Geosystems*, 11(3).
- Jørgensen, B. B. (1978). A comparison of methods for the quantification of bacterial sulfate reduction in coastal 1410 marine sediments: II Calculation from mathematical models. *Geomicrobiology Journal*, 1:29–47.

- Jourabchi, P., Cappellen, P. V., and Regnier, P. (2005). Quantitative interpretation of pH distributions in aquatic sediments: A reaction-transport modeling approach. *American Journal of Science*, 305(9):919–956.
- Jørgensen, B. B. and Kasten, S. (2006). Sulfur Cycling and Methane Oxidation. In Schulz, P. D. H. D. and Zabel, D. M., editors, *Marine Geochemistry*, pages 271–309. Springer Berlin Heidelberg.
- 1415 Kolmogorov, A. (1933). Sulla determinazione empirica di una leggi di distribuzione. *Giorn. Ist Ital. Attuari*, 4, 91.
- Krom, M. D. and Berner, R. A. (1980). Adsorption of phosphate in anoxic marine sediments1. *Limnology and Oceanography*, 25(5):797–806.
- Krumins, V., Gehlen, M., Arndt, S., Van Cappellen, P., and Regnier, P. (2013). Dissolved inorganic carbon 1420 and alkalinity fluxes from coastal marine sediments: Model estimates for different shelf environments and sensitivity to global change. *Biogeosciences*.
- Lee, C., Wakeham, S. G., and I. Hedges, J. (2000). Composition and flux of particulate amino acids and chloropigments in equatorial Pacific seawater and sediments. *Deep Sea Research Part I: Oceanographic Research Papers*, 47(8):1535–1568.
- 1425 Lenton, T. M. and Watson, A. J. (2000). Redfield revisited: 1. Regulation of nitrate, phosphate, and oxygen in the ocean. *Global Biogeochemical Cycles*, 14(1):225–248.
- Li, Y.-H. and Gregory, S. (1974). Diffusion of ions in sea water and in deep-sea sediments. *Geochimica et Cosmochimica Acta*, 38(5):703–714.
- Longhurst, A., Sathyendranath, S., Platt, T., and Caverhill, C. (1995). An estimate of global primary production 1430 in the ocean from satellite radiometer data. *Journal of Plankton Research*, 17(6):1245–1271.
- Mackenzie, F. T. (2005). *Sediments, Diagenesis, and Sedimentary Rocks: Treatise on Geochemistry, Second Edition*. Elsevier. 00000.
- Meile, C. and Van Cappellen, P. (2003). Global estimates of enhanced solute transport in marine sediments. *Limnology and Oceanography*, 48(2):777–786.
- 1435 Meysman, F. J. R., Middelburg, J. J., Herman, P. M. J., and Heip, C. H. R. (2003). Reactive transport in surface sediments. II. Media: an object-oriented problem-solving environment for early diagenesis. *Computers & Geosciences*, 29(3):301–318. 00067.
- Middelburg, J. J., Soetaert, K., and Herman, P. M. (1997). Empirical relationships for use in global diagenetic models. *Deep Sea Research Part I: Oceanographic Research Papers*, 44(2):327–344.
- 1440 Middelburg, J. J., Soetaert, K., Herman, P. M. J., and Heip, C. H. R. (1996). Denitrification in marine sediments: A model study. *Global Biogeochemical Cycles*, 10(4):661–673.
- Middelburg, J. J., Vlug, T., Jaco, F., and van der Nat, W. A. (1993). Organic matter mineralization in marine systems. *Global and Planetary Change*, 8(1):47–58.
- Mort, H. P., Adatte, T., Föllmi, K. B., Keller, G., Steinmann, P., Matera, V., Berner, Z., and Stüben, D. (2007). 1445 Phosphorus and the roles of productivity and nutrient recycling during oceanic anoxic event 2. *Geology*, 35(6):483–486. 00135.
- Munhoven, G. (2007). Glacial–interglacial rain ratio changes: Implications for atmospheric and ocean–sediment interaction. *Deep Sea Research Part II: Topical Studies in Oceanography*, 54(5–7):722–746.

- 1450 Najjar, R. G., Jin, X., Louanchi, F., Aumont, O., Caldeira, K., Doney, S. C., Dutay, J.-C., Follows, M., Gruber, N., Joos, F., Lindsay, K., Maier-Reimer, E., Matear, R. J., Matsumoto, K., Monfray, P., Mouchet, A., Orr, J. C., Plattner, G.-K., Sarmiento, J. L., Schlitzer, R., Slater, R. D., Weirig, M.-F., Yamanaka, Y., and Yool, A. (2007). Impact of circulation on export production, dissolved organic matter, and dissolved oxygen in the ocean: Results from Phase II of the Ocean Carbon-cycle Model Intercomparison Project (OCMIP-2). *Global Biogeochemical Cycles*, 21(3):GB3007.
- 1455 Palastanga, V., Slomp, C. P., and Heinze, C. (2011). Long-term controls on ocean phosphorus and oxygen in a global biogeochemical model. *Global Biogeochemical Cycles*, 25(3):GB3024.
- Pianosi, F., Beven, K., Freer, J., Hall, J. W., Rougier, J., Stephenson, D. B., and Wagener, T. (2016). Sensitivity analysis of environmental models: A systematic review with practical workflow. *Environmental Modelling & Software*, 79:214–232.
- 1460 Pianosi, F., Sarrazin, F., and Wagener, T. (2015). A Matlab toolbox for Global Sensitivity Analysis. *Environmental Modelling & Software*, 70:80–85.
- Pianosi, F. and Wagener, T. (2015). A simple and efficient method for global sensitivity analysis based on cumulative distribution functions. *Environmental Modelling & Software*, 67:1–11.
- 1465 Redfield, A. C. (1963). The influence of organisms on the composition of seawater. *The sea*, 2:26–77.
- Regnier, P., Dale, A. W., Arndt, S., LaRowe, D. E., Mogollon, J., and Van Cappellen, P. (2011). Quantitative analysis of anaerobic oxidation of methane (AOM) in marine sediments: A modeling perspective. *Earth-Science Reviews*, 106(1):105–130.
- Reimers, C. E., Lange, C. B., Tabak, M., and Bernhard, J. M. (1990). Seasonal spillover and varve formation 1470 in the Santa Barbara Basin, California. *Limnology and Oceanography*, 35(7):1577–1585.
- Reimers, C. E., Ruttenberg, K. C., Canfield, D. E., Christiansen, M. B., and Martin, J. B. (1996). Porewater pH and authigenic phases formed in the uppermost sediments of the Santa Barbara Basin. *Geochimica et Cosmochimica Acta*, 60(21):4037–4057.
- Ridgwell, A. and Hargreaves, J. C. (2007). Regulation of atmospheric CO₂ by deep-sea sediments in an Earth 1475 system model. *Global Biogeochemical Cycles*, 21(2):n/a–n/a.
- Ridgwell, A., Hargreaves, J. C., Edwards, N. R., Annan, J. D., Lenton, T. M., Marsh, R., Yool, A., and Watson, A. (2007). Marine geochemical data assimilation in an efficient Earth System Model of global biogeochemical cycling. *Biogeosciences*, 4(1):87–104. 00090.
- Ridgwell, A. and Zeebe, R. E. (2005). The role of the global carbonate cycle in the regulation and evolution of 1480 the Earth system. *Earth and Planetary Science Letters*, 234(3–4):299–315. 00172.
- Ruardij, P. and Van Raaphorst, W. (1995). Benthic nutrient regeneration in the ERSEM ecosystem model of the North Sea. *Netherlands Journal of Sea Research*, 33(3):453–483.
- Ruttenberg, K. C. (1993). Reassessment of the oceanic residence time of phosphorus. *Chemical Geology*, 107(3):405–409.
- 1485 Schulz, H. D. (2006). Quantification of Early Diagenesis: Dissolved Constituents in Pore Water and Signals in the Solid Phase. In Schulz, P. D. H. D. and Zabel, D. M., editors, *Marine Geochemistry*, pages 73–124. Springer Berlin Heidelberg.

- Seiter, K., Hensen, C., Schröter, J., and Zabel, M. (2004). Organic carbon content in surface sediments—defining regional provinces. *Deep Sea Research Part I: Oceanographic Research Papers*, 51(12):2001–2026.
- 1490 Shaffer, G., Malskær Olsen, S., and Pepke Pedersen, J. O. (2008). Presentation, calibration and validation of the low-order, DCESS Earth System Model (Version 1). *Geosci. Model Dev.*, 1(1):17–51. 00007.
- Slomp, C., Malschaert, J., and Van Raaphorst, W. (1998). The role of adsorption in sediment-water exchange of phosphate in north sea continental margin sediments. *Limnology and Oceanography*, 43(5):832–846.
- 1495 Slomp, C. P., Epping, E. H., Helder, W., and Van Raaphorst, W. (1996). A key role for iron-bound phosphorus in authigenic apatite formation in north atlantic continental platform sediments. *Journal of Marine Research*, 54(6):1179–1205.
- Smirnov, N. V. (1939). On the estimation of the discrepancy between empirical curves of distribution for two independent samples. *Bull. Math. Univ. Moscou*, 2(2).
- 1500 Soetaert, K., Herman, P. M. J., and Middelburg, J. J. (1996). A model of early diagenetic processes from the shelf to abyssal depths. *Geochimica et Cosmochimica Acta*, 60(6):1019–1040.
- Soetaert, K., Middelburg, J. J., Herman, P. M. J., and Buis, K. (2000). On the coupling of benthic and pelagic biogeochemical models. *Earth-Science Reviews*, 51(1–4):173–201.
- Stein, R., Rulkötter, J., and Welte, D. H. (1986). Accumulation of organic-carbon-rich sediments in the Late 1505 Jurassic and Cretaceous Atlantic Ocean — A synthesis. *Chemical Geology*, 56(1–2):1–32.
- Stolpovsky, K., Dale, A. W., and Wallmann, K. (2015). Toward a parameterization of global-scale organic carbon mineralization kinetics in surface marine sediments. *Global Biogeochemical Cycles*, 29(6):2015GB005087.
- Stumm, W. and Morgan, J. J. (2012). *Aquatic Chemistry: Chemical Equilibria and Rates in Natural Waters*.
- 1510 John Wiley & Sons.
- Teal, L., Bulling, M., Parker, E., and Solan, M. (2010). Global patterns of bioturbation intensity and mixed depth of marine soft sediments. *Aquatic Biology*, 2(3):207–218.
- Thullner, M., Dale, A. W., and Regnier, P. (2009). Global-scale quantification of mineralization pathways in marine sediments: A reaction-transport modeling approach. *Geochemistry, Geophysics, Geosystems*, 10(10).
- 1515 Thullner, M., Van Cappellen, P., and Regnier, P. (2005). Modeling the impact of microbial activity on redox dynamics in porous media. *Geochimica et Cosmochimica Acta*, 69(21):5005–5019.
- Tjiputra, J. F., Roelandt, C., Bentsen, M., Lawrence, D. M., Lorentzen, T., Schwinger, J., Seland, Ø., and Heinze, C. (2013). Evaluation of the carbon cycle components in the Norwegian Earth System Model (NorESM). *Geosci. Model Dev.*, 6(2):301–325. 00057.
- 1520 Toth, D. J. and Lerman, A. (1977). Organic matter reactivity and sedimentation rates in the ocean. *American Journal of Science*, 277(4):465–485.
- Tromp, T. K., Van Cappellen, P., and Key, R. M. (1995). A global model for the early diagenesis of organic carbon and organic phosphorus in marine sediments. *Geochimica et Cosmochimica Acta*, 59(7):1259–1284. 00164.
- 1525 Tsandev, I. and Slomp, C. (2009). Modeling phosphorus cycling and carbon burial during Cretaceous Oceanic Anoxic Events. *Earth and Planetary Science Letters*, 286(1–2):71–79.

- Ullman, W. J. and Aller, R. C. (1982). Diffusion coefficients in nearshore marine sediments. *Limnology and Oceanography*, 27(3):552–556.
- Van Cappellen, P. and Berner, R. A. (1988). A mathematical model for the early diagenesis of phosphorus and fluorine in marine sediments; apatite precipitation. *American Journal of Science*, 288(4):289–333.
- 1530 Van Cappellen, P. and Ingall, E. D. (1994). Benthic phosphorus regeneration, net primary production, and ocean anoxia: A model of the coupled marine biogeochemical cycles of carbon and phosphorus. *Paleoceanography*, 9(5):677–692.
- Van Cappellen, P. and Wang, Y. (1995). Metal cycling in surface sediments: modeling the interplay of transport and reaction. *Metal contaminated aquatic sediments*, pages 21–64.
- 1535 Van Cappellen, P. and Wang, Y. (1996). Cycling of iron and manganese in surface sediments; a general theory for the coupled transport and reaction of carbon, oxygen, nitrogen, sulfur, iron, and manganese. *American Journal of Science*, 296(3):197–243.
- van Weering, T. C. E., de Stigter, H. C., Boer, W., and de Haas, H. (2002). Recent sediment transport and accumulation on the NW Iberian margin. *Progress in Oceanography*, 52(2):349–371.
- 1540 Vanderborgh, J.-P. and Billen, G. (1975). Vertical distribution of nitrate concentration in interstitial water of marine sediments with nitrification and denitrification. *Limnology and Oceanography*, 20(6):953–961.
- Vanderborgh, J.-P., Wollas, R., and Bitten, G. (1977). Kinetic models of diagenesis in disturbed sediments. Part 2. Nitrogen diagenesis. *Limnology and Oceanography*, 22(5):794–803.
- 1545 Wakeham, S. G., Hedges, J. I., Lee, C., Peterson, M. L., and Hernes, P. J. (1997). Compositions and transport of lipid biomarkers through the water column and surficial sediments of the equatorial Pacific Ocean. *Deep Sea Research Part II: Topical Studies in Oceanography*, 44(9):2131–2162.
- Wang, Y. and Van Cappellen, P. (1996). A multicomponent reactive transport model of early diagenesis: Application to redox cycling in coastal marine sediments. *Geochimica et Cosmochimica Acta*, 60(16):2993–3014.
- 1550 00283.
- Wenzhöfer, F. and Glud, R. N. (2002). Benthic carbon mineralization in the Atlantic: a synthesis based on in situ data from the last decade. *Deep Sea Research Part I: Oceanographic Research Papers*, 49(7):1255–1279.
- Wolf-Gladrow, D. A., Zeebe, R. E., Klaas, C., Kötzinger, A., and Dickson, A. G. (2007). Total alkalinity: The explicit conservative expression and its application to biogeochemical processes. *Marine Chemistry*, 106(1–2):287–300.
- 1555